

12-8-2020

## **An Improved Foam Modeling Technique and Its Application to Petroleum Drilling and Production Practice**

Yanfang Wang

*Louisiana State University and Agricultural and Mechanical College*

Follow this and additional works at: [https://digitalcommons.lsu.edu/gradschool\\_dissertations](https://digitalcommons.lsu.edu/gradschool_dissertations)



Part of the [Complex Fluids Commons](#), [Energy Systems Commons](#), [Engineering Mechanics Commons](#), and the [Petroleum Engineering Commons](#)

---

### **Recommended Citation**

Wang, Yanfang, "An Improved Foam Modeling Technique and Its Application to Petroleum Drilling and Production Practice" (2020). *LSU Doctoral Dissertations*. 5430.

[https://digitalcommons.lsu.edu/gradschool\\_dissertations/5430](https://digitalcommons.lsu.edu/gradschool_dissertations/5430)

This Dissertation is brought to you for free and open access by the Graduate School at LSU Digital Commons. It has been accepted for inclusion in LSU Doctoral Dissertations by an authorized graduate school editor of LSU Digital Commons. For more information, please contact [gradetd@lsu.edu](mailto:gradetd@lsu.edu).

# AN IMPROVED FOAM MODELING TECHNIQUE AND ITS APPLICATION TO PETROLEUM DRILLING AND PRODUCTION PRACTICE

A Dissertation

Submitted to the Graduate Faculty of the  
Louisiana State University and  
Agricultural and Mechanical College  
in partial fulfillment of the  
requirements for the degree of  
Doctor of Philosophy

in

The Department of Petroleum Engineering

by

Yanfang Wang

B.S., China University of Petroleum at Beijing, 2012

M.S., University of Louisiana at Lafayette, 2014

May 2021

## ACKNOWLEDGMENTS

This PhD journey is a truly life-changing experience for me, and it would have been impossible for me to go through it without the support and guidance from many people.

First of all, I would like to express my sincere gratitude to the Craft & Hawkins Department of Petroleum Engineering, College of Engineering, Louisiana State University for financial support. Especially, I would thank my major advisor, Dr. Seung Ihl Kam, for his consistent support and guidance through each stage of the process. His hardworking and immense knowledge have also deeply impressed and inspired me.

I would like to thank other committee members (Dr. Paulo J. Waltrich, Dr. Wesley C. Williams, Dr. Celalettin E. Ozdemir, and Dr. Jianhua Chen) for their insightful comments and encouragement. My sincere thanks also goes to Dr. Dandina Rao, Dr. Mauricio Almeida, Dr. Yuanhang Chen, and Dr. Arash Dahi Taleghani for their wonderful courses.

I am also very thankful to my industrial collaborators at Pegasus Vertex, Inc. More specifically, I would like to thank Dr. Hu Dai and Gefei Liu for their great mentorship and guidance during my internships.

I also thank my fellow labmates including Dr. Mohammad Izadi, Caitlyn Thiberville, Hazem Fleifel, Tooba Riaz, and Doris Ortiz for the stimulating discussions and all the fun we have had.

I would also like to extend my deepest gratitude to my family, especially my parents Zhenyuan Wang and Chunlan Xu. They have provided me continued encouragement and endless support throughout my life. Thanks should also go to my loving and supportive husband, Dr. Yichen Jia, who always made me feel confident in my abilities. Last but not least, I feel very fortunate to have my Shiba Inu pet, Totoro, for her companionship during the COVID -19 outbreak.

## TABLE OF CONTENTS

ACKNOWLEDGMENTS .....	ii
LIST OF TABLES .....	v
LIST OF FIGURES .....	vi
ABSTRACT.....	x
CHAPTER 1. INTRODUCTION .....	1
1.1    Dissertation Statement and Contributions .....	3
1.2    Dissertation Organization .....	4
CHAPTER 2. LITERATURE REVIEW OF FOAM APPLICATIONS AND PRESENCE OF TWO FLOW REGIMES.....	5
2.1    Foam Applications in Petroleum Industry .....	5
2.1    Presence of Two Flow Regimes .....	11
CHAPTER 3. A NEW MODEL FOR FOAM FLOW IN PIPES AND ANNULI.....	22
3.1    Introduction.....	22
3.2    Motivation and Objectives .....	26
3.3    Methodology .....	29
3.4    Conclusions.....	53
CHAPTER 4. MODELING OF FOAM-ASSISTED WELLBORE CLEANUP AND DRILLING PROCESSES WITH BOTH DRY- AND WET-FOAM RHEOLOGICAL PROPERTIES .....	55
4.1    Introduction.....	55
4.2    Objectives .....	59
4.3    Methodology .....	60
4.4    Results and Discussions.....	68
4.5    Conclusions.....	87
CHAPTER 5. NUMERICAL MODELING AND SIMULATION OF FOAM-ASSISTED MUD CAP DRILLING PROCESSES.....	88
5.1    Introduction.....	88
5.2    Objectives .....	96
5.3    Methodology .....	98
5.4    Results and Discussions.....	107
5.5    Conclusions.....	129
CHAPTER 6. CONCLUSIONS AND FUTURE WORKS.....	131



6.1	Conclusions .....	131
6.2	Future Works .....	132
REFERENCES .....		134
VITA .....		141

## LIST OF TABLES

3. 1 Summary of nine foam model parameters determined in this study .....	39
3. 2 Comparison of three different foam simulation methods .....	53
4. 1 Nine input parameters for foam flow inside drill pipe.....	65
4. 2 Nine input parameters for foam flow in the annulus .....	65
4. 3 Field data for foam circulation modeling.....	69
4. 4 Comparison of three different foam simulation methods .....	76
5. 1 Nine foam model parameters used for frictional pressure loss in this study.....	105
5. 2 Input data for foam PMCD well control process .....	106
5. 3 Flow rate data and measured pressure data for Point A, B, C .....	128
5. 4 Comparisons of predicted circulation pressure with different foam models .....	129

## LIST OF FIGURES

2. 1 Beyer et al.'s model: (a) foam viscosity vs. foam quality and (b) viscosity contours .....	12
2. 2 Sanghani and Ikoku's model: (a) foam viscosity vs. foam quality (b) viscosity contours ....	13
2. 3 Reidenbach et al.'s model: (a) foam viscosity vs. foam quality (b) viscosity contours .....	14
2. 4 Pressure contour map developed using Sanghani and Ikoku data .....	15
2. 5 Pressure contour map developed using Briceno and Joseph data .....	16
2. 6 Pressure contour map developed using Guzman et al.'s data .....	17
2. 7 Contour maps for inclination angle $0^\circ$ (left) and $90^\circ$ (right) downward flow: pressure drop (A); apparent viscosity (B) .....	18
2. 8 Pressure drop contour map for surfactant foams .....	19
2. 9 Pressure drop contour map for surfactant foams in the presence of oil .....	20
2. 10 Pressure drop contour map for polymer-added surfactant foams .....	21
3. 1 Experimental data from surfactant foam flow .....	24
3. 2 Model fit to experimental data proposed by Edrisi and Kam (2013) .....	25
3. 3 Schematic figures comparing previous model and this new model .....	27
3. 4 A schematic figure showing nine parameters in this new model .....	34
3. 5 A schematic figure showing the model parameters .....	37
3. 6 Rheograms showing the relationship between shear stress and shear rate .....	37
3. 7 A schematic of a complete pressure contour map .....	38
3. 8 Conversion of pressure contours into apparent foam viscosity contours .....	40
3. 9 Apparent foam viscosity obtained at fixed superficial liquid rates .....	41
3. 10 A schematic figure showing 12 data points of interest in the Low-Quality regime .....	43
3. 11 Liquid layer thickness at different gas and liquid injection rates .....	44
3. 12 Relationship between friction factor and Reynolds number .....	45

3. 13 A schematic of foam drilling process using U-tube concept .....	46
3. 14 Steady-state simulation results for foam circulation without formation fluid influx: (a) pressure (b) foam quality (c) foam density (d) total velocity .....	49
4. 1 Frictional pressure loss contours from surfactant foam flow experiments.....	58
4. 2 A schematic figure showing nine parameters in the new foam rheology model .....	59
4. 3 A schematic on how to determine the frictional pressure gradient in Domain 1 .....	62
4. 4 A schematic on how to determine the frictional pressure gradient in Domain 2 .....	63
4. 5 A schematic on how to determine the frictional pressure gradient in Domain 3 .....	63
4. 6 Schematics of U-tube concept wellbore configurations: (a) vertical well (b) inclined well (c) horizontal well .....	67
4. 7 Steady-state simulation results for the vertical well .....	70
4. 8 Steady-state simulation results for the inclined well .....	71
4. 9 Steady-state simulation results for the horizontal well .....	72
4. 10 Simulated paths along the drill pipe (left) and annulus (right): (a)(b) vertical well, (c)(d) inclined well, (e)(f) horizontal well.....	74
4. 11 Steady-state simulation results for the vertical well with formation water influx .....	77
4. 12 Steady-state simulation results for the inclined well with formation water influx .....	78
4. 13 Steady-state simulation results for the horizontal well with formation water influx.....	79
4. 14 Simulated paths with formation water influx along the drillpipe (left) and annulus (right): (a)(b) vertical well, (c)(d) inclined well, (e)(f) horizontal well .....	80
4. 15 Steady-state simulation results for the vertical well with formation gas influx .....	81
4. 16 Steady-state simulation results for the inclined well with formation gas influx.....	82
4. 17 Steady-state simulation results for the horizontal well with formation gas influx .....	83
4. 18 Simulated paths with formation gas influx along the drillpipe (left) and annulus (right): (a)(b) vertical well, (c)(d) inclined well, (e)(f) horizontal well.....	84
4. 19 Steady-state simulation results of apparent viscosity for the vertical well without influx ..	85

4. 20 Steady-state simulation results of apparent viscosity for the vertical well with formation water influx.....	86
4. 21 Steady-state simulation results of apparent viscosity for the vertical well with formation gas influx .....	86
5. 1 A schematic of fluid flow in a typical PMCD operation for bullheading.....	90
5. 2 Offshore drilling schematic with RCD .....	91
5. 3 Foam-assisted bullheading process when foam is not in contact with formation gas .....	99
5. 4 Foam-assisted bullheading process when foam is in contact with formation gas but remains stable.....	101
5. 5 Foam-assisted bullheading process when foam is in contact with formation gas and becomes unstable.....	102
5. 6 Foam model that has both dry and wet rheological behaviors.....	104
5. 7 Foam flow regime map for foam flowing in annulus .....	108
5. 8 Base Scenario results showing vertical locations of different fluid zones with time [min].	109
5. 9 Base Scenario results showing pressure profile changing with time .....	110
5. 10 Base Scenario results showing pressure profile at different times .....	111
5. 11 Base Scenario results showing foam quality profile with time.....	112
5. 12 Base Scenario results showing foam density profile with time .....	112
5. 13 Base Scenario results showing foam velocity profile with time .....	113
5. 14 Base Scenario results showing injection pressure at the annular surface with time .....	114
5. 15 Scenario 1 results showing vertical locations of different fluid zones with time [min] ....	115
5. 16 Scenario 1 results showing pressure profile changing with time.....	116
5. 17 Scenario 1 results showing pressure profile at different times .....	116
5. 18 Scenario 1 results showing foam quality profile with time .....	117
5. 19 Scenario 1 results showing foam density profile with time .....	118

5. 20 Scenario 1 results showing foam velocity profile with time.....	118
5. 21 Scenario 1 results showing injection pressure at the annular surface with time.....	119
5. 22 Scenario 2 results showing vertical locations of different fluid zones with time [min] ....	120
5. 23 Scenario 2 results showing pressure profile changing with time.....	121
5. 24 Scenario 2 results showing pressure profile at different times .....	121
5. 25 Scenario 2 results showing foam quality profile with time .....	122
5. 26 Scenario 2 results showing foam density profile with time .....	123
5. 27 Scenario 2 results showing foam velocity profile with time.....	123
5. 28 Scenario 2 results showing injection pressure at the annular surface with time.....	124
5. 29 Well trajectory of field-scale testing and survey data.....	126
5. 30 Job chart of field-scale testing in real time .....	127
5. 31 Three near-steady-state data points and the sketch of pressure contours .....	128

## ABSTRACT

Foam is one of the most common used multiphase fluid in petroleum industry. Because of its low density, high capacity of lifting and carrying cuttings, low cost and compatibility with formations, foam has become more superior than the conventional drilling mud when depleted reservoir pressure, severe lost circulation, or unstable borehole are encountered. In general, the success of foam applications rely on the understanding of the fundamentals of foam rheology in downhole conditions.

Foam rheology has been studied for decades. Conventional foam rheological models usually fail to interpret the monitored circulating pressure changes in operation, not to mention foam behaviors in downhole. Understanding bubble size and foam texture impacts at different foam quality ranges in the foam model development become very significant.

A new foam rheological model based on Low-Quality Regime (LQR) and High-Quality Regime (HQR) behaviors is developed. This new model, which originally came from comprehensive foam flow experiments, together with the visualization of foam texture and bubble distribution, is proved to be easily and conveniently implemented for industry use in this study. With the newly developed foam model, we apply it in the following two foam applications in petroleum industry.

First of all, a foam drilling and wellbore clean-up application with foam is investigated. These scenarios consider foam circulation into 10000 ft long wells at different inclination angles with a long vertical, inclined, or horizontal trajectory. The results are compared with two existing foam modeling techniques. The conclusions show that, with or without formation fluid influx, the new foam model demonstrates the robustness of the new modeling technique in all scenarios capturing

foam flow characteristics better, whenever the situation forms stable fine-textured foams or unstable coarse-textured foams.

Second, foam-assisted mud cap drilling for gas migration situation, which simulates using foam to suppress gas kicks under certain well and fluid conditions, is presented. The results show how mud-cap drilling parameters change at different operating conditions and scenarios. Moreover, a set of field data from a wellbore clean-up with foam operation is demonstrated and the circulating pressure changes provide the evidence of Two Flow Regimes.



## CHAPTER 1. INTRODUCTION

Foams are two-phase mixtures in which gas bubbles (the internal phase) are separated by interconnecting thin films of liquid (the external phase). Surface-active agents (surfactants, or commonly called foaming agents) are designed to trap the gas phase for a desired time period. Gas fraction in the whole foam mixture, which is referred to as “foam quality”, defines how much foam is dry or wet. With a sufficient amount of liquid, wet foams tend to have spherical bubbles with relatively large Plateau borders (the liquid-accumulated areas between gas bubbles) at low capillary pressure, while dry foams have polyhedral bubbles with very thin foam films and tiny Plateau borders at high capillary pressure. Foam quality affects bubble sizes and shapes and thus the resulting interactions (between individual bubbles, between bubbles and pipe wall, and between bubbles and surrounding liquid, for example). Bubble size distribution in foam mixture is defined as “foam texture” – if the mixture is dominated by a large population of well-developed tiny bubbles, it is called fine-textured foam; otherwise it is called coarse-textured foam.

Experimental investigation of foam rheology can be classified into three main categories: using capillaries, rotational viscometers, and pipes. Although foam consists of two phases, some of the simple early day approaches often considered it a homogeneous mixture with pre-specified density and viscosity based on experimental data. Foam viscosity slowly increases with foam quality, when foam quality increases up to roughly 70% (i.e., more bubbles means a higher possibility of bubble-to-bubble and bubble-to-wall interactions to increase foam viscosity). For foam quality roughly between 70% and 85%, foam viscosity dramatically increases with foam quality (i.e., not much space is available to avoid interactions any longer). For foam quality higher than a certain threshold value, around 86-92%, foam viscosity dramatically decreases with foam quality. Of course, these intervals are case- and material-specific, depending on pipe inclination, pipe

diameter, roughness, injection pressure or flow rate, fluid properties, and so on (Xia and Chai, 2012; Saxena et al., 2016), but the general trend still seems valid.

Due to the unique characteristics such as low density, high viscosity, Non-Newtonian rheology, high compressibility, foam has been widely chosen as superior choice in the following fields: underbalanced drilling, wellbore cleaning, enhanced oil recovery, cementing and fracking, artificial lift and gas blockage and so on. On the other hand, the uniqueness of foam raises three critical issues that motivate this work.

Critical Issue 1: Among many developed foam rheological models from literature, those models can hardly explain or predict the monitored pressure changes from the gauges (e.g. circulating pressure). The poor understanding of foam rheology change underground will cause the failure of field operation or even severe safety issues.

Critical Issue 2: Numerical simulation of complex fluid flow in wellbore with Non-Newtonian rheology can be very difficult to handle. Besides of the expensive computation costs, the handling of Non-Newtonian rheological property of foam fluid may require lots of parameters and uncertainties that could affect foam behavior. A simple yet sophisticated modeling work is demanding for field applications.

Critical Issue 3: Foam is a multiphase fluid with gas and liquid phases. A successful foam application requires accurate monitoring of gas and liquid injection simultaneously. Failure to control gas and liquid injection rates would first cause foam stabilities issues, and then cause the failure of the job.

All the above mentioned issues stem the complicated and mysterious characteristics of foam when used in different environments and applications. This motivates us to discover a more generalized foam model and dig some foam applications.

## 1.1 Dissertation Statement and Contributions

To improve the understanding of foam behavior and foam applications in petroleum industry, we develop a new foam model and discover two foam applications in this work. The main contributions of this dissertation can be summarized as follows:

- We first present the creation of a new foam model with 9 foam parameters. These parameters allow the model to capture foam rheological properties in the high-quality and low-quality regimes. By introducing a smooth transition between the two regimes, this model can capture experimental data more realistically. Based on the Power-Law rheology model, the 9 parameters contain 3 to define the range of gas and liquid flow rates and corresponding frictional pressure losses of interest, 4 to fit the Power-Law rheology of wet and dry foams, and last 2 to capture the sensitivity of foam rheology to gas and liquid rates. Some key parameters for foam flow in pipe can also be obtained from this study such as apparent viscosity, thickness of water film, and dimensionless friction factor for foam flows in pipe and annuli. This work is also reported in our research paper (Wang et al., 2017).
- Then we present the application of the new foam model into the foam circulation associated with well cleanup and conventional near-balanced drilling process. Together with the 9-parameter foam rheology model, a semi-steady-state finite difference model is developed to simulate the foam drilling process. Important outputs such as pressure, foam density, foam quality and velocity are plotted with depth based on different scenarios. This work is reported in our research paper (Wang et al., 2018).
- We then present the second foam application, which is a special type of managed pressure drilling process called foam mud cap drilling. This technique has been

successfully used when drilling thick highly-fractured sour reservoirs or carbonate/karst formations where severe fluid loss or sour gas migration is encountered. At these situations, lost circulation is of serious concern because blocking or plugging the wide fractures is impossible and inefficient. Using viscous foam fluid as cap fluid to directly inject into the annulus with accurate control of annular pressure, problems might be solved efficiently. We describe and simulate different scenarios with respect to the response time and foam properties at interface. We will show fluid positions and annular injection pressures in real time. The simulation results will help improve the understanding of field operations of injecting foam to suppress gas migration to control the wells. This work is reported in our research paper (Wang et al., 2020).

## 1.2 Dissertation Organization

The rest of the dissertation is organized as follows. Chapter 2 introduces foam applications in petroleum industry and the concept of Two Foam Flow Regimes. Chapter 3 presents a new foam model that can handle rheology of wet and dry foams across a wide range of gas and liquid velocities. And this bring the following chapters about how such a versatile foam model can be applied to various foam applications in petroleum industry. Chapter 3 presents the foam model applied to a wide range of hole cleaning and drilling scenarios. Chapter 4 presents foam-assisted mud cap drilling process with gas migration situation for well control. Finally, Chapter 5 discusses the conclusions and the limitations of our work presented in the dissertation and our recommendations.

## CHAPTER 2. LITERATURE REVIEW OF FOAM APPLICATIONS AND PRESENCE OF TWO FLOW REGIMES

### 2.1 Foam Applications in Petroleum Industry

As we know, foam has been widely used in many fields in petroleum industry. This section covers the literature reviews about foam applications in the following aspects: Foam Drilling Field Applications; Foam Drilling Hydraulic Simulations; Foam Applications in Production and Completion Engineering; Foam Applications in Enhanced Oil Recovery for Mobility Control.

#### 2.1.1 Foam Drilling Field Applications

As one kind of untraditional drilling fluid, foam bring many benefits while drilling a well. These benefits are reflected in both operational and economical aspects: improved rate of penetration (ROP) and bit life, reduced non-productive time (NPT) and drilling cost, improved cutting transportation, reduced formation damage, and so on.

In 1994, PETROBRAS (Lage et al., 1996) started to apply foam to drill vertical wells in Carmopolis Field, in both overbalanced and underbalanced conditions. The success of improved productivity inspired them to drill short radius horizontal wells in Candeias Field. Also in 1995, foam drilling applied in the high permeability and low pressure sandstone reservoirs in Parana Basin showed the success of reducing formation damage.

Foam drilling application is not just limited to onshore under pressured formations, offshore drilling with foam can also bring benefits. Two wells in the Santa Barbara Channel were redrilled with preformed stable foam where lost circulation had occurred in past conventional drilling (Hall and Roberts, 1984). Drilling offshore with foam met the offshore lost circulation, well deviation and directional needs.

Sepulveda et al. (2008) reported a recyclable oil-based foam drilling fluid (OBDF) system to drill in deep, high temperature, sour environment located in Deep Gulf Coast. Together with polymer viscosifiers, the nitrified diesel base foam can stay stable up to 450°F (232°C) according to the laboratory results. The drilling results showed effective control of lost circulation, minimal risk of formation damage, excellent hole cleaning, as well as improved bit life and ROP.

### 2.1.2 Foam Drilling Hydraulic Simulations

As one kind of complex fluid, foam makes the determination of the optimum combination of gas and liquid injection rates very difficult in foam drilling and circulations. Modeling of foam rheology is the key issue in hydraulics design in order to predict the bottomhole pressure accurately and to optimize different controllable parameters for effective cutting removal (Ozbayoglu et al., 2000). Ozbayoglu et al. conducted a comparative study to investigate the predictive performance of existing foam hydraulic models such as Beyer et al. (1972), Blauer et al. (1974), Sanghani and Ikoku (1983), Gardiner et al. (1988) and Valko and Economides (1992). A computer program was developed with incorporation of these foam models, and the results were used to compare with their experimental results. The comparison of predicted and measured pressure losses indicated that there is no “best” model that can describe foam flow behavior under all conditions. The difference between the predicted and measured pressure losses can be between 2% to 250%.

Unlike conventional incompressible drilling fluids, it is not possible to calculate the frictional pressure and hydrostatic pressure separately and then to determine the overall pressure drop in foam drilling. The reason is that in drilling with foam, the frictional and hydrostatic pressure influence each other. Numerical methods seem to be the best approach when dealing with compressible fluids such as foam (Paknejad et al., 2007).

Paknejad et al. (2007) developed a foam simulator using a Finite Difference Method (FDM). Besides of foam hydraulics, cutting removal simulation is also incorporated. Heat transfer is also incorporated by solving the energy balance equations in the wellbore. And foam rheology is characterized by the Power-Law model. They also conducted sensitivity analysis of key drilling parameters that would affect the circulating bottomhole pressure (Paknejad et al., 2009). They analyzed the parameters based on two categories: uncontrollable parameters and controllable parameters.

### 2.1.3 Foam Applications in Production and Completion Engineering

Besides the widely usage in drilling engineering, foam also is well known in liquid unloading process, foam fracturing, as well as foamed cementing.

**Liquid unloading.** With the depletion of the reservoir, the reduced gas flow rate, in some sense no longer be effective in transporting the liquid phase to the wellhead and they will accumulate at bottom hole and lead to liquid loading. When a well is loading liquid, it may still produce at a low gas rate, intermittently or it may not produce at all. The accumulation of liquid phase will further reduce the gas flow rate upward in tubing and aggravate liquid loading. The pioneer works by Bernadiner (Bernadiner, M. G., 1991) investigated the application of foaming agent to assist gas lift in depleted reservoirs. Injecting foaming agent into liquid column will form surfactant solution with certain concentration. The formation of foam by injecting gas at certain flow rate would force part of the liquid come out, and the bottom hole pressure would decrease.

Among different methods to control liquid loading and optimize well production and economics (such as gas lift, plunger lift, usage of Coiled Tubing or velocity strings, foaming agents), foaming is attractive: foamers do not need downhole modification, can be easily tested on

existing wells and facilities and are chemically compatible with corrosion inhibitors, so that the same injection points and devices can be used (Farina et al., 2012).

The main reason for the low application of foam for liquid unloading is that foam stability issue due to the existence of liquid hydrocarbons or condensates (Frag et al., 2016). If the liquid phase is only water, foam can have higher strength. If both water and hydrocarbons are present in wellbore, on the other hand, foam is formed mainly within the water phase and the foam assists in carrying along the liquid hydrocarbons. Foams created in hydrocarbons is not stable and will soon separate.

**Foam fracturing.** As one unusual kind of fracturing fluid, foam's success in use should be attributed to the following two rheological properties among many: first is its very low fluid leak-off coefficient; second is its excellent sand-carrying capability (Bullen and Bratrud, 1976). Because of that, foam shows many advantages in fracturing over conventional fracturing fluids.

In many Russian oilfields such as Volga-Urals and Western Siberian Basin (Oussoltsev et al., 2008), because of reservoir pressure depletion, the filtration leak-off of stimulation fluids had impacted the reservoir productivity. It also affected the possibility of flow the well back after stimulation treatments. Using foam system in particular to viscoelastic based foam can provide a better fluid-loss control, efficient post-treatment flowback, as well as the reduced consumption of liquid pumped overall.

McAndrew et al. (2017) conducted experiments to measure the transport of proppant by foams under high pressure (2000 psi (13789520 Pa)-3000 psi (20684280 Pa)) and also developed computational fluid dynamics (CFD) model. Their results showed that proppants can be transported by foam further than water due to foam's high suspension capability.



When fracturing unconventional shales, high foam deterioration and insufficient viscosity have been the major concerns with foam. Ahmed et al. (2019) conducted laboratory study to investigate the stability and foam properties of foam with different additives. Their results showed that at HTHP condition, polymer-free CO<sub>2</sub> foam can produce higher stability and relatively equally high viscosity compared to polymer-added CO<sub>2</sub> foam due to the fact that the added polymer had been degraded at HTHP condition.

Recently, a new hydraulic fracturing process incorporating a system of ultra-high quality foam and ultra-lightweight proppant has been successfully employed for multi-zone fracking stimulation of horizontal shale gas wells (Brannon et al., 2009). And both vertical and horizontal wells had been treated with this process in Big Sandy, located in the eastern USA. The cumulative production after the first 30 days were observed to be 200% greater than the offset wells.

**Foam cementing.** Unlike neat foam, foamed cement, or nitrified cement is formed when injecting gas, usually nitrogen, into base slurry at high pressure. Foamed cements are used extensively in lost circulation zones, depleted zones, or low formation fracture gradients are encountered and a low-density cement system is required.

Experiments were conducted to test the effect of foam structure on fluid loss property (Rozieres and Ferriere, 1991). The results show that an increase in gas volume decreased the fluid loss. Therefore, compared with conventional cement system, foamed cement is more suitable with severe cement loss conditions. More recently, foamed cement was applied to resolve the lost circulation problem by plugging the thief zone (Moore et al., 2005; Fomenkov et al, 2018).

The lower-density property of foamed cement leads to lower hydrostatic pressure. The (Equivalent Circulating Density) ECDs along the annulus can be carefully designed to avoid

exceeding the fracture pressure at weak zone. This is extremely significant in low fracture gradient formation otherwise severe losses might be encountered (Joao et al., 2017).

Besides onshore application, foamed cement use has expanded into regions with shallow water flows (SWF), for example, in deep water operations and isolating fragile formations (Doherty, 2007; Jacobs, 2015). Foamed cements can be designed to have variable hydrostatic gradients to satisfy density requirements in annulus; compared to conventional cements, it also has fast setting time according to laboratory studies (Dusterhoft, 2003), which is a very significant aspect when cementing unconsolidated SWF zone in deep water operation.

#### 2.1.4 Foam Applications in Enhanced Oil Recovery for Mobility Control

CO<sub>2</sub> enhanced oil recovery (CO<sub>2</sub> EOR) has been commercially implemented in the United States since early 1970s. However, the major challenge in implementing CO<sub>2</sub> EOR in the field has been mobility control of CO<sub>2</sub>. Due to the low density of CO<sub>2</sub>, gravity segregation can easily occurs, and as result, the volumetric sweep efficiency is low, so as well as the recovery factor. CO<sub>2</sub> foam EOR technology on the other hand, can offer a robust method for CO<sub>2</sub> mobility control (Heller, 1994). Foaming the gas phase for improved sweep efficiency has been proved in the laboratory and field for more than 50 years. Lee et al. (2016) investigated how the dimensionality change from laboratory-measured data to field-scale treatments can affect foam rheological properties. Izadi and Kam recently investigated the EOR modeling work (Izadi and Kam, 2019) and the optimization of injection strategies (Izadi and Kam, 2020) related with supercritical CO<sub>2</sub> foam.

Many successful field pilot tests have been reported such as CO<sub>2</sub>-foam field test conducted in Salt Creek, WY (Mukherjee et al., 2016) and SAG treatment for conformance control in Lower Mirador formation, Cusiana Field, Columbia (Ocampo et al. 2013; Rossen et al. 2017). Ortiz et al.

(2019) conducted modeling work with nanoparticle-stabilized supercritical CO<sub>2</sub> foam using some reservoir conditions from Lisama Field.

## 2.1 Presence of Two Flow Regimes

The essence of our new foam model development and foam applications in this study is based on the two flow regimes concept. The concept of two flow regimes indicates that pressure loss in foam flow or foam viscosity changes differently with foam quality when foam quality reaches the critical foam quality. Therefore, foam can be categorized as low-quality regime and high-quality regime foams separated by the critical foam quality value.

The concept of two flow regimes on foam is not solely found in a certain experimental study but can be found in many existing foam models and previous experimental studies. Gajbhiye (2011) investigated three existing foam models and three foam experimental studies: Beyer et al. (1972), Sanghani and Ikoku (1983), and Reidenbach et al. (1986); Sanghani and Ikoku (1983), Briceno and Joseph (2003), and Guzman et al. (2005). He plotted the outcomes of these studies in the form of pressure contours or foam viscosity contours as a function of injection velocities in order to evaluate the presence of two flow regimes.

In Beyer et al.'s model (1972), the slip velocity is correlated with liquid volume fraction and wall shear stress, the equations are shown below:

$$\mu_o = \frac{1}{(7200LVF+267)}, \text{ for liquid volume fraction from 0.02 to 0.1,} \quad (2.1)$$

$$\text{and } \mu_o = \frac{1}{(2533LVF+733)}, \text{ for liquid volume fraction from 0.1 to 0.2,} \quad (2.2)$$

where  $\mu_o$  is the Bingham plastic viscosity, and LVF presents liquid volume fraction of the foam.

Figure 2.1 shows the plots of foam viscosity based on Equation (2.1) and Equation (2.2) (Figure 2.1(a) and viscosity contour (Figure 2.1(b)). The contour map seems to show low-quality regime with finite slopes, and did not reflect the two flow regimes concept.

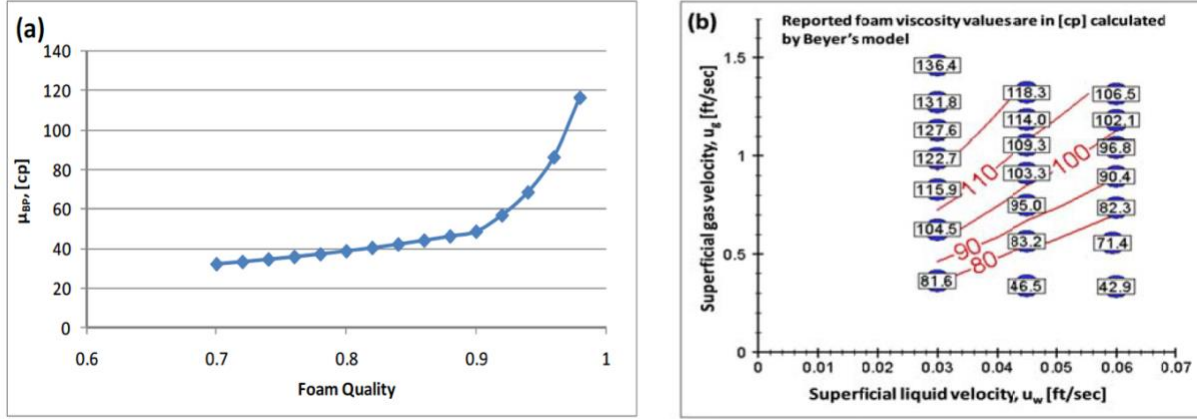


Figure 2. 1 Beyer et al.'s model: (a) foam viscosity vs. foam quality and (b) viscosity contours

In Sanghani and Ikoku's model (1983), the effective foam viscosity is correlated with the power law model parameters  $K$  and  $n$  as below:

$$\mu_e = K \left( \frac{2n+1}{3n} \right)^n \left( \frac{12v_f}{D_H} \right)^{n-1} \quad (2.3)$$

$$K = -0.15626 + 56.147\Gamma - 312.77\Gamma^2 + 576.65\Gamma^3 + 63.96\Gamma^4 - 960.46\Gamma^5 - 154.68\Gamma^6 + 1670.2\Gamma^7 - 937.88\Gamma^8 \quad (2.4)$$

$$n = 0.095932 + 2.365\Gamma - 10.467\Gamma^2 + 12.955\Gamma^3 + 14.467\Gamma^4 - 39.673\Gamma^5 + 20.625\Gamma^6 \quad (2.5)$$

where  $v_f$  is foam velocity,  $D_H$  is hydraulic diameter, and  $\Gamma$  is foam quality.

Figure 2.2 shows the plots of foam viscosity based on Equation (2.3) through Equation (2.5) (Figure 2.2(a) and viscosity contour (Figure 2.2(b)). This model implies the presence of two flow regimes.

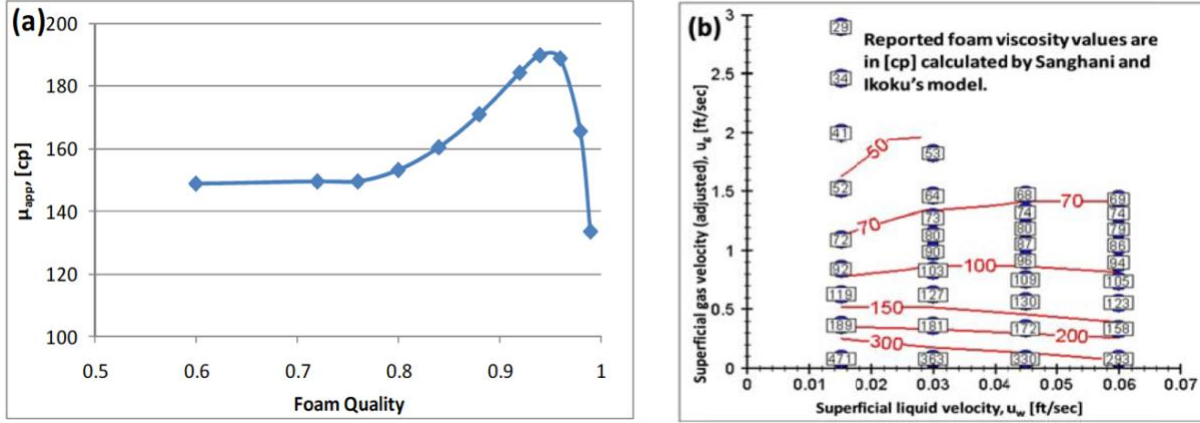


Figure 2. 2 Sanghani and Ikoku's model: (a) foam viscosity vs. foam quality (b) viscosity contours

In Reidenbach et al.'s model (1986), two separate equations were developed for foam quality less than 60% and more than 60%, respectively. The apparent yield point ( $\tau_{yp}$ ), consistency index (K), and behavior index (n) were computed with least-square regression for a fixed foam quality. The apparent viscosity ( $\mu_a$ ) is given by the following equations:

$$\mu_a = \tau_{yp} \left( \frac{8v}{d} \right)^{-1} + K \left( \frac{8v}{d} \right)^{n-1} \quad (2.6)$$

$$\text{where } \tau_{yp} = C_1 \Gamma \text{ for } \Gamma < 0.6 \text{ and } \tau_{yp} = C_2 e^{C_3 \Gamma} \text{ for } \Gamma > 0.6, \quad (2.7)$$

$$\text{and } K = K_{liquid} \times e^{(C_1 \Gamma + C_2 \Gamma^2)} \quad (2.8)$$

where  $\Gamma$  is foam quality, d is internal diameter of pipe, v is bulk velocity and  $K_{liquid}$  is consistency index for liquid phase. The constants  $C_1$ ,  $C_2$  and  $C_3$  depend on surfactant concentration, foam texture, and physical properties of mixture and conduit.

Figure 2.3 shows the plots of foam viscosity based on Equation (2.6) through Equation (2.8) (Figure 2.3(a) and viscosity contour (Figure 2.3(b)). This model also implies the presence of two flow regimes. The curves of pressure contours are connected from upper left to lower right, it seems like the transition region between high-quality regime and low-quality regime.

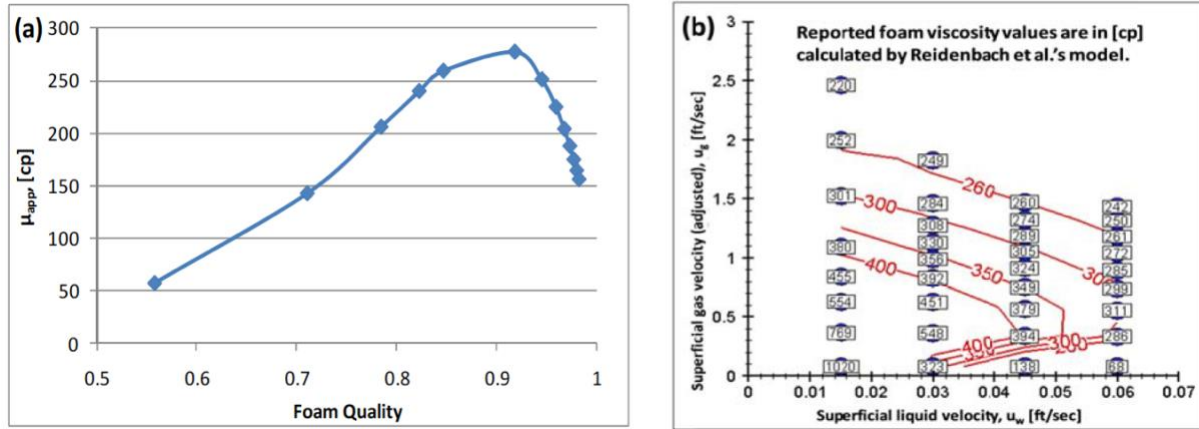


Figure 2. 3 Reidenbach et al.'s model: (a) foam viscosity vs. foam quality (b) viscosity contours

Gajbhiye (2011) also used Sanghani and Ikoku's experimental data to plot in the way of pressure contours. Figure 2.4 shows their raw pressure data together with the general trend of pressure contours. It indicates that the contours show finite slopes similar to the high-quality regime.

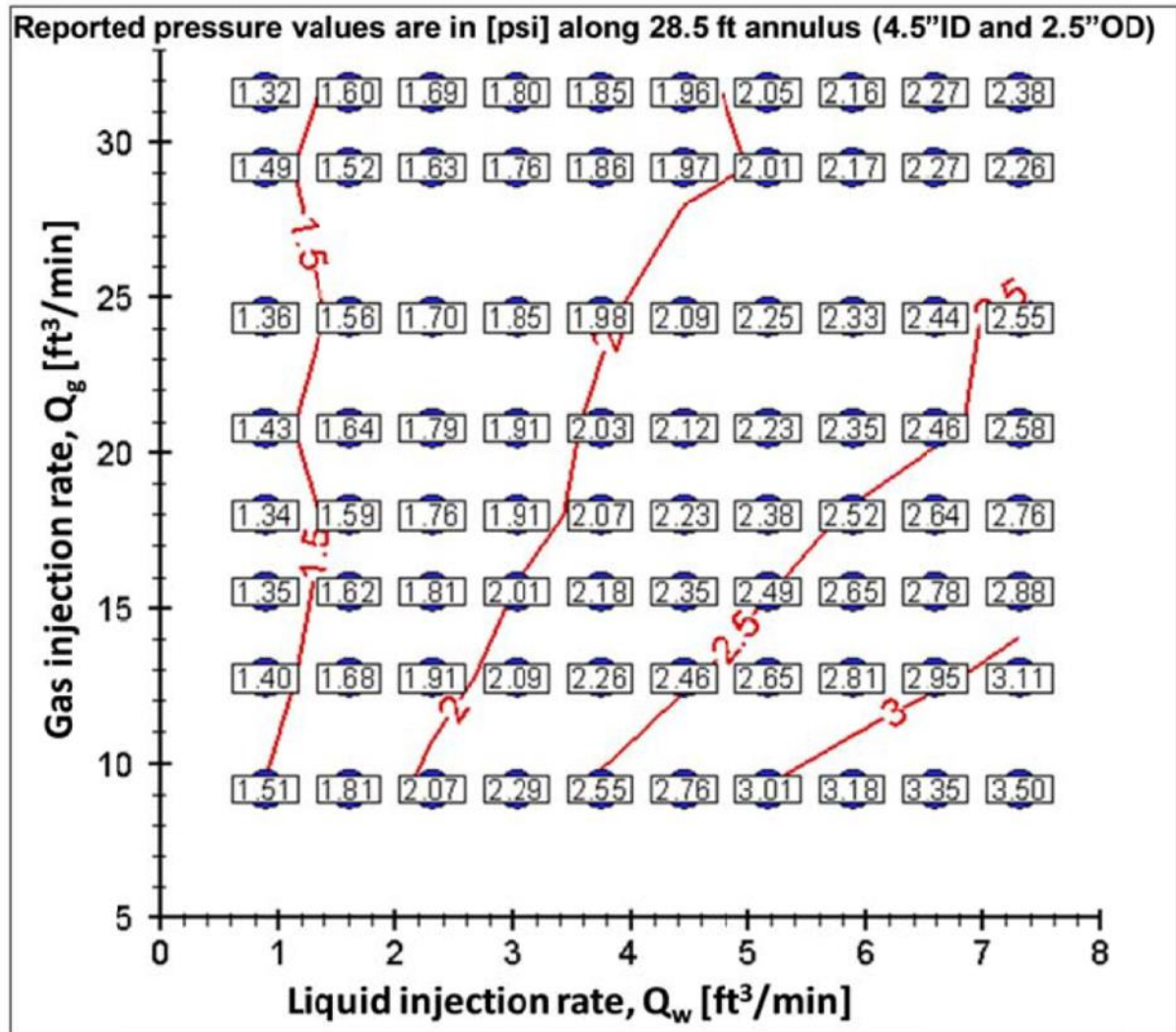


Figure 2. 4 Pressure contour map developed using Sanghani and Ikoku data

Figure 2.5 shows the pressure contour map with Briceno and Joseph's experimental data (2003). The pressure contours are almost horizontal similar to the behavior of the low-quality regime.

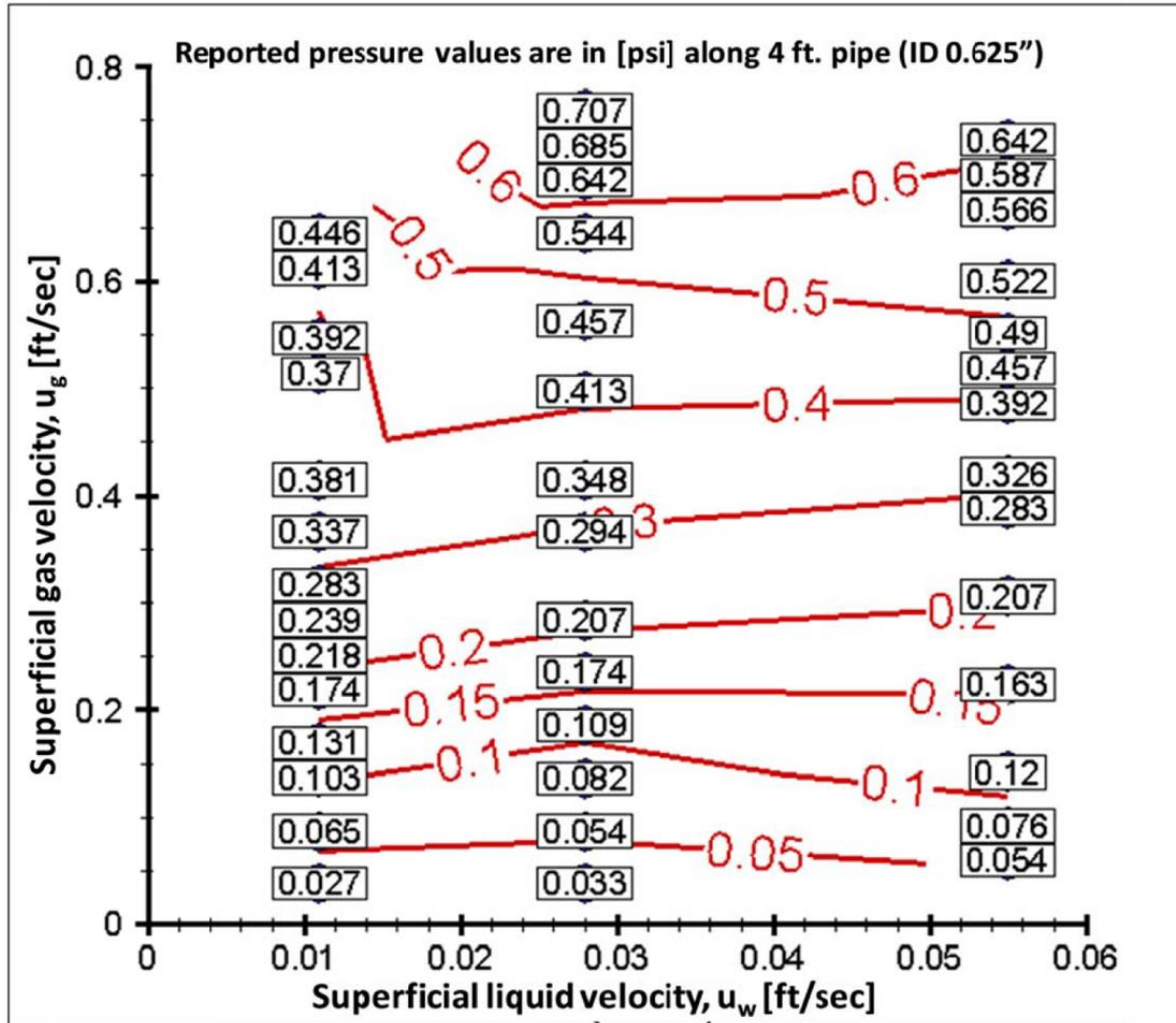


Figure 2. 5 Pressure contour map developed using Briceno and Joseph data

Lastly, Guzman et al.'s experimental data (2005) was used to plot as pressure contour map as shown in Figure 2.6. This set of experimental data also do not explicitly reflect the two flow regimes. Similar to Reidenbach et al.'s model (1986), the curves of pressure contours are also connected from upper left to lower right, it indicates that there might be a transition region between high-quality regime and low-quality regime.



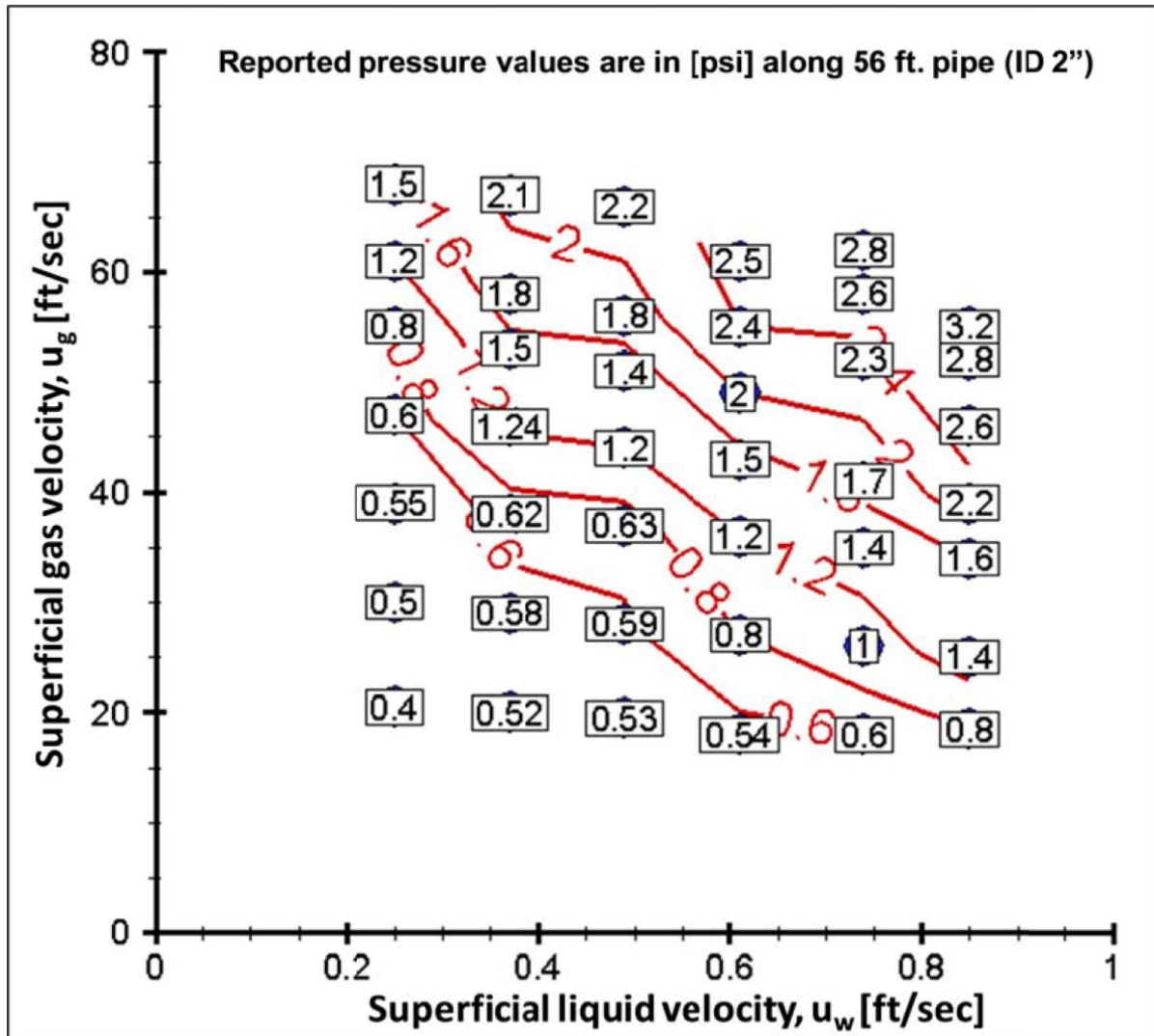


Figure 2. 6 Pressure contour map developed using Guzman et al.'s data

From these six studies of foam models or foam experiments, we can notice that many existing foam models can somehow explicitly or implicitly reflect the presence of two flow regimes. However, due to different experimental conditions, or gas and liquid injection rates, the limited experimental data we showed previously might not show the typical pressure contour map of two flow regimes for foam flow.

The following parts introduced previous foam experimental studies conducted from our research group at Louisiana State University. Data were plotted in the manner of contour map to show the presence of two flow regimes.

Gajbhiye and Kam (2012) also tested the effect of inclination angle on the presence of two flow regimes. Figure 2.7 showed the contour maps of pressure and calculated apparent viscosity for downward flow with inclination angle  $0^\circ$  (horizontal) and  $90^\circ$  (vertical), respectively. We can clearly see both pressure drop contours and viscosity contours showed two flow regimes, which are separated by the critical foam quality curve. Moreover, there is a wide transition in between.

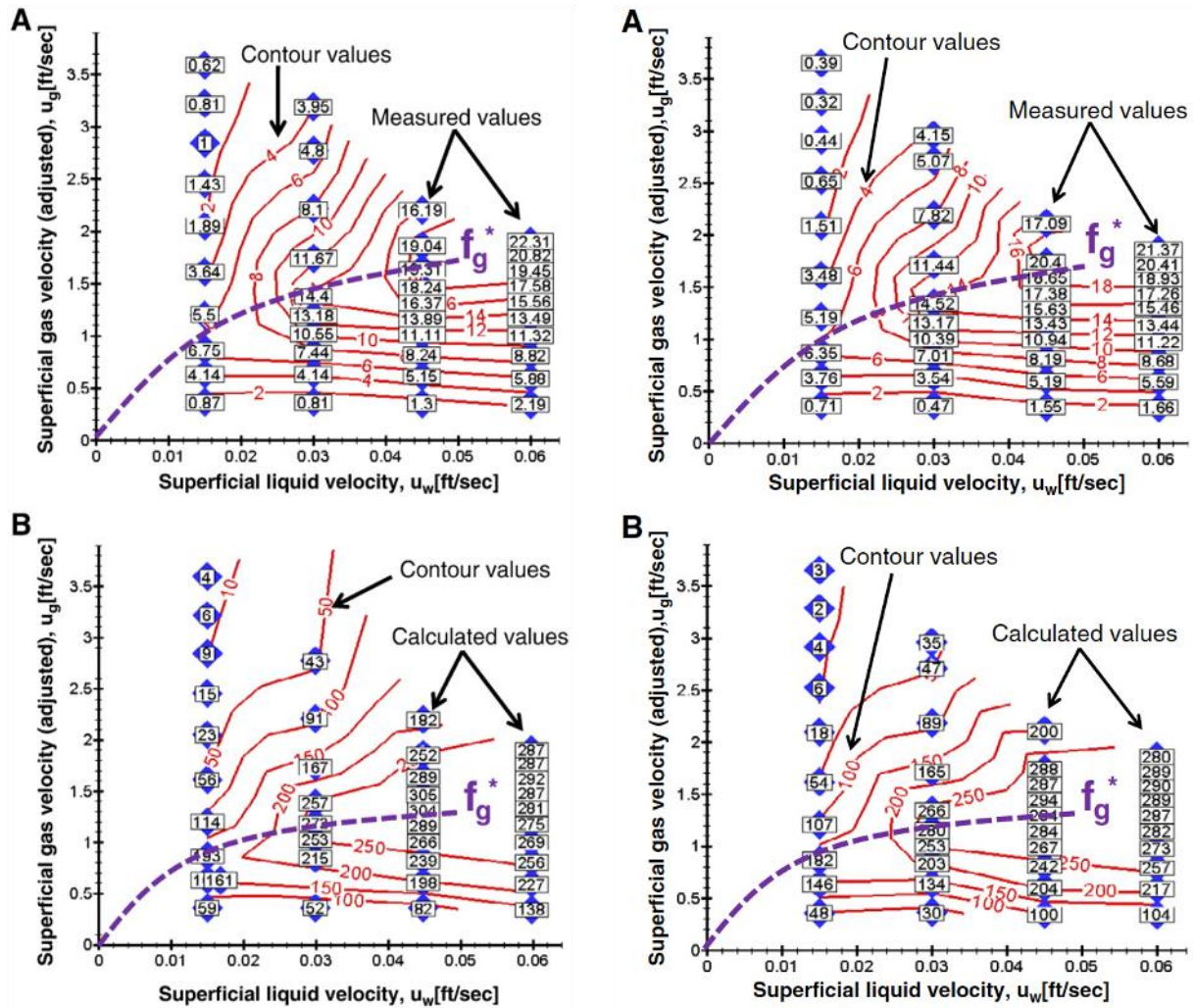


Figure 2. 7 Contour maps for inclination angle  $0^\circ$  (left) and  $90^\circ$  (right) downward flow: pressure drop (A); apparent viscosity (B)

Later, Edrisi et al. (2014) investigated the sensitivity of two flow regimes with additives such as polymer and oil. Figure 2.8 through Figure 2.10 presented the pressure drop contour maps showing the measured pressure drops as function of gas and liquid injection velocities. We can see when polymer or oil were added with surfactant solution, the presence of two flow regimes seemed not to disappear. It is worth to mention that in the case with polymer, the contour map showed chaotic transition region that is unlike other cases.

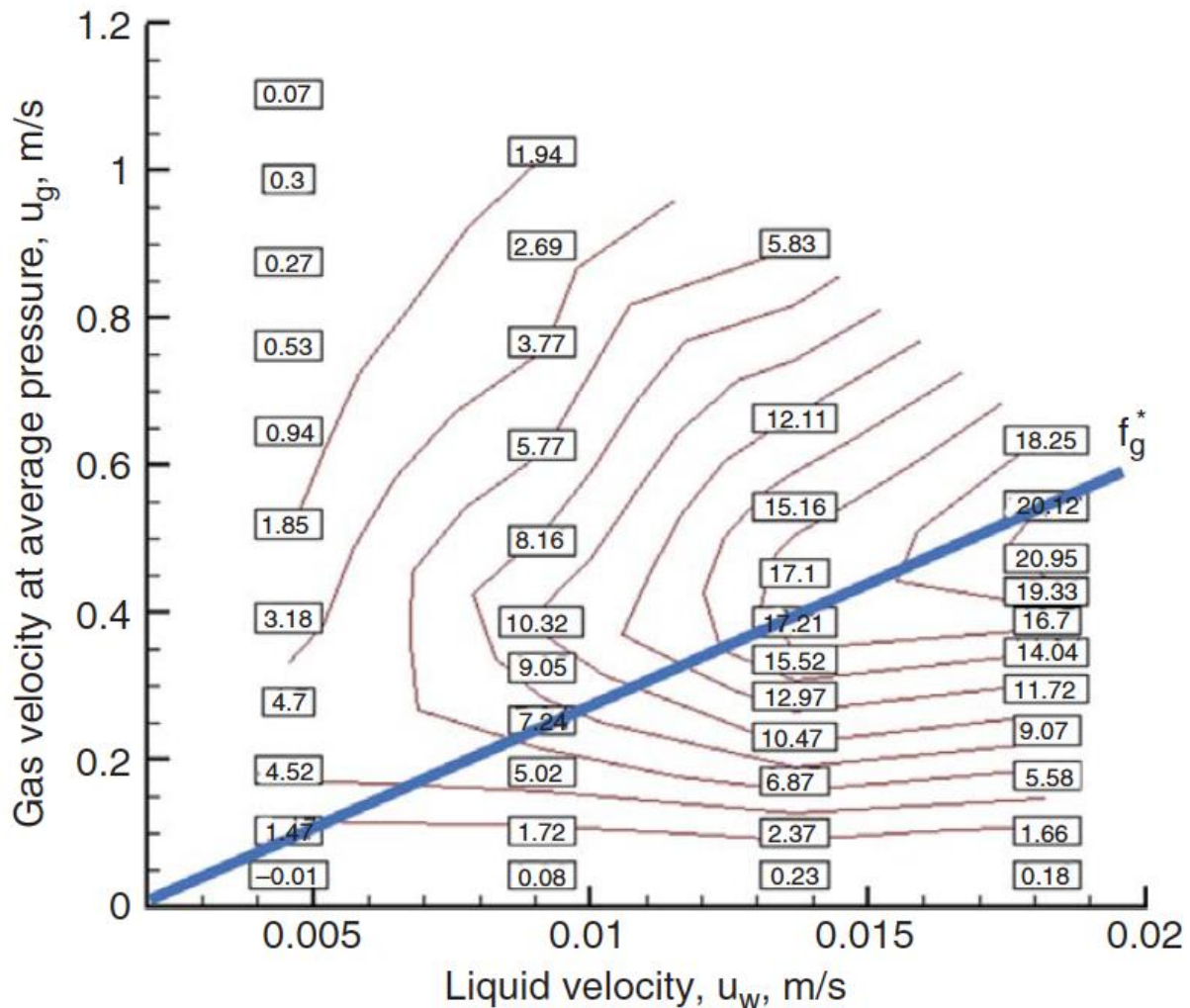


Figure 2. 8 Pressure drop contour map for surfactant foams

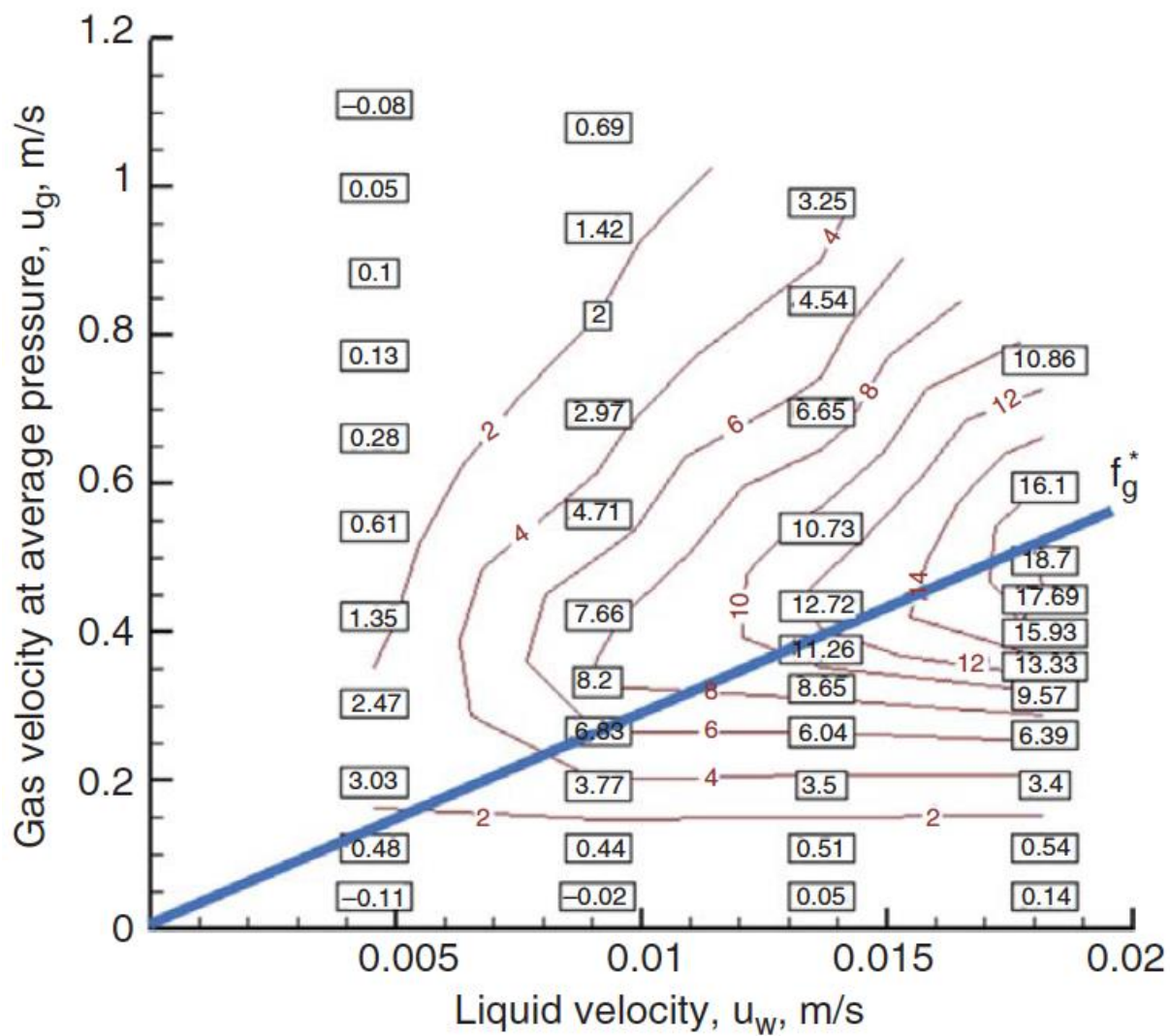


Figure 2. 9 Pressure drop contour map for surfactant foams in the presence of oil



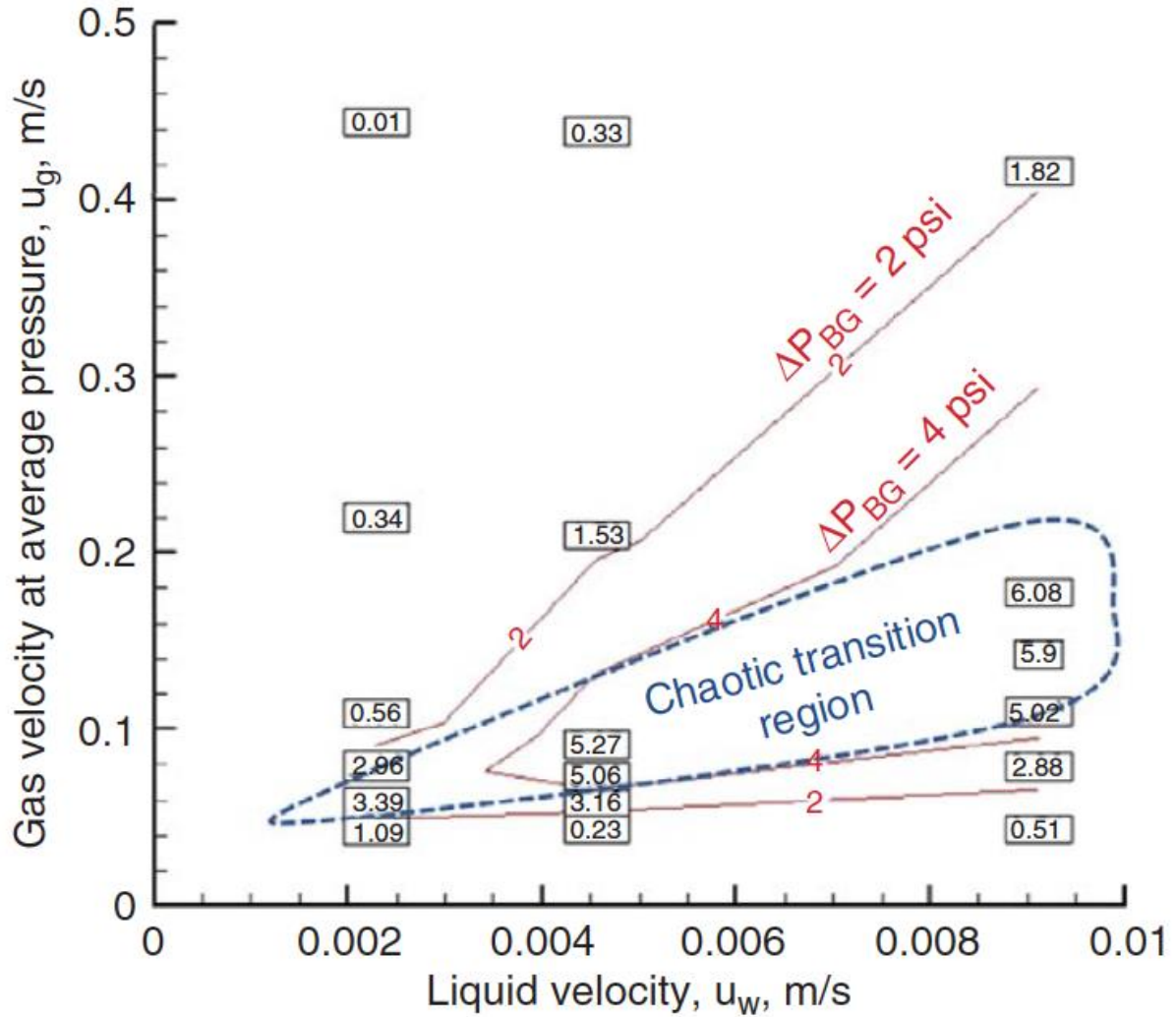


Figure 2. 10 Pressure drop contour map for polymer-added surfactant foams

Throughout the whole literature review from foam applications to foam models showing two flow regimes concept, we have confidence that developing a more robust foam model at the base of two flow regimes concept is very valuable. More importantly, implementations of the developed foam model to improve the understanding of foam behaviors in wellbore is also demanding. This way will get us closer to the success of field applications with foam.

## CHAPTER 3. A NEW MODEL FOR FOAM FLOW IN PIPES AND ANNULI

### 3.1 Introduction

Foam flow in pipe has been regarded as a challenging topic because of its complex structures and stability issues (Deshpande and Barigou, 2000; Briceno and Joseph, 2003; Wang et al., 2016). Although foam has been widely used in numerous applications such as improved and enhanced oil recovery (I/EOR), drilling, cementing, liquid and solid removal, fracturing and so on, there is still much room to improve the modeling, simulation, and analysis of relevant applications.

#### 3.1.1 Foam Rheology Fundamentals

A good number of experimental studies show that foam can be modeled as a Power-Law fluid reasonably well, if the rheology at low shear rates is not of interest. For example, Sanghani and Ikoku (1983) conducted foam flow experiments in the annulus with drill pipe (OD 1.5 inch (0.0381 m) and casing (ID 4.5 inch (0.1143 m)), both about 28.5 ft (8.6868 m) long. The range of foam quality tested was from 0.65 to 0.95, and the shear rates ranged from 150 to 1000  $\text{sec}^{-1}$ . The calculated foam effective viscosity was in the range of 60 cp (0.06 Pa.s) to 500 cp (0.5 Pa.s). They formulated empirical equations for the effective foam viscosity as a function of foam quality by using a Power-Law model with parameters  $K$  and  $n$ . Foam flow characteristics also strongly depend on pipe diameter and the interaction between the pipe wall and flowing foam mixture. By conducting experiments in small pipes and capillary tubes, Mooney (1931) found that the presence of a wall significantly influences the flow behavior and, as a result, such a wall effect should not be neglected. Furthermore, they observed that a thin liquid layer forming at the pipe wall acts as a lubricant such that a relatively uniform foam core can slide on the liquid layer at the wall. This results in a lower-than-expected shear stress at a given shear rate, which, in turn, yields a lower than expected foam viscosity, due to wall slippage. Deshpande and Barigou (2000) showed that

the wall slip effect is more pronounced in small-diameter pipes/capillaries, where bubble size is comparable to the conduit diameter, and diminishes with pipe diameter. Sherif et al. (2015) performed experiments in three 4-m parallel transparent pipe sections to investigate oil-based foam rheology with varying foam quality from 34%-68%. The base liquid was prepared by mixing mineral oil with diesel. Their results confirmed that the lubricating effect observed in aqueous foams was found to be consistent with oil-based foams.

### 3.1.2 Recent Approach with Two Flow Regimes

Recent experiments by Bogdanovic et al. (2009) were conducted with two different pipe sizes (0.36 inch (0.0091 m) and 0.957 inch (0.0243 m) inner diameters, and lengths of about 12 ft (3.6576 m)) with nitrogen and various surfactants commonly used in drilling and completion. The pressure measurements along the pipe showed two different foam flow behaviors at fixed liquid velocity – a low-quality regime in which the pressure drop increases with increasing gas velocity, and a high-quality regime in which the pressure drop decreases with increasing gas velocity. Figure 3.1 shows similar experimental results obtained by Edrisi and Kam (2013), where the threshold value of foam quality necessary to separate the two flow regimes was defined as  $f_g^*$ .

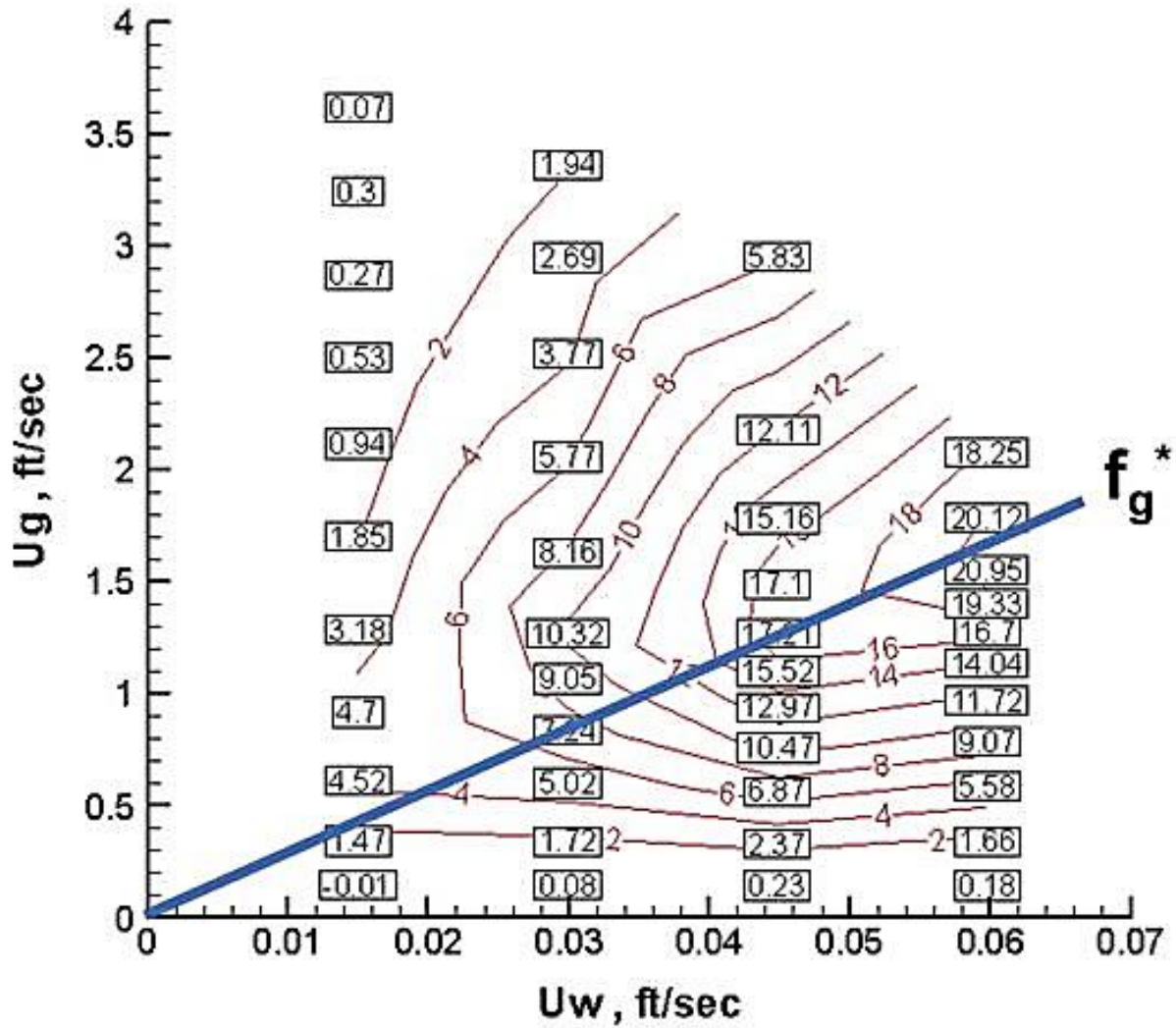


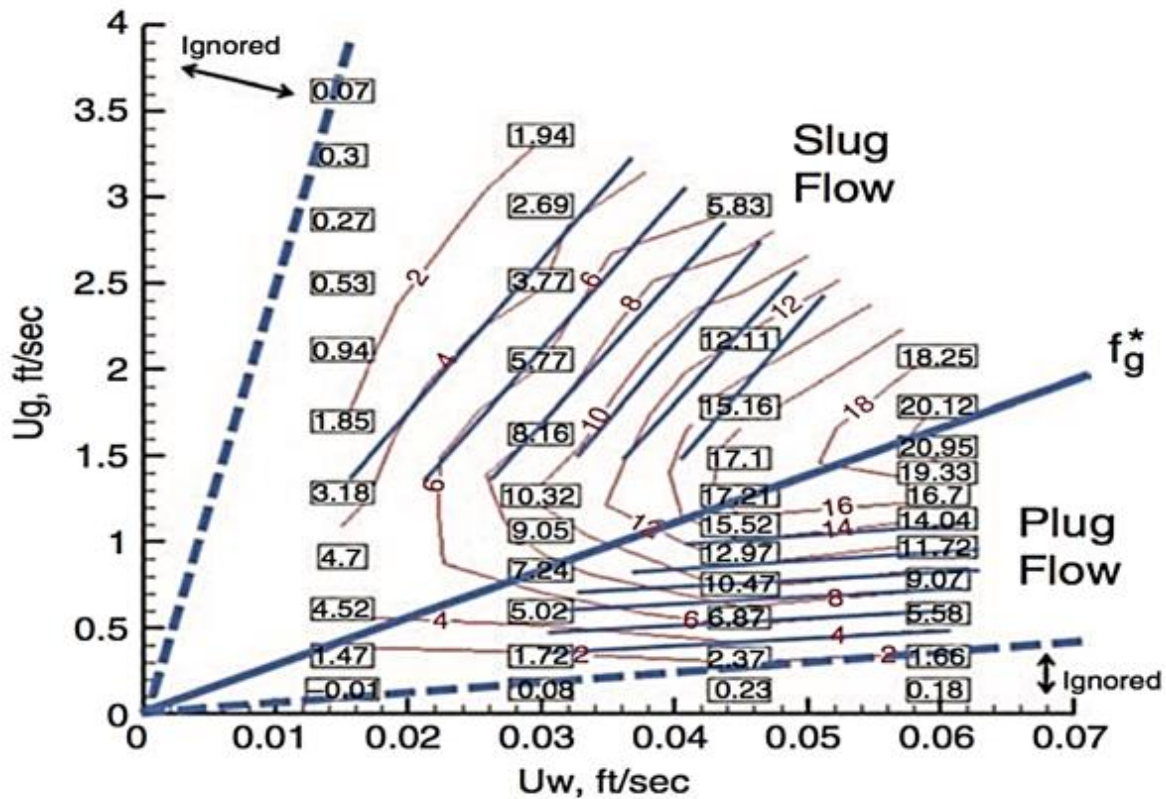
Figure 3. 1 Experimental data from surfactant foam flow

Gajbhiye and Kam (2011, 2012) further extended the experiments with visual cells in horizontal and inclined directions (i.e.,  $0^\circ$ ,  $45^\circ$ , and  $90^\circ$ , both upward and downward). In addition to the size of bubbles in flowing foams, they visualized that the high-quality regime would show a slug flow pattern (i.e., repetition of free gas and fine-textured foams), and the low-quality regime shows plug flow pattern with homogeneous foam mixtures.

Edrisi et al. (2014) conducted similar experiments to investigate the effects of oil and polymers. Although foam stability in the presence of oil and polymers added more complexity to the analysis,



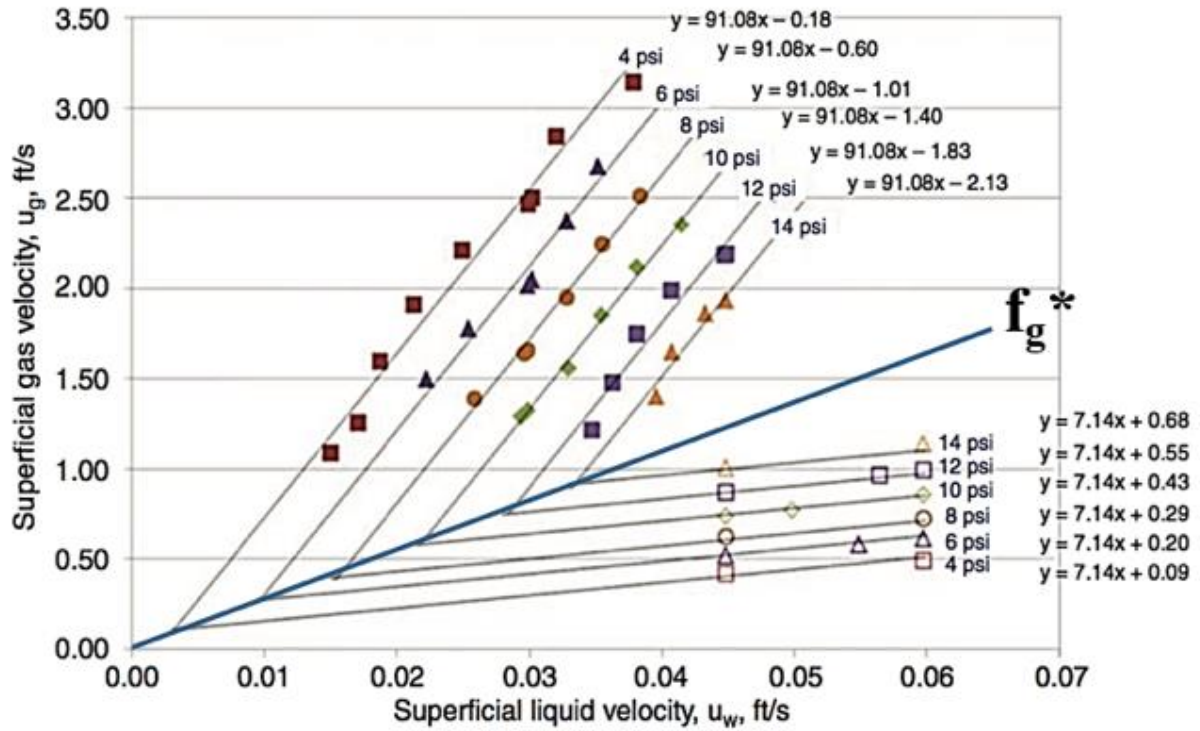
the presence of two distinct flow regimes was consistently confirmed. The threshold value of foam quality,  $f_g^*$ , was shown to go down by adding oils, due to lower foam stability, and go up in the presence of polymers, due to higher water density and improved foam stability. Following those experimental studies that showed two distinct flow regimes, Edrisi and Kam (2013) proposed a foam rheological model to capture the trend in the high-quality and low-quality regimes, as shown in Figure 3. 2 (a) and Figure 3. 2 (b).



(a) Pressure Contours on the Original Data

Figure 3. 2 Model fit to experimental data proposed by Edrisi and Kam (2013)

(fig. cont'd.)



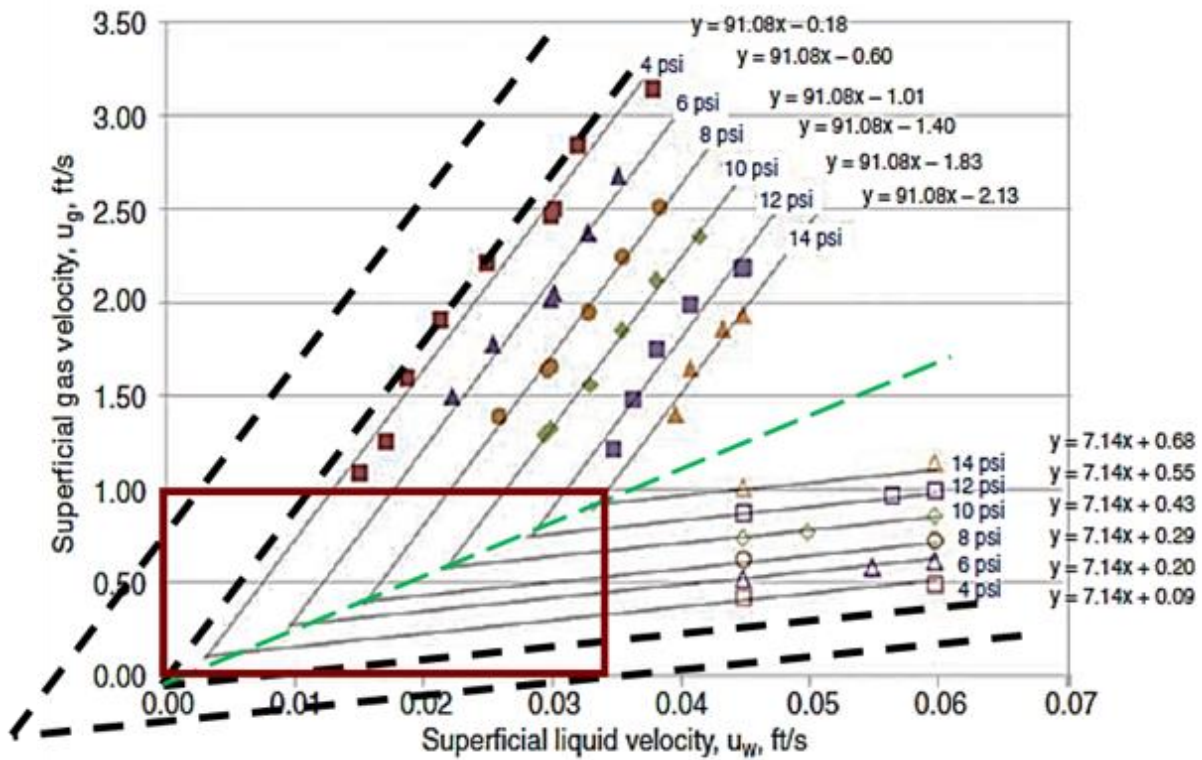
(b) Pressure Contour Map Reconstructed by the Model

As a first step, the model employed the Power-Law model along the  $f_g^*$  line that required the consistency index,  $K$ , and Power-Law exponent,  $n$ , which can be determined based on the gap between pressure contours. The two representative slopes of the pressure contours in both regimes then defined how sensitive the pressure drop was to the liquid and gas velocities. These two families of parallel lines intersected at the  $f_g^*$  line and, as a result the pressure contour map was approximated.

### 3.2 Motivation and Objectives

Although the previous modeling effort (Edrisi and Kam, 2013) captured the trend of pressure contours in both regimes, it left some significant shortcomings, as shown in Figure 3.3 (a): (i) by defining foam rheology along the  $f_g^*$  line, the model has essentially one type of foam rheology that is shared by both high-quality and low-quality regimes; (ii) for those pressure contours with

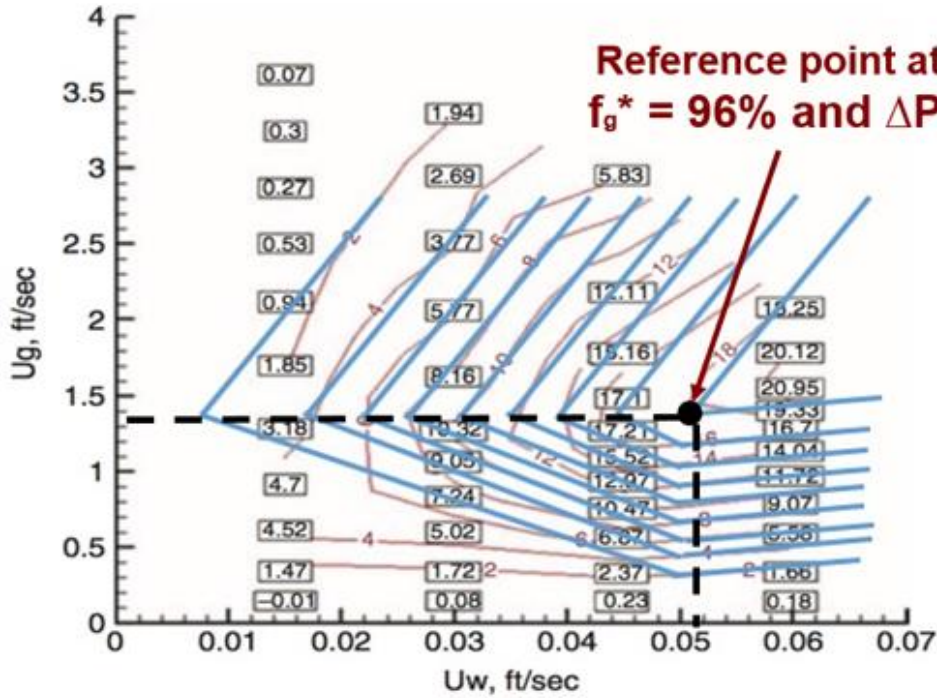
relatively low values of pressure drops (for example, 2 psi (13790 Pa)), the model may crash with negative velocity values near the  $f_g^*$  line; and (iii) the modeled pressure contours did not mimic the smooth transition between the two regimes, which is typically shown in the lab data.



(a) Shortcomings of the Previous Work

Figure 3. 3 Schematic figures comparing previous model and this new model

(fig. cont'd.)



(b) Improved Model Introduced in This Study

The objective of this study was to develop a new foam model by improving the previous foam model of Edrisi and Kam (2013) such that: (i) the model would have the ability to exhibit two different types of foam rheology independently in both regimes, and (ii) the model could handle a wide range of pressure and velocity conditions. The schematic of Figure 3. 3 (b) shows how these goals were achieved by introducing a reference point ( $u_{wRef}$ ,  $u_{gRef}$ ) in the pressure contour plot such that: (i) two types of foam rheology were defined separately along each of the lines ( $u_{wRef} = 0$  and  $u_{gRef} = 0$ ), and (ii) the smooth transition was made by interpolation to connect the contours of the two flow regimes.

After showing the procedure for model fit, the authors also present how to extract other valuable properties during foam flow, such as foam viscosity, liquid layer thickness at the wall, and friction factor to determine the frictional pressure loss during foam flow. As a final step, the robustness of this model is demonstrated from an example of a foam-assisted drilling process.

### 3.3 Methodology

#### 3.3.1 Fundamentals of Foam Flow in Pipes

For a two-phase flow of water and gas (including foam), the total pressure drop ( $\Delta P_t$ ) consists of three major components, as given in Equation (3.1).

$$\Delta P_t = \Delta P_h + \Delta P_a + \Delta P_f \quad (3.1)$$

where,  $\Delta P_t$  is the total pressure loss;  $\Delta P_h$  is the hydrostatic pressure loss;  $\Delta P_a$  is the pressure loss due to acceleration;  $\Delta P_f$  is the frictional pressure loss.

The pressure drop due to acceleration is often neglected unless the cross-sectional area changes dramatically or the fluid is reactive. The hydrostatic pressure loss  $\Delta P_h$  [psi] is expressed as Equation (3.2).

$$\Delta P_h = 0.052 \rho_m \quad (3.2)$$

where,  $\rho_m$  is the density of mixture (i.e., foams) [ppg].

The mixture density is commonly calculated as shown in Equation (3.3) and Equation (3.4).

$$\rho_m = \rho_g \left( \frac{Q_g}{Q_t} \right) + \rho_L \left( \frac{Q_L}{Q_t} \right) = \rho_g (f_g) + \rho_L (f_L) \quad (3.3)$$

$$Q_t = Q_g + Q_L \quad (3.4)$$

where,  $\rho_g$ ,  $\rho_L$  are gas and liquid densities [ppg];  $f_g$ ,  $f_L$  are gas and liquid flowing fractions;  $Q_t$  is the total flow rate [gpm]; and  $Q_g$  and  $Q_L$  represent gas and liquid flow rates [gpm].

Unlike the liquid density, the density of highly compressible gas phase is a strong function of pressure and temperature, as shown in Equation (3.5).

$$\rho_g = \frac{PM}{ZRT} \quad (3.5)$$

where, P and T are pressure [psia] and temperature [R]; M is the molecular weight [g/mol]; R is

the universal gas constant [J/mol.K]; and Z is the compressibility factor. The compressibility factor, Z is also a function of pressure, temperature and composition.

The expression for the frictional pressure loss ( $\Delta P_f$ ) depends on flow rheology (Bourgoyne et al., 1986). For Newtonian fluid in two-phase flow, Equation (3.6) is used if it is laminar flow, and Equation (3.7) if it is turbulent flow.

$$\Delta P_f = \frac{\mu_m v_m}{1,500 d^2} \quad (3.6)$$

$$\Delta P_f = \frac{f \rho_m v_m^2}{25.8 d} \quad (3.7)$$

where,  $\rho_m$  and  $\mu_m$  are mixture density [ppg] and viscosity [cp]; d is pipe internal diameter [inch];  $v_m$  is the mean flow velocity [ft/s]; and f is dimensionless Fanning friction factor. Note that for laminar flow, the Fanning friction factor is given in Equation (3.8).

$$f = \frac{16}{\text{Re}} \quad (3.8)$$

for turbulent flow (smooth pipe), the empirical Equation (3.9) and Equation (3.10) can be used.

$$f = \frac{0.0791}{\text{Re}^{0.25}} \quad (3.9)$$

$$\text{Re} = \frac{928 \rho_m v_m d}{\mu_m} \quad (3.10)$$

where, Re is the dimensionless Reynolds number. Note that the mixture viscosity  $\mu_m$  [cp] can be replaced by apparent foam viscosity  $\mu_{app}$  [cp] for non-Newtonian fluid, as shown in Equation (3.11).

$$\mu_{app} = 47900 \frac{\tau_w}{\dot{\gamma}_w} \quad (3.11)$$

where,  $\tau_w$  is the wall shear stress [lbf/ft<sup>2</sup>]; and  $\dot{\gamma}_w$  is wall shear rate [s<sup>-1</sup>].

By using the hold-up of each of the phases ( $H_g$  and  $H_L$  for gas and liquid hold-up, respectively),

the mean fluid velocity ( $v_m$  [ft/s]) for flow in pipe, which is no other than total superficial velocity ( $u_t$  [ft/s]), is expressed by Equation (3.12).

$$v_m = u_t = u_w + u_g = \frac{Q_t}{2.448d^2} \quad (3.12)$$

where,  $u_g$  and  $u_w$  are superficial gas and liquid velocities [ft/s];  $u_t$  is the total superficial velocity [ft/s]. Note that the wall shear stress ( $\tau_w$  [lbf/ft<sup>2</sup>]) and wall shear rate ( $\dot{\gamma}_w$  [s<sup>-1</sup>]) on the conduit walls can be expressed by Equation (3.13) and Equation (3.14), respectively.

$$\tau_w = 3d \frac{\Delta P_t}{L} \quad (3.13)$$

$$\dot{\gamma}_w = \frac{96u_t}{d} \quad (3.14)$$

where,  $L$  is the conduit length [ft].

The flow can be modelled by the Power-Law model, which is the case with this study, the equations above can be written as follows in Equations (3.15 – 3.17). (all units are the same as defined above):

$$\tau_w = K\dot{\gamma}_w^n \quad (3.15)$$

$$\mu_{app} = K\dot{\gamma}_w^{n-1} \quad (3.16)$$

$$\Delta P_f = \frac{Kv_m^n}{144000d^{1+n}} \left( \frac{3+1/n}{0.0416} \right)^n \quad (3.17)$$

where,  $K$  is the consistency index and  $n$  is the Power-Law exponent. Note that both  $K$  and  $n$  should be identified from experimental data.

For fine-textured foam flowing in pipe, it can be approximated by plug flow, that is, a foam core located at the center of pipe sliding on a lubricating thin liquid layer at the wall. Briceno and Joseph (2003) suggested a simplified method to analyze the system as shown in Equation (3.18) in SI units: from force balance,

$$\Delta PA = \tau_{wL} LS \quad (3.18)$$

where,  $\Delta P$  is the pressure loss term;  $\tau_{wL}$  is the shear stress within the liquid film;  $A$  is the cross-sectional area of the pipe;  $L$  is the length of the pipe (or, segment of interest), and  $S$  is the perimeter of cylindrical foam core (that is concentric to the pipe). Therefore,  $LS$  represents the surface area of foam core over the length of  $L$ .

If the thickness of liquid layer at the wall ( $\delta_L$ ) is very thin, then the velocity gradient ( $dv/dy$ ) (or, shear rate ( $\dot{\gamma}$ ) equivalently) can be approximated by Newtonian flow, given in Equation (3.19).

$$\dot{\gamma} = \frac{\partial v}{\partial y} \approx \frac{u_t}{\delta_L} \quad (3.19)$$

where,  $\Delta v$  is velocity at the foam-liquid interface, i.e. velocity at the wall;  $\Delta y$  is distance to the foam-liquid interface, i.e. distance to the wall);  $u_t$  is the velocity of foam core and  $\delta_L$  is the thickness of water film at the wall. Because the shear stress in the liquid film ( $\tau_{wL}$ ) can be expressed by Equation (3.20):

$$\tau_{wL} = \mu_L \frac{u_t}{\delta_L} \quad (3.20)$$

where,  $\mu_L$  is the liquid viscosity. The liquid layer thickness ( $\delta_L$ ) can be written as follows in Equation (3.21).

$$\delta_L = \frac{S\mu_L u_t}{A \left( -\frac{\Delta P}{L} \right)} \quad (3.21)$$

For the friction factor of foam flow in pipe, the following expressions are used, given in Equations (3.22 – 3.23).

$$f = \frac{\tau_w}{\frac{1}{2} \rho_L u_t^2} \quad (3.22)$$

$$\tau_w = \frac{A\Delta P}{LS} \quad (3.23)$$



Note that the friction factor ( $f$ ) is dimensionless which later can be related to dimensionless Reynolds number, as given in Equation (3.24).

$$\text{Re} = \frac{\rho_L u_t A}{\mu_L S} \quad (3.24)$$

Note that this definition of Reynolds number is valid when foam forms plug flow surrounded by liquid film, showing lubricating effect.

### 3.3.2 New Foam Model Proposed in This Study

The new foam model in this study has 9 model parameters to capture the flow behavior presented in the pressure contours constructed from laboratory flow tests in a wide range of gas and liquid velocities, as shown in Figure 3. 4 . There are three parameters to define the reference point (i.e.,  $u_{w\text{Ref}}$ ,  $u_{g\text{Ref}}$ ,  $\Delta P_{\text{Ref}}$ ), two parameters to capture the trend of linear slopes in the pressure contour lines in both high-quality and low-quality regimes ( $m_H$  and  $m_L$ ), and two Power-Law model parameters for each of the two flow regimes ( $K_H$ ,  $n_H$ ;  $K_L$ ,  $n_L$ ). Note that the boundary between the high-quality and low-quality regimes,  $f_g^*$ , is simply determined by other model parameters, i.e.,  $f_g^* = u_{g\text{Ref}}/(u_{w\text{Ref}}+u_{g\text{Ref}})$ . More details about these parameters are described below.

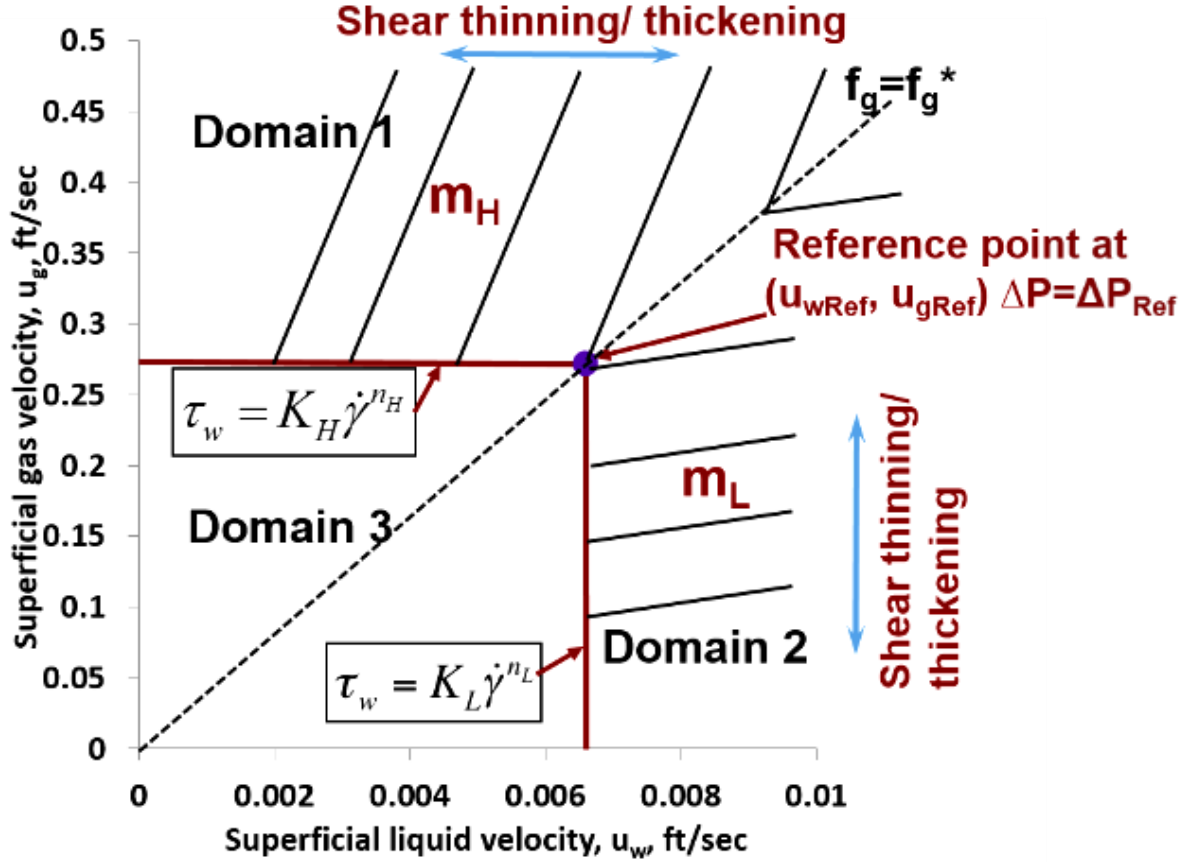


Figure 3. 4 A schematic figure showing nine parameters in this new model

Suppose a series of laboratory flow tests are plotted in a form of pressure contours (Figure 3. 3 (b)). As a first step, a reference point,  $(u_{wRef}, u_{gRef})$ , is selected such that (i) the rectangular area connecting  $(0, 0)$ ,  $(u_{wRef}, 0)$ ,  $(0, u_{gRef})$ , and  $(u_{wRef}, u_{gRef})$  covers the range of pressure contour map that needs to be treated by a smooth transition (this transition named as Domain 3, see Figure 3. 4 ) and (ii) the point sits on the boundary between the two flow regimes (i.e.,  $f_g^* = u_{gRef}/(u_{gRef}+u_{wRef})$ ). Note that the pressure contour corresponding to  $(u_{wRef}, u_{gRef})$  is given by  $\Delta P_{Ref}$ . The second step is to capture the trend of linear pressure contours, outside Domain 3, in the high-quality regime (Domain 1 in Figure 3. 4 ) and in the low-quality regime (Domain 2 in Figure 3. 4 ). The pressure contours based on the original data (Figure 3. 3 (b)) can be captured by a series of straight lines with the average slopes, that is,  $m_H$  and  $m_L$  the average slopes in the high-quality

regime and in the low-quality regime, respectively. Note that  $m_H$  is much larger than  $m_L$ , meaning that the pressure drop is sensitive to “both” gas and liquid velocities in the high-quality regime, while “only” sensitive to gas velocity in the low-quality regime.

The final step is to determine foam rheology in each regime by using Power-Law rheology model, which in some sense defines how a family of pressure contours are separated graphically in the contour plot (For example, if they are equally spaced, it implies that the rheology is near-Newtonian with  $n$  value of around 1, while if the gaps between pressure contours grow or diminish with total velocity ( $u_t$ ), the rheology is shear-thickening with  $n$  greater than 1 or shear-thinning with  $n$  less than 1, respectively.). Among various possible options, this study uses the horizontal line from  $(0, u_{gRef})$  to  $(u_{wRef}, u_{gRef})$  to determine foam rheology in the high-quality regime (i.e.,  $K_H$  and  $n_H$ ; Equation (3.15)), and the vertical line from  $(u_{wRef}, 0)$  to  $(u_{wRef}, u_{gRef})$  to determine foam rheology in the low-quality regime (i.e.,  $K_L$  and  $n_L$ ; Equation (3.15)). The selection of these lines are somewhat arbitrary, but the use of above-mentioned lines helps maintain a small number of model parameters. It should be noted that, outside Domain 3, the boundary between the two regimes is primarily determined by  $n_H$  and  $n_L$  values – if they are the same, the line separating the two flow regimes tends to be straight; if one is greater than the other, the line is curved towards that domain, however.

As a result, this new model captures three domains (Domain 1, Domain 2, and Domain 3 for the high-quality regime, low-quality regime, and transition in between, respectively) with a total of 9 model parameters ( $u_{wRef}$ ,  $u_{gRef}$ ,  $\Delta P_{Ref}$ ,  $m_H$ ,  $m_L$ ,  $K_H$ ,  $n_H$ ,  $K_L$ , and  $n_L$ ).

### 3.3.3 Model Fit to Pressure Contour Map

In order to demonstrate the procedure required for model fit, this study uses an experimental data from Edrisi and Kam (2013) as an example (Figure 3. 2 (a)) in which nitrogen and 0.5 wt%

Stepanform surfactant solutions are injected into 0.38 inch (0.0096 m) ID and 8.5 ft (2.5908 m) long stainless steel horizontal pipe. Figure 3. 4 shows a schematic drawing to define and extract all nine model parameters.

First of all, the reference point of  $(u_{wRef}, u_{gRef}) = (0.034 \text{ ft/s (0.0104 m/s), } 0.93 \text{ ft/s (0.2835 m/s)})$ , providing  $f_g^* = 96.5\%$ , is selected at  $\Delta P_{Ref} = 14 \text{ psi (96527 Pa)}$ , which allows the rectangular box for Domain 3 to be determined. Then, a series of parallel pressure contours in both high-quality regime and low-quality regime are drawn from  $\Delta P = 2 \text{ psi (13790 Pa)}$  to  $14 \text{ psi (96527 Pa)}$  with the interval of  $4 \text{ psi (27579 Pa)}$ . The average slopes of these straight pressure contours are determined to be  $90.0$  and  $7.0$  for  $m_H$  and  $m_L$ , respectively. One may choose different pressure contours with different intervals, but it does not make much difference in this holistic approach. Figure 3. 5 shows the results up to this point. As a next step, the Power-Law model parameters can be calculated from the relationship between the pressure drop and total velocity ( $K_H$  and  $n_H$  in Figure 3. 6 (a) for the high-quality regime along  $(0, u_{gRef})$  to  $(u_{wRef}, u_{gRef})$ ;  $K_L$  and  $n_L$  in Figure 3. 6 (b) for the low-quality regime along  $(u_{wRef}, 0)$  to  $(u_{wRef}, u_{gRef})$ ). The curve fit shows  $K_H = 0.1349 \frac{\text{dyne-s}^{1.2202}}{\text{cm}^2}$  and  $n_H = 1.2202$  for the high-quality regime, and  $K_L = 0.0027 \frac{\text{dyne-s}^{1.2074}}{\text{cm}^2}$  and  $n_L = 1.2074$  for the low-quality regime.

Finally, Domain 3 showing the transition can be completed by connecting pressure contours exhibiting the same values from both regimes, as shown in Figure 3. 7. The figure also shows the boundary between two flow regimes and one pressure contour beyond the reference point ( $\Delta P = 18 \text{ psi}$ ). Table 3. 1 shows a summary of all nine model parameters.

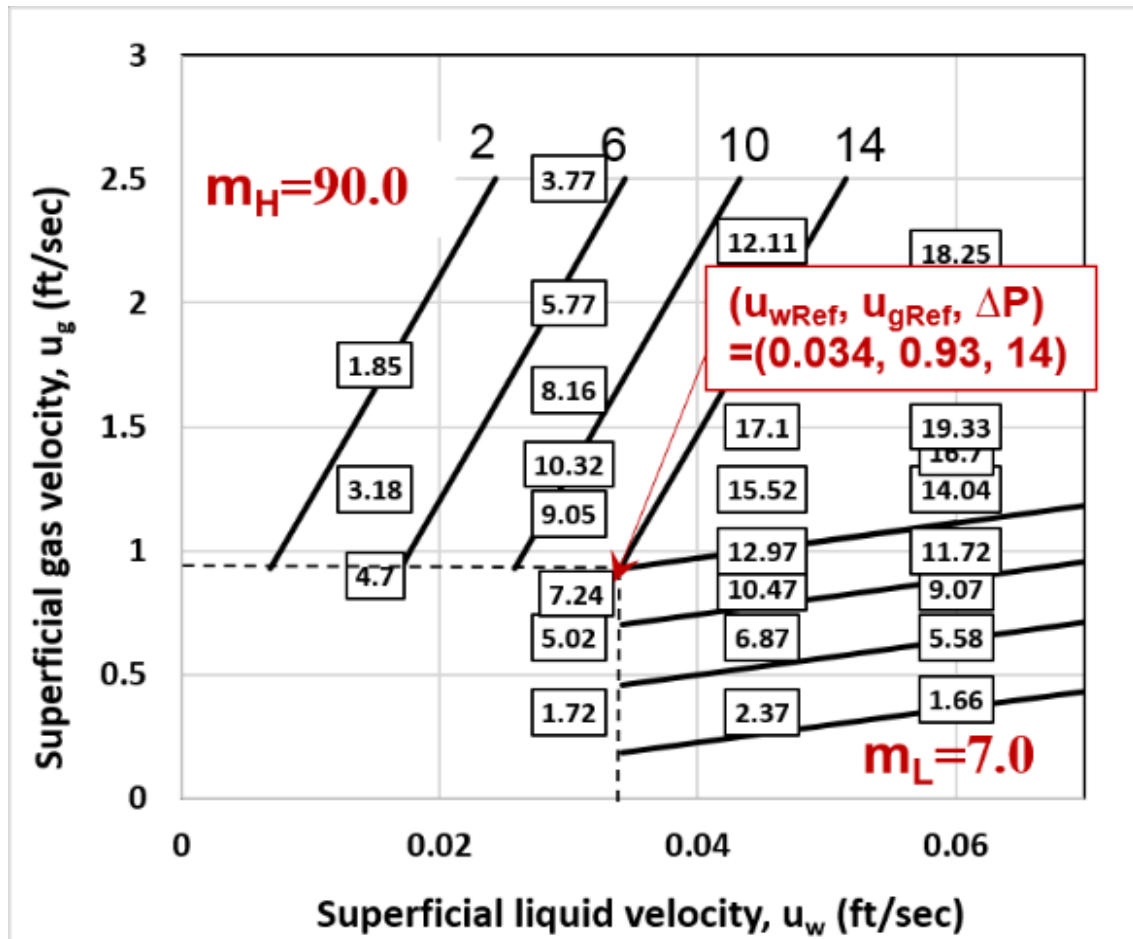
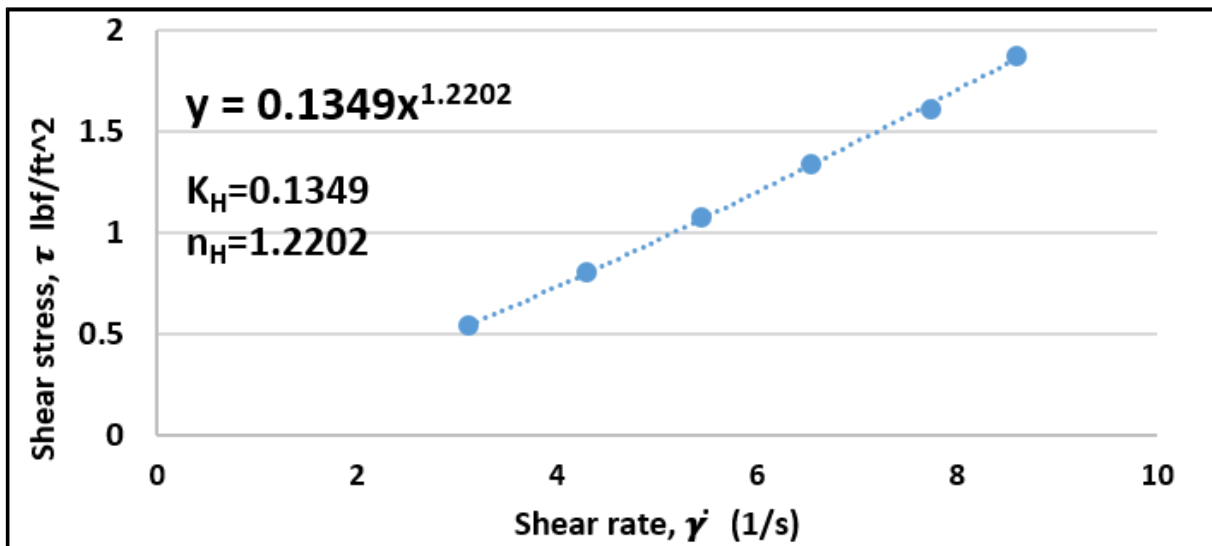


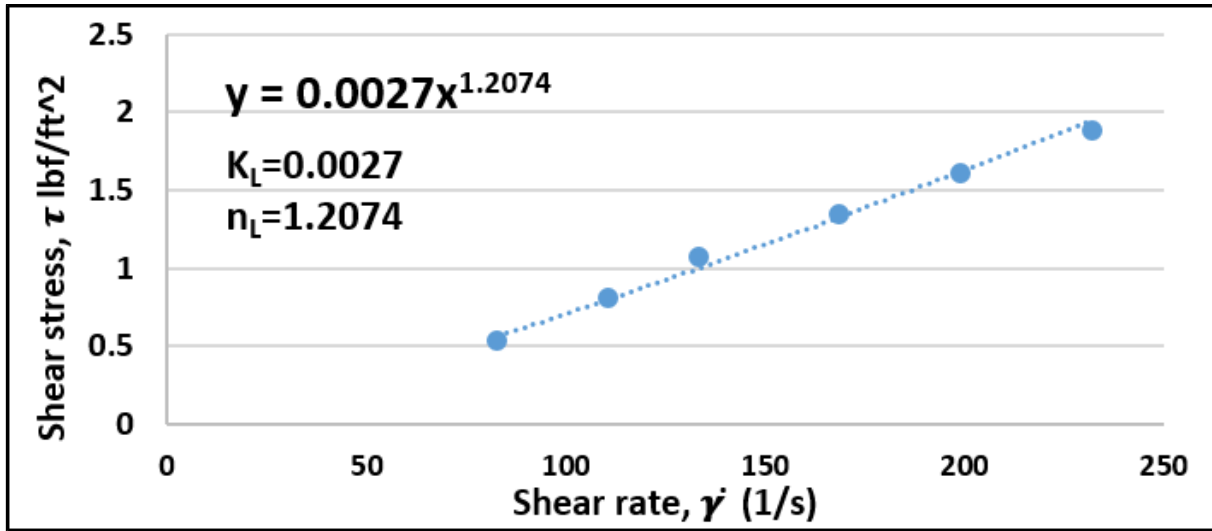
Figure 3. 5 A schematic figure showing the model parameters



(a)  $K_H$  and  $n_H$  in the High-Quality Regime

Figure 3. 6 Rheograms showing the relationship between shear stress and shear rate

(fig. cont'd.)



(b)  $K_L$  and  $n_L$  in the Low-Quality Regime

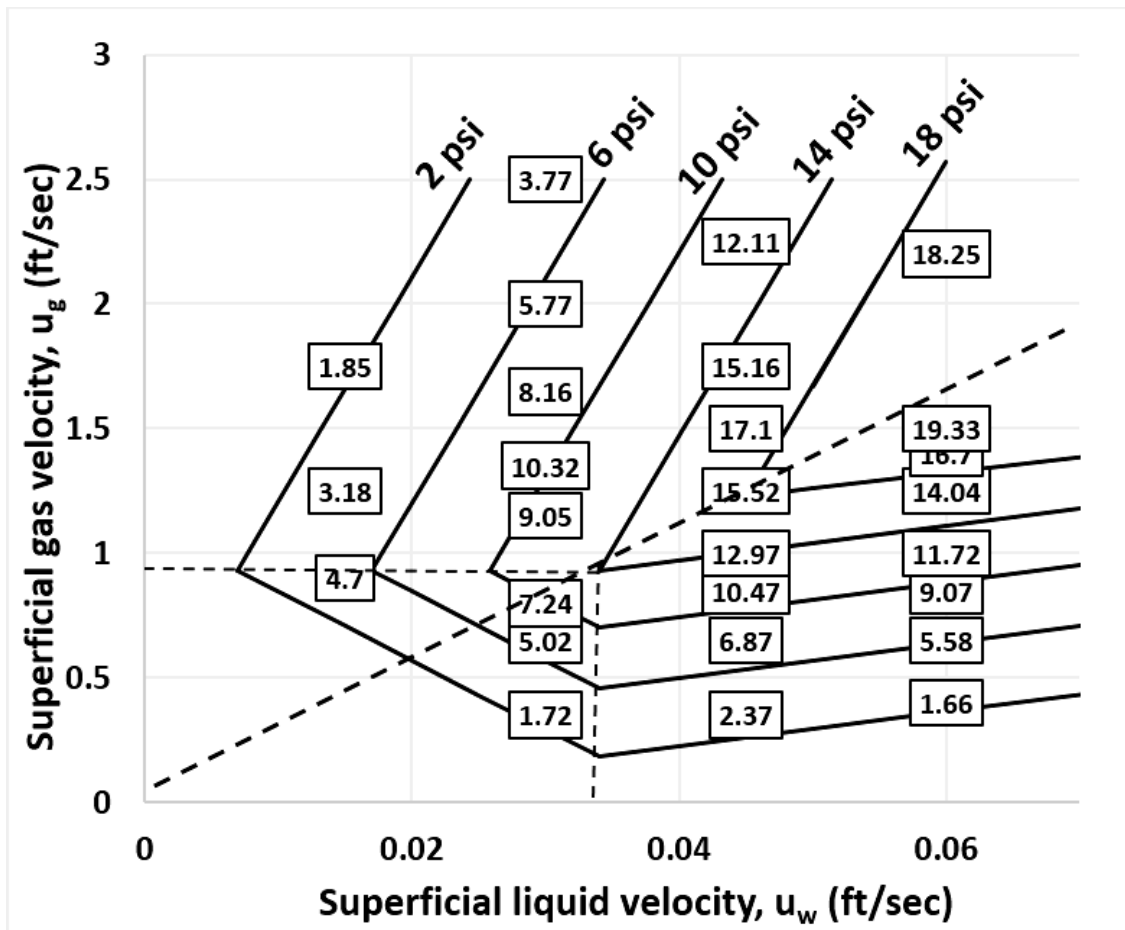


Figure 3. 7 A schematic of a complete pressure contour map

Table 3. 1 Summary of nine foam model parameters determined in this study

Parameters		Units	
$u_{wRef}$	Superficial liquid velocity at reference point	0.034	ft/s
$u_{gRef}$	Superficial gas velocity at reference point	0.93	ft/s
$\Delta P_{Ref}$	Pressure drop at reference point	14	Dimensionless
$m_H$	Average slope in high-quality regime	90	Dimensionless
$m_L$	Average slope in low-quality regime	7	Dimensionless
$K_H$	Consistency index in high-quality regime	0.1349	$\frac{\text{dyne} - \text{s}^{1.2202}}{\text{cm}^2}$
$n_H$	Power-Law Exponent in high-quality regime	1.2202	Dimensionless
$K_L$	Consistency index in low-quality regime	0.0027	$\frac{\text{dyne} - \text{s}^{1.2074}}{\text{cm}^2}$
$n_L$	Power-Law Exponent in low-quality regime	1.2074	Dimensionless

### 3.3.4 Implication of the Model for Other Flow Characteristics

Although this study first constructs pressure contours as a function of gas and liquid velocities and then turn them into foam rheology using rheograms, some previous studies in the literature prefer using apparent foam viscosity for more practical purposes. By using Equations (3.12-3.16), one can plot apparent viscosity contours calculated by Power-Law model, the result of which is shown in Figure 3. 8 . The filled square symbols represent the points at which actual pressure measurements are collected from the experiments and apparent foam viscosities are calculated. The position of the reference point is also shown by the filled circle.

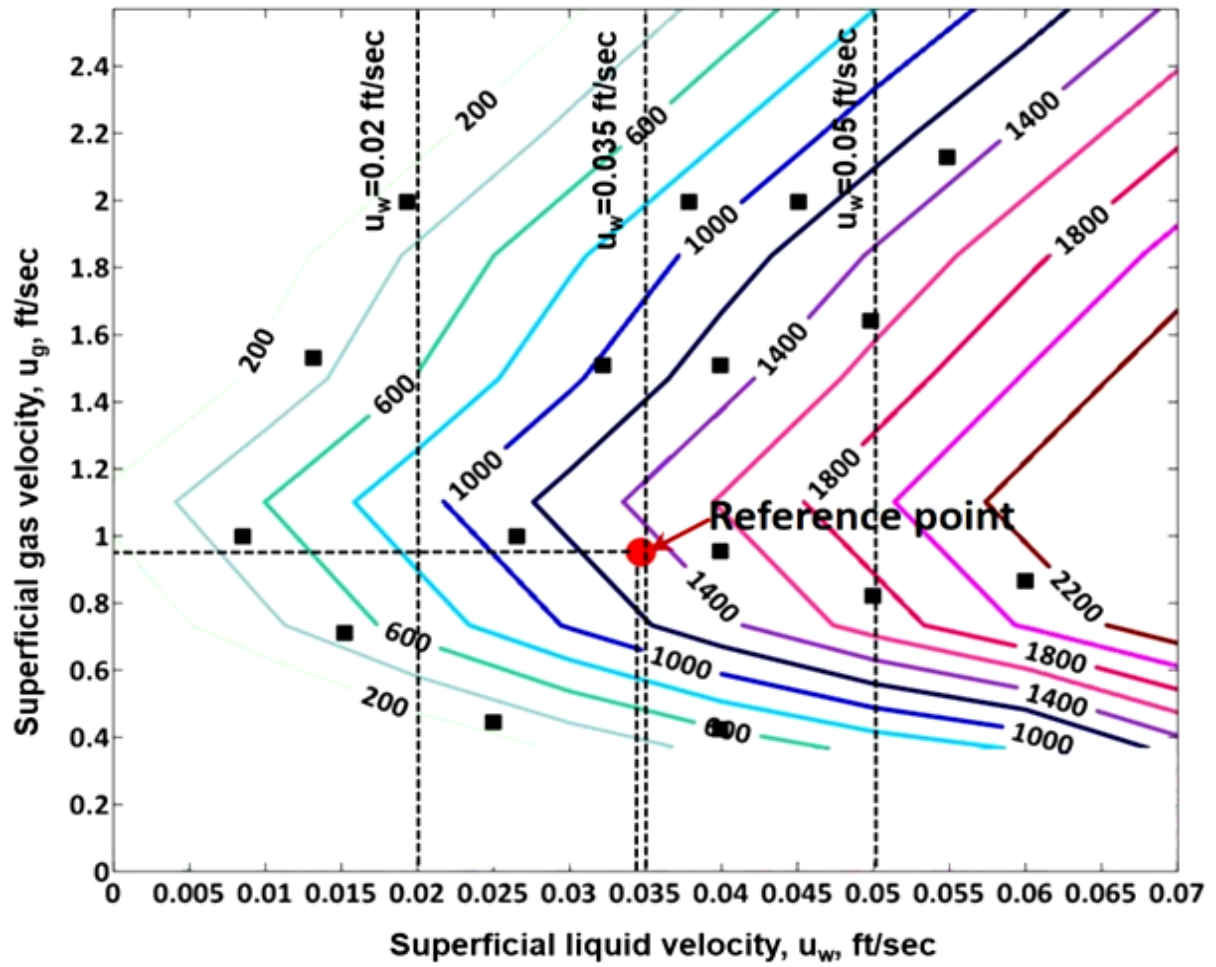


Figure 3. 8 Conversion of pressure contours into apparent foam viscosity contours



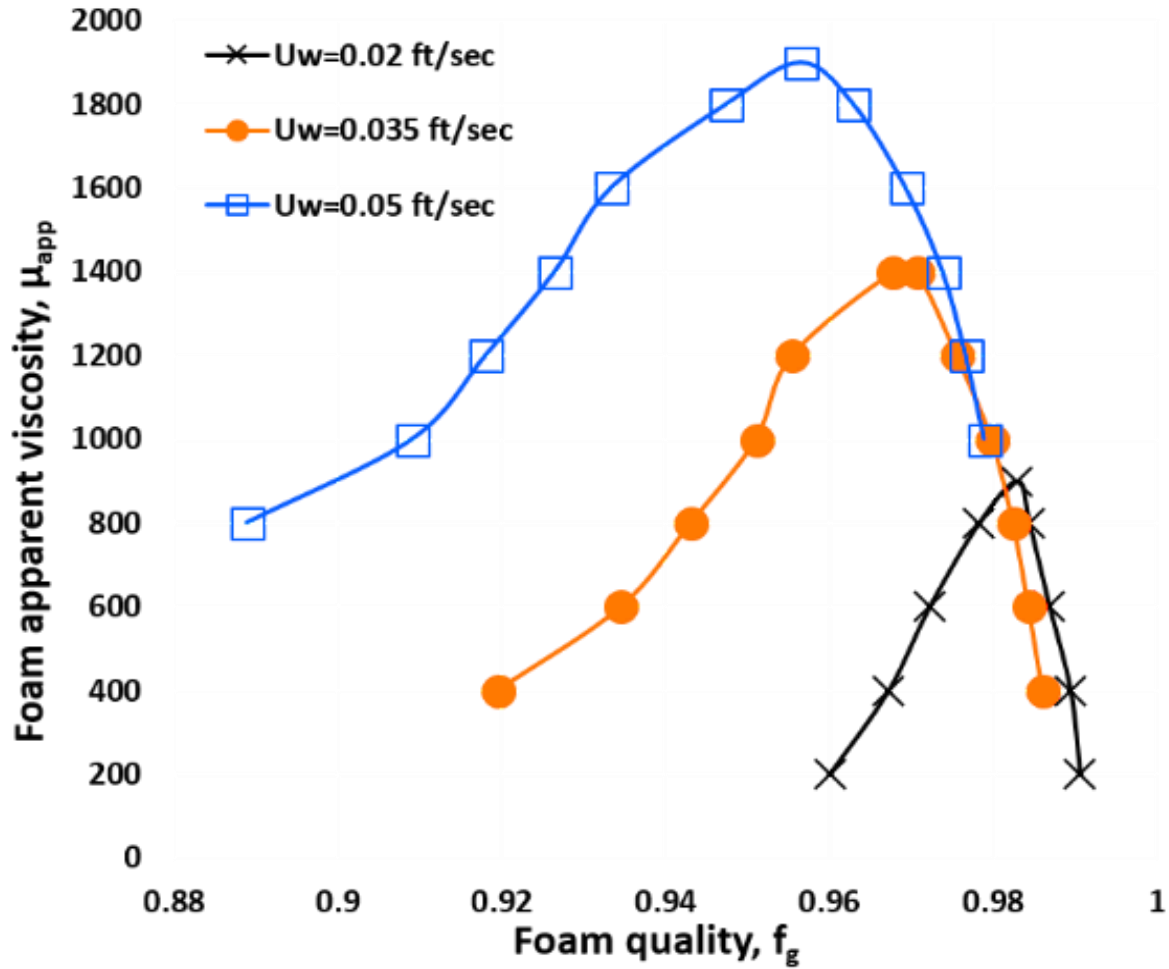


Figure 3. 9 Apparent foam viscosity obtained at fixed superficial liquid rates

Once the viscosity contours, ranging from 200 cp (0.2 Pa.s) to 2200 cp (2.2 Pa.s), are constructed in a wide range of gas and liquid velocities of interest as shown in Figure 3. 8 , one may apply the map in order to estimate how foam viscosity varies during certain applications. For example, in foam drilling applications (shown in the following section for more detail) the process has relatively constant liquid velocities with gas velocities varying significantly due to compressibility. For three superficial liquid velocities in such an application (as shown by the vertical dotted lines such as  $u_w = 0.02$  ft/s (0.0061 m/s), 0.035 ft/s (0.0107 m/s), and 0.05 ft/s (0.0152 m/s) in Figure 3. 8 ), Figure 3. 9 shows apparent foam viscosities as a function of foam quality (i.e., varying  $u_g$  at fixed  $u_w$ ). One may notice that the results from viscosity contours

resemble the trend reported by previous studies – foam mixture becomes more viscous with  $u_g$  for relatively wet foams, while less viscous with  $u_g$  for relatively dry foams. It is because of foam stability: adding more gas to already stable wet foams increase viscosity due to increasing bubble-to-bubble interactions during shear flow, while adding more gas to unstable dry foams decreases viscosity due to more active bubble coalescence.

For foams in the low-quality regime, the flow of a relatively homogeneous foam mixture allows the thickness of liquid film at the wall to be determined (Equation (3.21)) under the influence of lubricating effect. In order to analyze how liquid-film thickness changes, 12 data points in the low-quality regime are selected as shown in the contour map of Figure 3. 10 , that is, four  $u_g$  values ( $u_g = 0.184$  ft/s (0.0561 m/s), 0.46 ft/s (0.1402 m/s), 0.70 ft/s (0.2134 m/s), and 0.93 ft/s (0.2835 m/s)) at each of three  $u_w$  values ( $u_w = 0.0341$  ft/s (0.0104 m/s), 0.045 ft/s (0.0137 m/s), and 0.06 ft/s (0.0183 m/s)), the reference point being point 1. The liquid layer thickness corresponding to each point in Figure 3. 10 is calculated by Equation (3.21) and shown in Figure 3. 11 . As expected, (i) at fixed liquid velocity ( $u_w$ ), the thickness of liquid layer at the wall ( $\delta_L$ ) becomes thicker, as gas velocity decreases (or, as foam becomes wetter, equivalently), and (ii) at fixed gas velocity ( $u_g$ ), the thickness of liquid layer becomes thicker, as liquid velocity increases (or, as foam becomes wetter, once again). It is interesting to note that the reference point (point 1 in Figure 3. 10 ) has the minimum  $\delta_L$  and the change in  $\delta_L$  can be significant as foam becomes wetter (for example,  $\delta_L$  increases from 0.001319 inch (0.000034 m) to 0.426 inch (0.0108 m), almost 320 times increase, comparing point 1 to point 12).

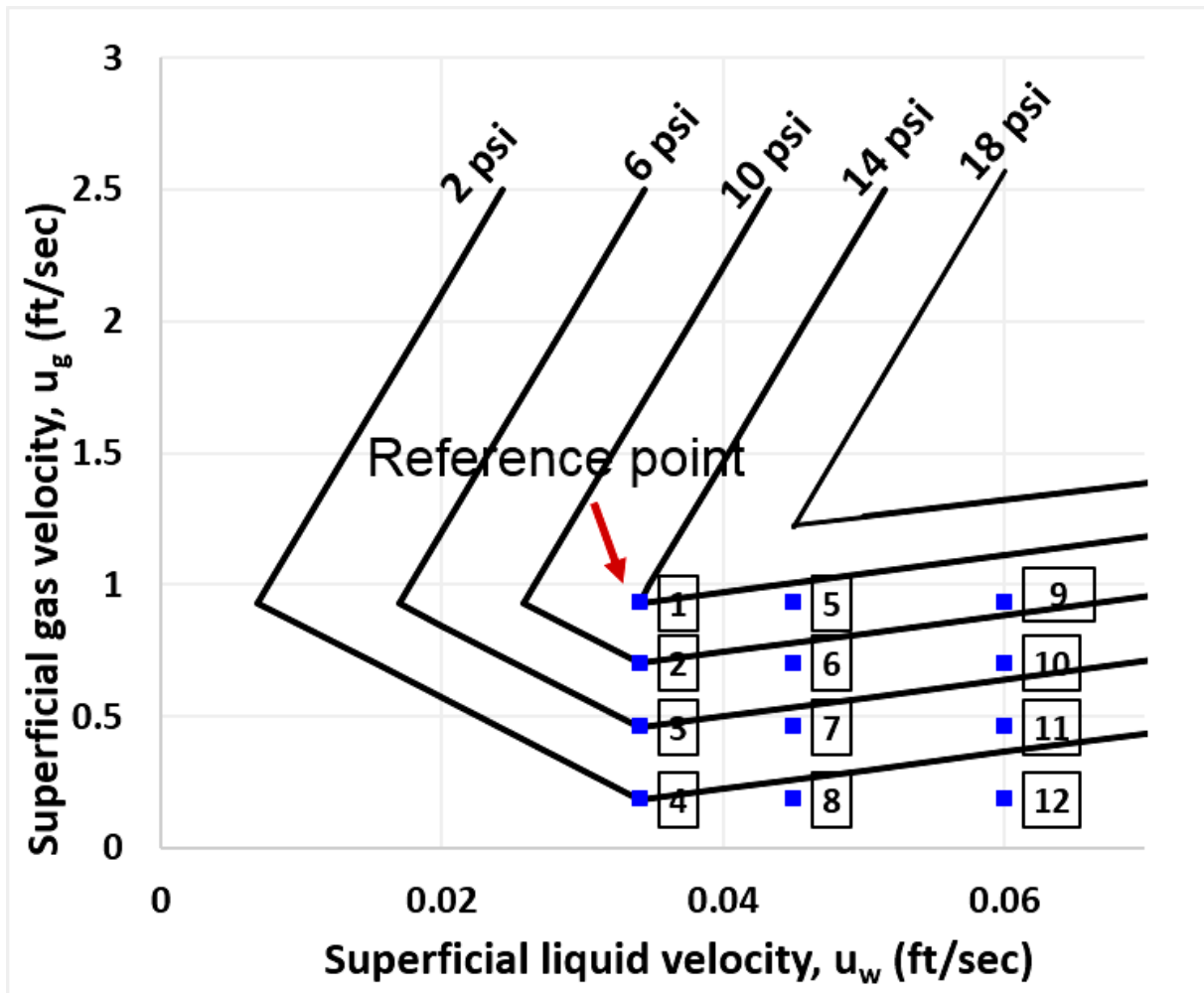


Figure 3. 10 A schematic figure showing 12 data points of interest in the Low-Quality regime

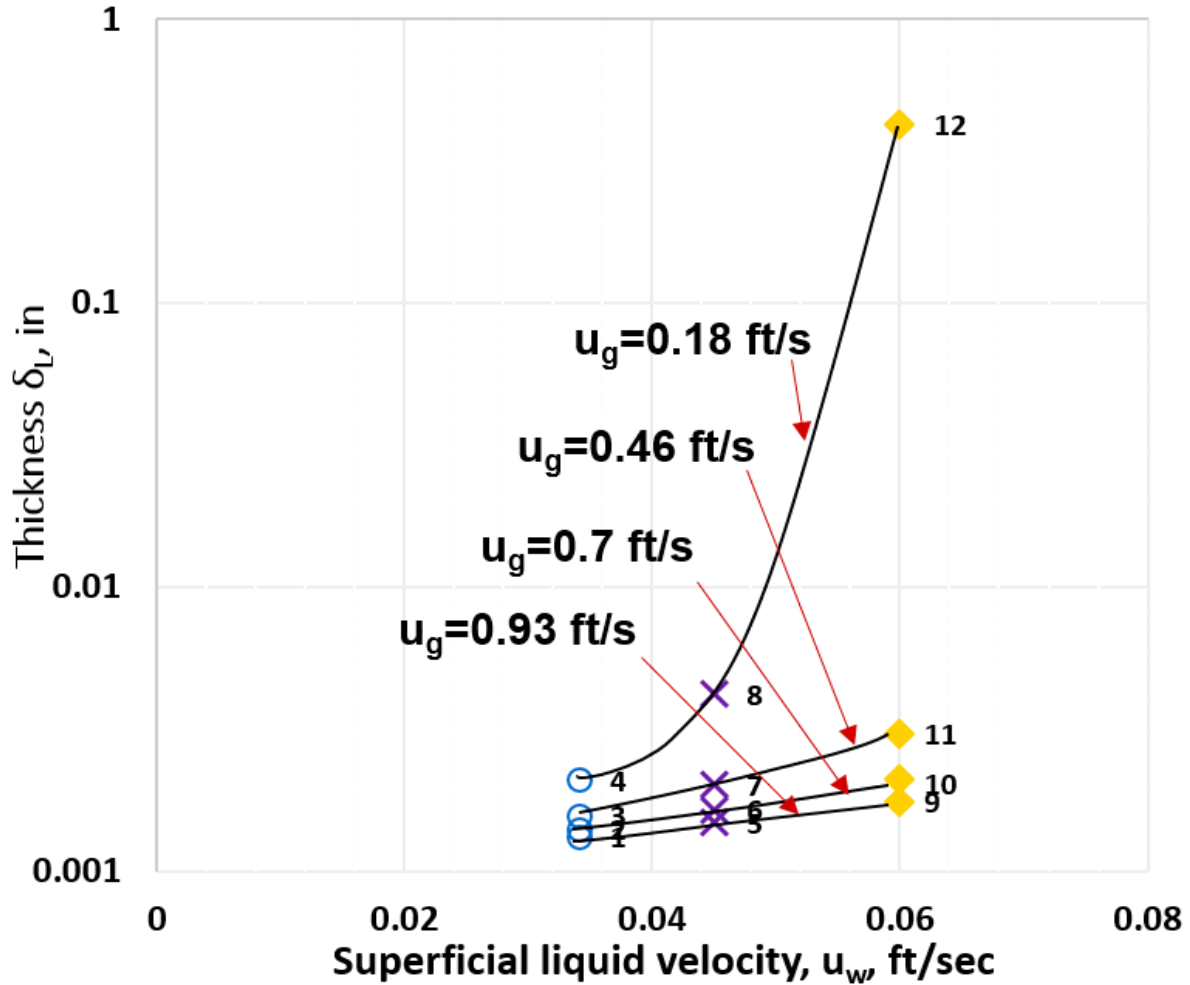


Figure 3. 11 Liquid layer thickness at different gas and liquid injection rates

In addition to pressure drop and apparent viscosity, the use of friction factor is sometimes handy to quantify the flow of non-Newtonian fluids. The frictional pressure loss through the pipe depends on many parameters such as pipe diameter, density of fluid, viscosity of fluid, and average flow velocity, which are often grouped into dimensionless Reynolds number (see Equations (3.22-3.24) for example). For the 10 points from Figure 3. 10 (excluding point 1 and point 12), the frictional factor ( $f$ ) for foams in the low-quality regime is plotted as a function of Reynolds number ( $Re$ ) as shown in Figure 3. 12 . More specifically, the best-fit straight line equation in log-log plot shows a relationship, as Equation (3.25):

$$f = \frac{0.1408}{\text{Re}_L^{0.584}} \quad (3.25)$$

Where,  $f$  is the foam friction factor;  $\text{Re}_L$  is the Reynolds number for low-quality foam.

It is interesting to find that the exponent is about 0.584 (data points all in the laminar flow regime ( $\text{Re}_L < 2400$ ) due to high-viscosity foam mixture), which can be contrasted with 0.25 and 1 for turbulent and for laminar flow of Newtonian fluid, respectively (Equations (3.8-3.9)). This deviation from the Newtonian fluid describes indirectly the complexity of foam flow behavior.

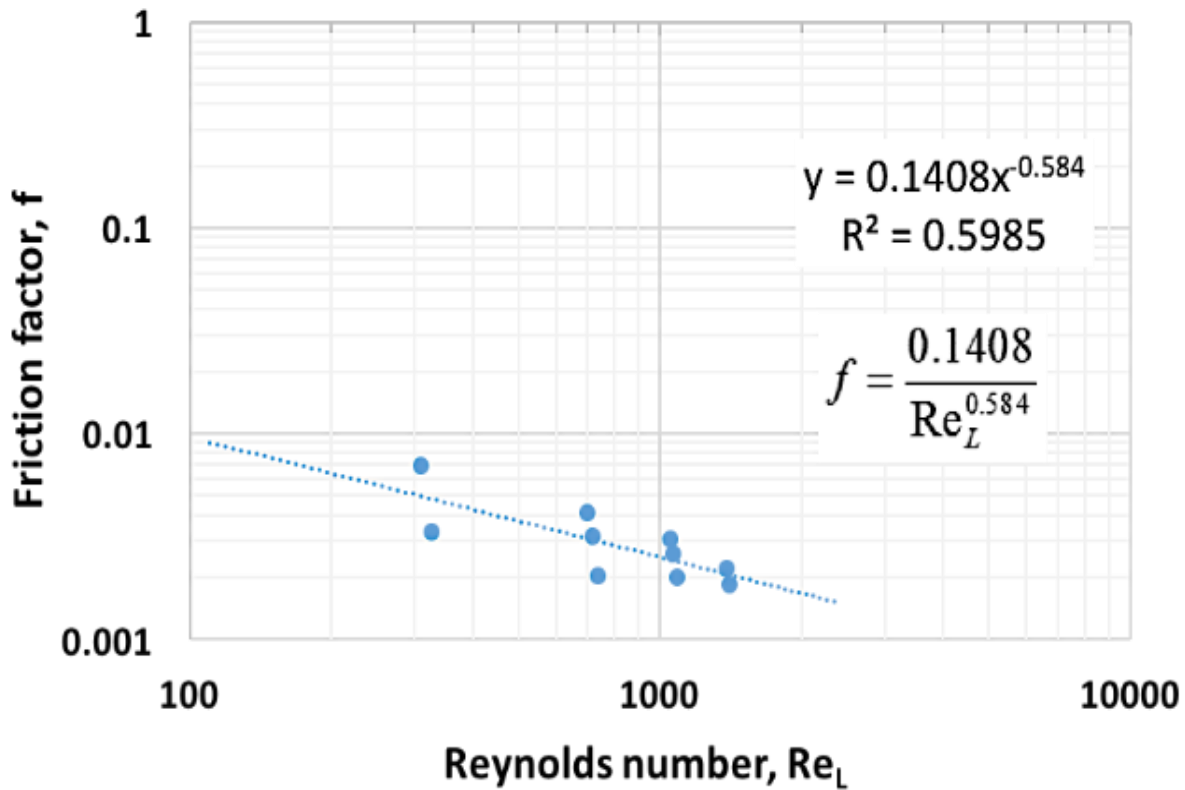


Figure 3. 12 Relationship between friction factor and Reynolds number

### 3.3.5 Application to Foam Drilling Process

As an example application of this new model, a foam drilling hydraulics simulator is developed and presented in this study. In the literature, there exist a few underbalanced drilling hydraulics

simulators developed from steady-state to transient simulators. For comparison, this study uses correlations from Chen et al. (2007, 2009), which developed homogeneous foam rheology for polymer stabilized foams, for the low-quality regime foams, and it uses correlations from Edrisi and Kam (2015) for the high-quality regime foams.

Figure 3. 13 shows a schematic of the drilling process with U-tube concept for a 10,000 ft (3048 m) vertical well (i.e. drill string on the left-hand-side column and annulus on the right-hand-side column, both connected through bit nozzles at the bottom). Wellbore diameter is 8.5 inch (0.2159m), and the drill string outer diameter is 5 inch (0.127m). At the bottom hole, the bit is assembled with 3 nozzles with a diameter of 0.375 inch (0.009525m).

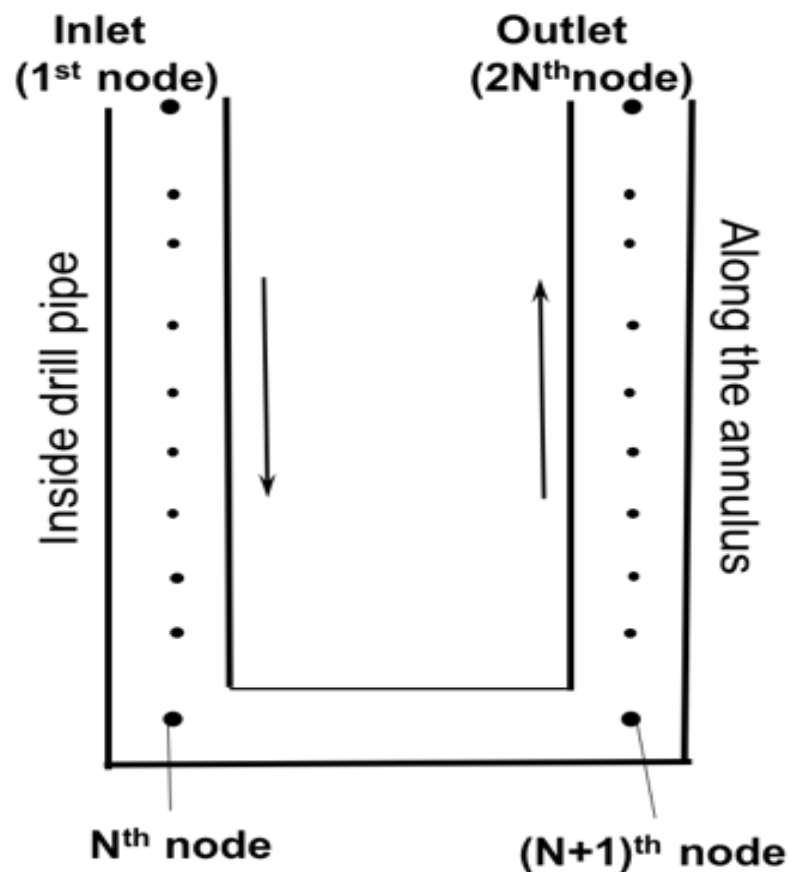


Figure 3. 13 A schematic of foam drilling process using U-tube concept

The direction of calculation is from the wellhead downward to the bottom hole for drill pipe

flow, and then upward from the bottom hole to the top of annulus for annulus flow. In calculation, the wall roughness is assumed to be negligible, the surface temperature 80°F (26°C), the wellbore and fluid temperatures the same as formation temperature (which has a gradient of 1.5°F/100ft (2.732°C/100m)), the liquid phase water, and the gas phase nitrogen. The overall iterative calculations are carried out by assuming drilling pipe pressure (i.e., the pressure at the 1<sup>st</sup> node) to satisfy the specified backpressure (i.e., the pressure at the 2N<sup>th</sup> node, which is 100 psia (689476 Pa)) at given gas and liquid circulation rates ( $Q_g = 1300$  scfm (0.611 m<sup>3</sup>/s) and  $Q_L = 40$  gpm (0.0025 m<sup>3</sup>/s)). The basic procedure is shown as follows:

1. Construct the computational U-tube domain for 2N cells for drill string and annulus, with each node representing the center of each cell, as shown in Figure 3. 13 .
2. Specify the boundary conditions, that is, the outlet pressure as well as gas and liquid rates.
3. Assume inlet pressure at the 1<sup>st</sup> node.
4. For each cell in the drilling string, compute  $\Delta P_a$ ,  $\Delta P_h$ ,  $\Delta P_f$ , and then the total pressure drop  $\Delta P_t$ , to determine the pressure at the next node.
5. Between the N<sup>th</sup> and (N+1)<sup>th</sup> nodes, there is a pressure drop through the drill bit, which is given by Equation (3.26).

$$\Delta P_{bit} = \frac{8.311 \times 10^{-5} \rho_m Q_t^2}{(0.95A)^2} \quad (3.26)$$

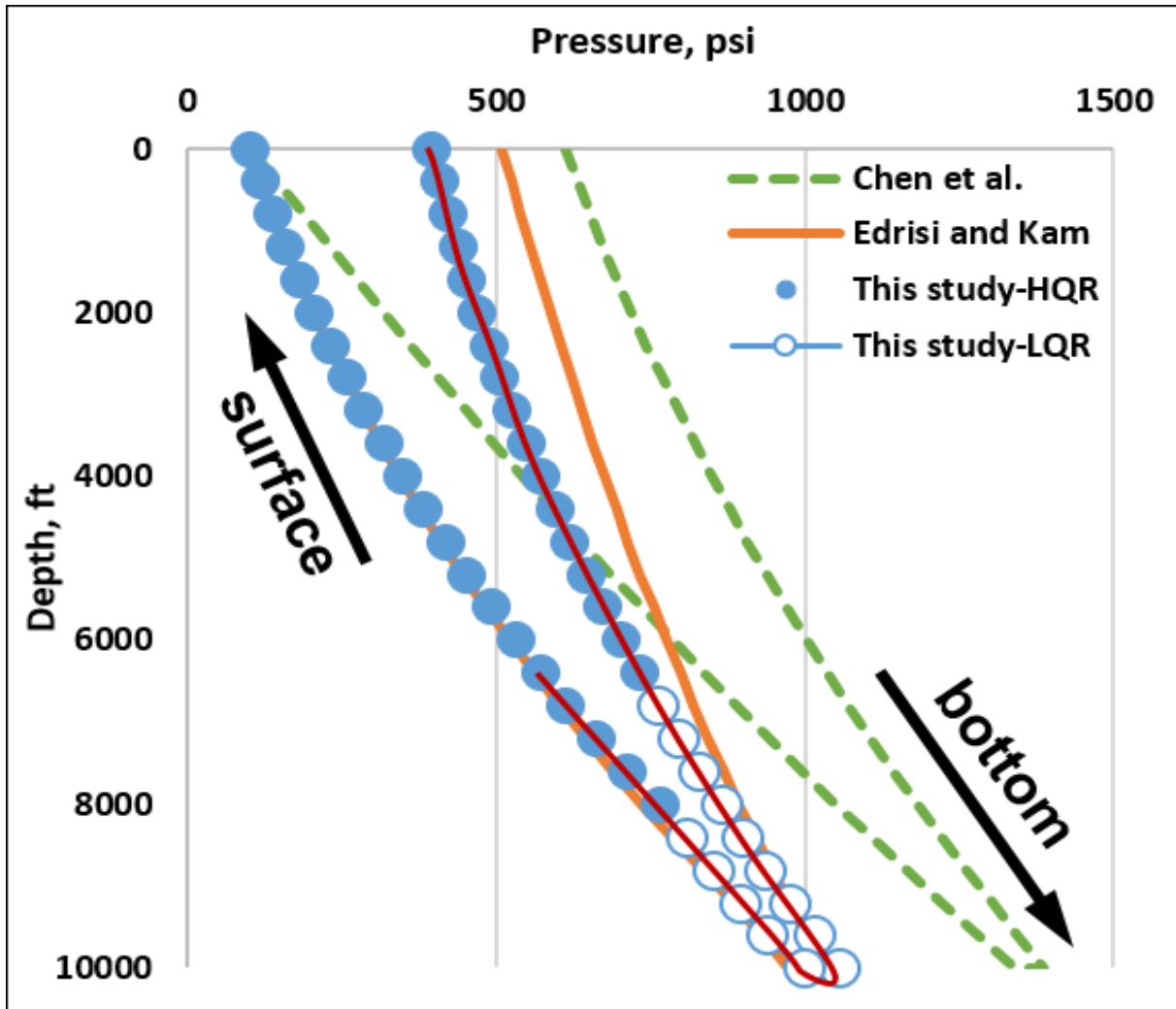
where,  $\rho_m$  is mixture density [ppg];  $Q_t$  is total flow rate [gpm];  $A$  is total nozzle area [in<sup>2</sup>]; and  $\Delta P_{bit}$  is pressure drop through nozzles [psig].

6. Similarly, continue the calculations upwards along the annulus for each node until the last node 2N<sup>th</sup> is reached at the outlet.
7. Evaluate if the calculated pressure at the last node is close enough to the pre-specified backpressure. If not, go to step 3 with a new assumed value of inlet pressure and repeat

calculations; otherwise, accept it as a final solution.

Figure 3. 14 shows the results of foam drilling simulations in terms of pressure profile, foam quality, foam density, and total velocity for three different methods of modeling. First of all, it should be noted that Edrisi and Kam's model (2013) cannot be used for low circulation rates (see the discussions in Figure 3. 3 ) due to the absence of smooth transition. This is why relatively high  $Q_g$  and  $Q_L$  values are used for this simulation. Second, in all three methods, the pressure profile (Figure 3. 14 (a)) shows the same backpressure values of 100 psia (689476 Pa) (as an input) that corresponds to 0.97 of foam quality at the surface in the foam quality profile (Figure 3. 14 (b)), which determines foam density and total velocity along the hole (Figure 3. 14 (c)) and Figure 3. 14 (d)). Third, the results are in general consistent as expected, for example, foam quality is reduced with increasing pressure, foam density increases with increasing depth, total velocity decreases with increasing depth and so on, primarily due to the compressibility of gas phase.

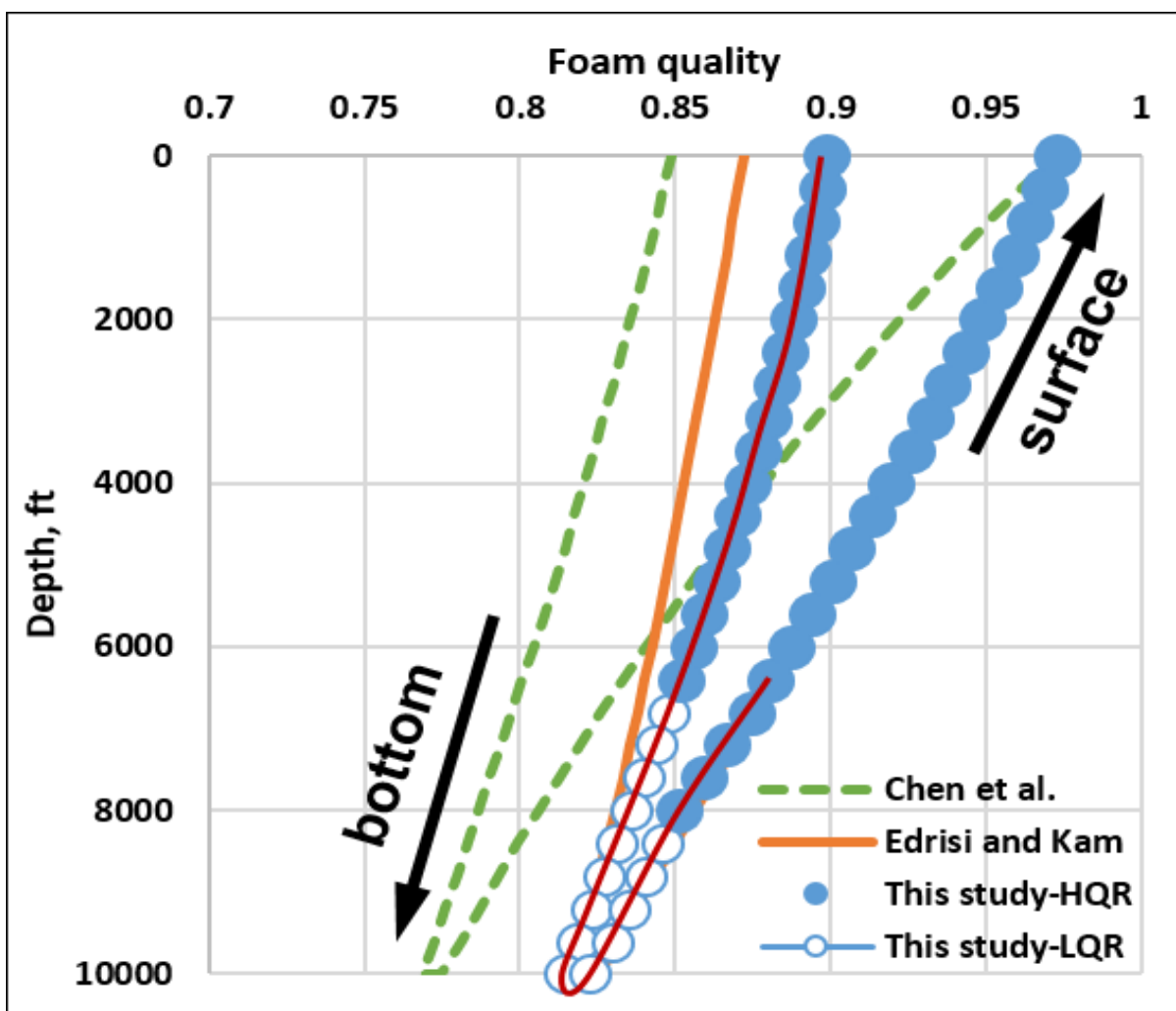




(a) Pressure

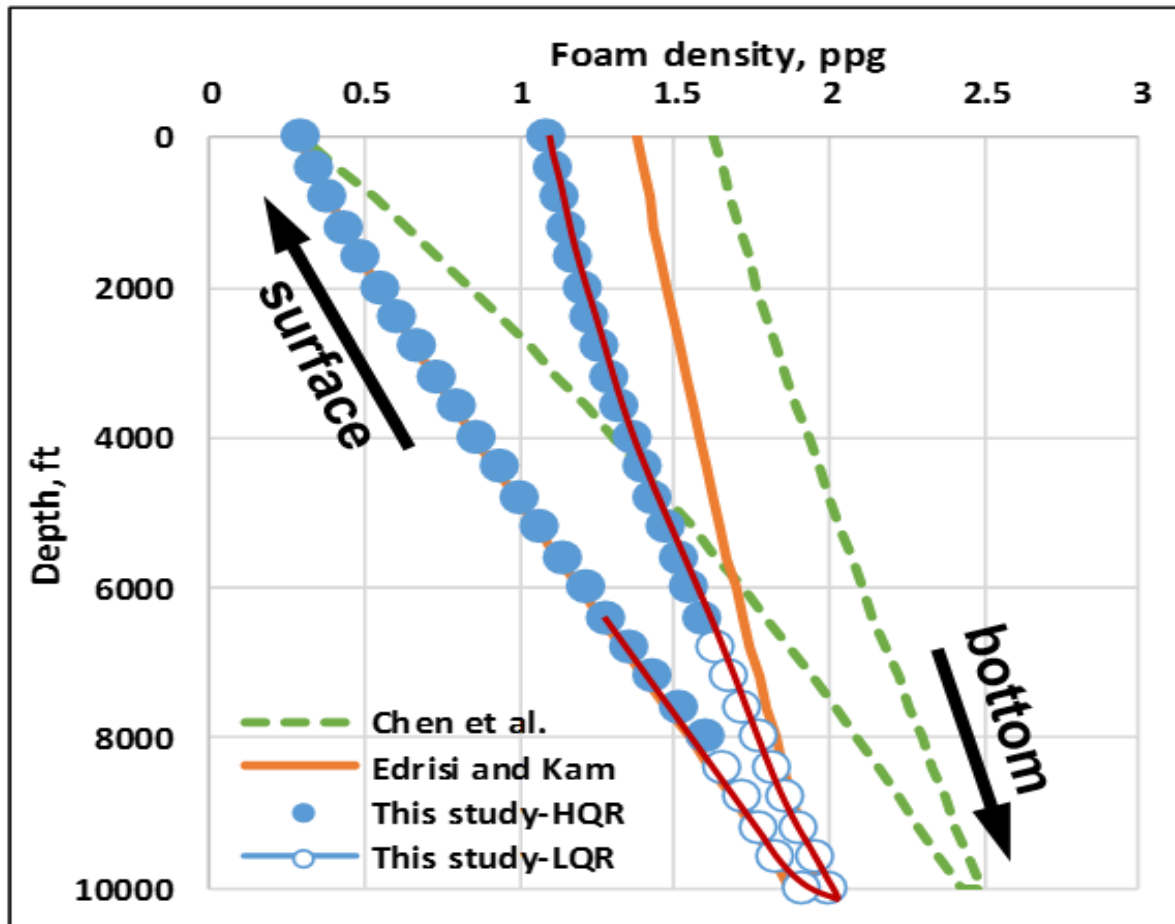
Figure 3. 14 Steady-state simulation results for foam circulation without formation fluid influx: (a) pressure (b) foam quality (c) foam density (d) total velocity

(fig. cont'd.)



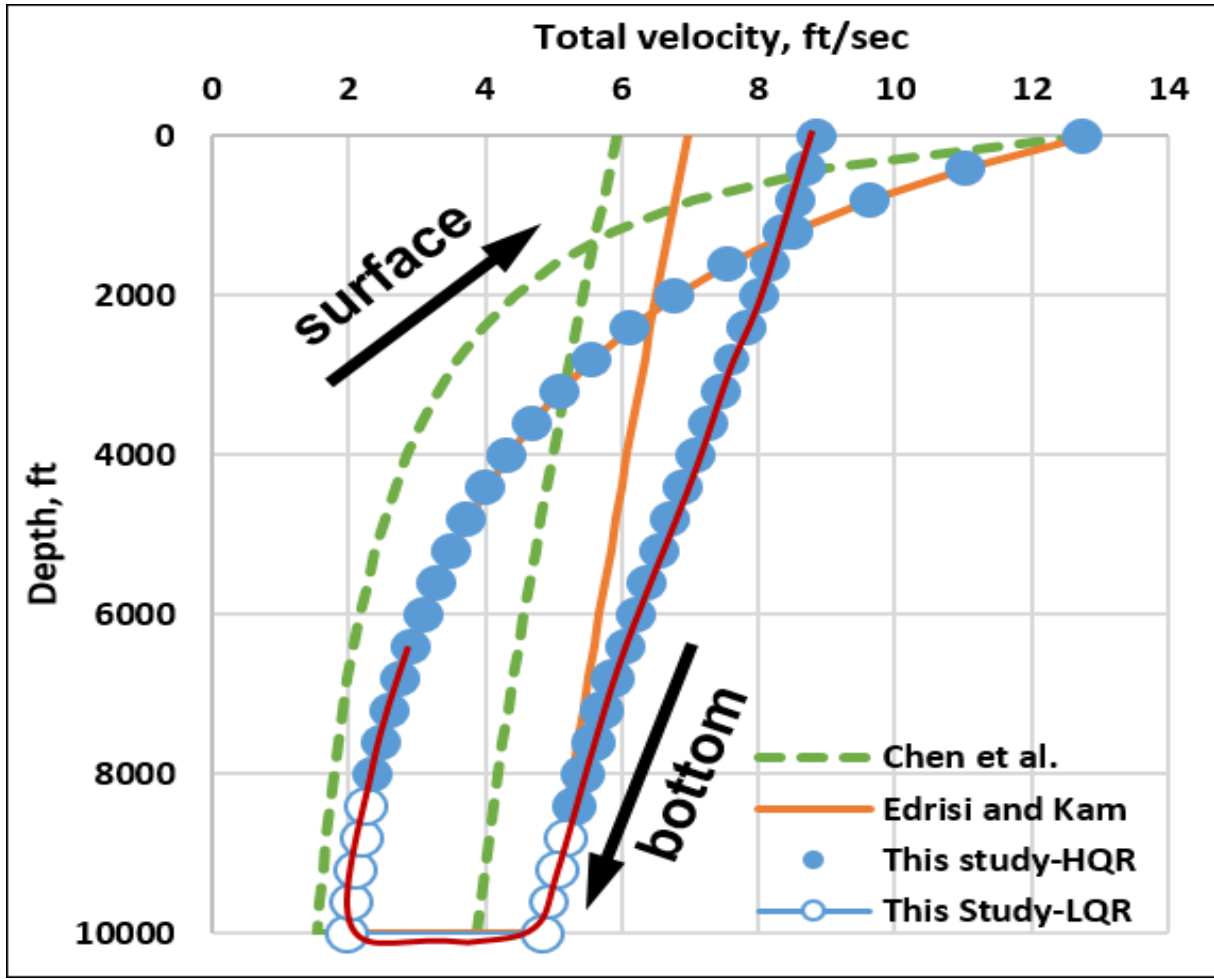
(b) Foam Quality

(fig. cont'd.)



(c) Foam Density

(fig. cont'd.)



(d) Total Velocity

Figure 3. 14 reveals that (i) the model based only on the low-quality-regime foams (referred to as “Chen et al.” in dashed green lines) deviates significantly by missing unstable foam flow characteristics for dry foams, and (ii) even the model with two flow regimes (referred to as “Edrisi and Kam” in solid orange lines) shows the level of errors that cannot be neglected by not incorporating transition (500 psia (3447380 Pa) vs. 400 psia (2757904 Pa) at the inlet, 1.4 ppg (167.67 kg/m<sup>3</sup>) vs. 1.05 ppg (125.82 kg/m<sup>3</sup>) foam density, and so on). Note that the results from the new model in this study is referred to as “This study” represented by circles (i.e., open circles for  $f_g > f_g^*$  and filled circles for  $f_g < f_g^*$ ) and the dotted red lines on the top represent the portion of the graph in the transition (Domain 3). Table 3. 2 summarizes the comparison of three different

methods in terms of bottom hole pressure (BHP), bottom hole foam quality, bottom hole density, bottom hole total velocity, and injection pressure. The relative errors are shown as well.

Table 3. 2 Comparison of three different foam simulation methods

	This model	Chen et al.	Edrisi and Kam
BHP, psi	996	1341 (26%)	973 (2%)
BH Foam Quality, %	82	77 (6%)	83 (1%)
Inlet Pressure, psi	395	611 (35%)	509 (22%)
BH Density, ppg	1.91	2.43 (21%)	1.88 (2%)
BH Total Velocity, ft/s	1.95	1.54 (26%)	1.99 (2%)

### 3.4 Conclusions

A new foam model has been established in this study to characterize foam flow in pipes. The model incorporates unstable slug-flow-pattern dry foam rheology (referred to as high-quality regime), stable plug-flow-pattern wet foam rheology (referred to as low-quality regime), and a transition in between. This study can be concluded with the following major outcomes.

This new foam model overcomes the limitations in the previous model by (i) allowing two separate and independent foam rheological properties in the high-quality and low-quality regimes and (ii) introducing a smooth transition between the two regimes to capture experimental data more realistically. The model requires nine model parameters – three ( $u_{wRef}$ ,  $u_{gRef}$ ,  $\Delta P_{Ref}$ ) to define the transition region, four to capture Power-Law rheology in both high-quality and low-quality regimes ( $K_H$ ,  $n_H$ ,  $K_L$ ,  $n_L$ ), and two to describe the sensitivity of steady-state pressure drops as a function of gas and liquid velocities in both regimes ( $m_H$ ,  $m_L$ ).

This study also demonstrates how some of the key parameters for foam flow in pipes can be decided. For example, how apparent foam viscosity can be mapped out in a wide range of gas and liquid velocities, how the thickness of water film at the wall (as an origin of lubricating effect) varies with the changes in gas and liquid contents, and how the dimensionless friction factor,

required for frictional pressure loss calculations, can be calculated as a function of experimental conditions (which can be grouped into Reynolds number).

This new model is applied to foam drilling application and compared with two other models in the literature – one only based on low-quality regime foams, and the other based on both high-quality regime and low-quality regime foams. The error analysis shows that there is a unique benefit of using the model presented in this study in predicting responses such as pressure, foam quality, foam densities, and total velocity. More detailed analysis in a wide range of drilling scenarios remains as a future study.

## CHAPTER 4. MODELING OF FOAM-ASSISTED WELLBORE CLEANUP AND DRILLING PROCESSES WITH BOTH DRY- AND WET-FOAM RHEOLOGICAL PROPERTIES

### 4.1 Introduction

The use of foams, as a mixture of gas and surfactant solutions, has been widely applied to numerous onshore and offshore wells. Foam drilling and cleanup technology, among many, can bring many benefits, including minimizing water usage and formation damage, avoiding lost circulation, extending drill bit life, lowering treatment costs, and improving cutting and solid transport efficiency. In conventional drilling mud applications, the deeper the well, the higher the hydrostatic pressure of the mud, and thus the higher the possibility to induce fractures or wellbore instability problems. (Rojas et al., 2002, Chen et al., 2006, Nugroho et al., 2017).

Foam may be generated either at the injection point (known as in-situ generation) or by passing through a porous medium or coiled tubing generator. When foam or foamed mud is injected, the hydrostatic pressure can be reduced by the lower mixture density, and the fluid viscosity can be improved by the foam films (or, lamellae) separating bubbles. Moreover, the density and viscosity of foamed mud can be adjusted further depending on the need, by controlling total flowrate ( $Q_t$ , that is, the sum of gas and liquid rates (i.e.,  $Q_t = Q_g + Q_w$ )), gas fraction ( $f_g$ , that is, also known as foam quality), surfactant compositions and concentrations, chemical additives, and so on. Because the gas phase in the foam mixture is compressible, total flowrate ( $Q_t$ ) and foam quality ( $f_g$ ) are sensitive to the surrounding pressure and temperature conditions.

Foam has also been a versatile means of transporting solids (such as sands in production wells or cuttings in drilling wells). In Okpobiri and Ikoku's study (1986), a semi-empirical method was developed to predict the frictional pressure losses caused by solid/foam slurry flow and the transition between foam and mist flows. The results showed that mostly laminar flow regime was observed with the foam quality ( $f_g$ ) ranging from 55% (i.e., minimum at the bottom hole) and 96%

(i.e., maximum at the annular surface). Li and Kuru (2003a, 2003b) and Osunde and Kuru (2006) investigated cutting transport with foam in vertical wells and horizontal wells using numerical modeling. The results showing cutting transport efficiency were analyzed as a function of gas and liquid rates, reservoir influx, circulation rates and borehole geometry. Chen et al. (2007, 2009) conducted a similar experimental study in horizontal downhole to investigate foam rheology and the effect of temperature and pressure on cutting transport efficiencies in a range of pipe geometries, multiple phases, and inclination angles. Saxena et al. (2017) also investigated foam flow experimentally in various pipe diameters with and without cuttings involved. Tested at three different qualities (75, 83, and 88%), the results showed that the frictional pressure drop increased with the total volumetric rate or velocity. In addition, higher foam viscosity and lower foam density were caused by increasing foam quality ( $f_g$ ), and the presence of cutting particles resulted in additional pressure drops. In spite of numerous studies, there still is a gap between experimental data and numerical simulations even in commercial software, as reported by Nakagawa et al. (1999). There have also been attempts to model the non-Newtonian rheological properties of foam-solid mixtures (Kam et al., 2002; Kam and Rossen, 2002).

A clear understanding of foam rheology is very important to predict various operations associated with foam drilling or cleanup processes. In addition to foam quality ( $f_g$ ), foam texture, which is referred to as average bubble size and bubble-size distribution, is another key parameter to characterize the rheological properties of foams. A series of recent foam experimental studies in a range of pipe sizes and inclination angles and in the presence of polymers (Bogdanovic et al., 2009; Gajbhiye and Kam, 2011, 2012; Edrisi et al., 2014) presented the concept of a threshold foam quality,  $f_g^*$ , above which bubbles are unstable and bubble stability is very sensitive to foam quality, and below which bubbles are stable with relatively uniform bubble sizes, as shown in



Figure 4. 1 . An example of the experimental data sets with frictional pressure drop contours at various flow rates in Figure 4. 1 presents the high-quality regime where  $f_g > f_g^*$  and the pressure drop decreases with increasing gas velocity ( $u_g$ ) at given liquid velocity ( $u_w$ ), showing unstable slug flow pattern (i.e., repetition of free gas and fine-textured foams). On the contrary, it presents the low-quality regime where  $f_g < f_g^*$  and the pressure drop increases with increasing gas velocity ( $u_g$ ) at given liquid velocity ( $u_w$ ), showing stable plug flow pattern (i.e., flow of only stable and fine-textured foams). This threshold foam quality ( $f_g^*$ ) between the high-quality regime and low-quality regime varies depending on surfactant types and concentrations, presence of additives, pipe characteristics, and many other experimental conditions. Edrisi and Kam (2013) proposed a foam model to capture the presence of the two regimes and related foam properties by using 5 model parameters. Edrisi and Kam (2015) applied the model to see the implication of the two foam flow regimes in large-scale foam circulation tests.

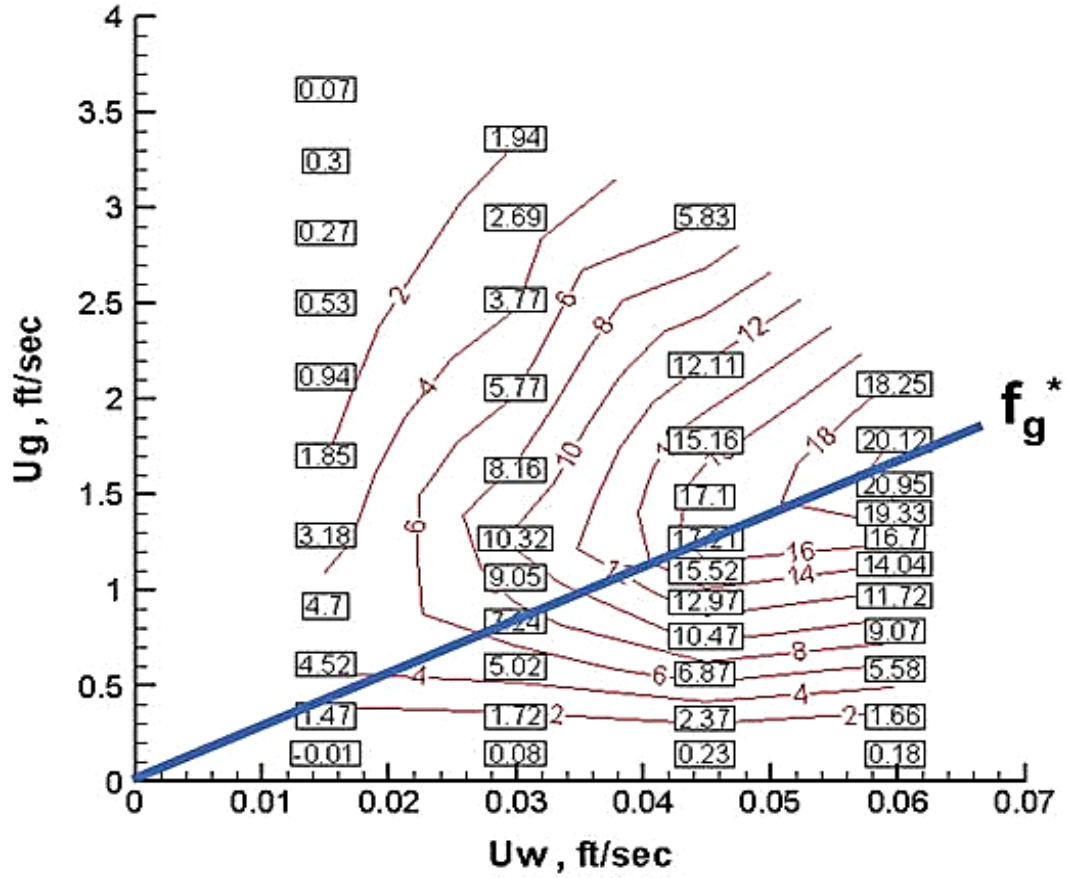


Figure 4. 1 Frictional pressure loss contours from surfactant foam flow experiments

Recently, Wang et al. (2017) developed a new modeling technique, as shown in Figure 4. 2 , which overcame the limitations of Edrisi and Kam's model (2013). By introducing 9 model parameters as shown in Figure 4. 2 , this new model allows both high-quality regime (Domain 1 in Figure 4. 2 ) and low-quality regime (Domain 2 in Figure 4. 2 ) to have its own rheological properties independently, defined by two Power-Law parameters in each regime (i.e., consistency index and Power-Law exponent ( $K_H$  and  $n_H$  in the high-quality regime;  $K_L$  and  $n_L$  in the low-quality regime)). Such an improvement was possible by introducing a reference point (i.e., reference flow rates  $U_{wRef}$  and  $U_{gRef}$ , and corresponding reference frictional pressure drop  $\Delta P_{Ref}$ , as shown by ( $U_{wRef}$ ,  $U_{gRef}$ ,  $\Delta P_{Ref}$ ) in Figure 4. 2 ) where foam rheology can be defined along the boundary lines of the transition region (Domain 3 in Figure 4. 2 ). There are two other model parameters, the

average slope of pressure contours ( $m_H$  and  $m_L$  in the high-quality and low-quality regimes, respectively), to define the sensitivity of foams to gas and liquid velocities. Note that the boundary between the high-quality and low-quality regime,  $f_g^*$ , is determined by the foam quality at the reference point, i.e.,  $f_g^* = u_{gRef}/(u_{wRef} + u_{gRef})$ . Domain 3 in Figure 4. 2 is simply a transition region connecting contour lines with the same pressure drops in Domain 1 and Domain 2. Wang et al. (2017) has more details about this modeling technique.

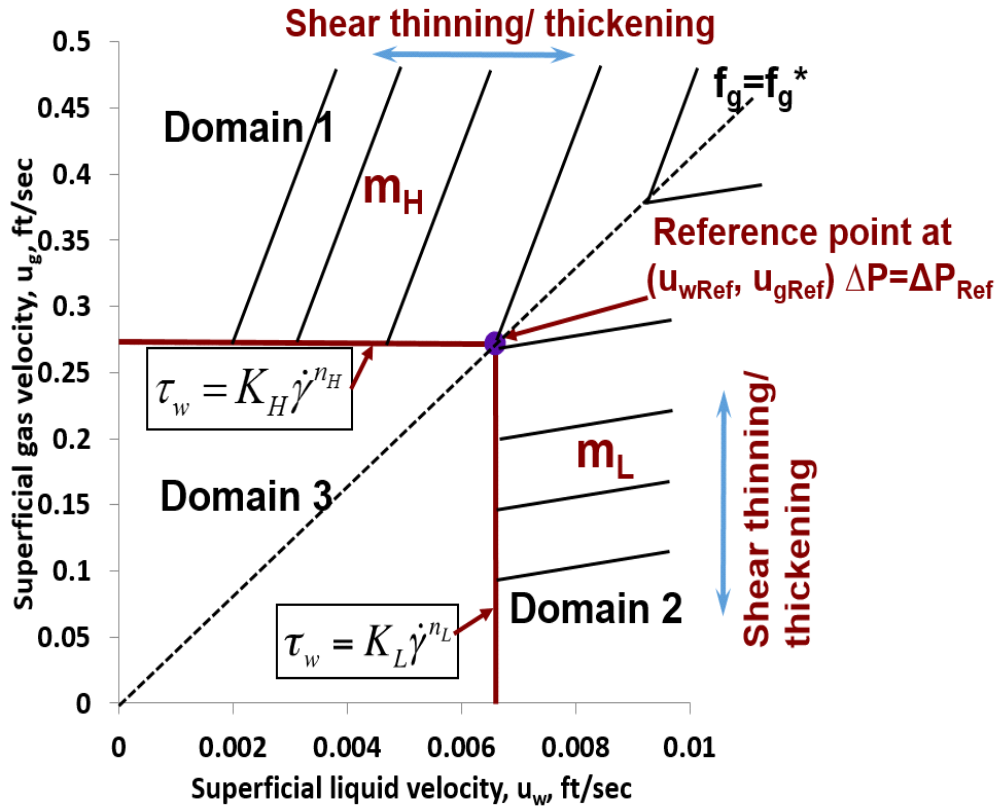


Figure 4. 2 A schematic figure showing nine parameters in the new foam rheology model

#### 4.2 Objectives

The objective of this study is to apply Wang et al.'s model (2017) to three different scenarios of drilling and cleanup field applications – a vertical well, an inclined well (or, a well with mainly inclined segment), and a horizontal well (or, a well with mainly horizontal segment), all with 10000 ft (3048 m) lengths – and to demonstrate the robustness of the model. The results are compared

with Chen's model (2009) (i.e., a model with only stable foams (meaning the low-quality regime)) and Edrisi and Kam's model (2013) (i.e., a model with both high-quality and low-quality regimes, but foam rheology in both regimes dependent upon each other). This study also extends investigation into the cases when there is a formation influx of water or gas.

### 4.3 Methodology

For foam flow in drill pipe or annulus, according to the momentum-balance equation, the total pressure drop ( $\Delta P_t$ ) consists of three major components, hydrostatic pressure loss ( $\Delta P_h$ ), acceleration pressure loss ( $\Delta P_a$ ), and frictional pressure loss ( $\Delta P_f$ ), i.e.,

$$\Delta P_t = \Delta P_h + \Delta P_a + \Delta P_f \quad (4.1)$$

where the hydrostatic pressure loss  $\Delta P_h$  is expressed as follows:

$$\Delta P_h = 0.052\rho_m \quad (4.2)$$

The equations below are used to calculate mixture density ( $\rho_m$ ), total flow rate ( $Q_t$ ), total mixture velocity ( $u_t$ ), and compressible gas density ( $\rho_g$ ):

$$\rho_m = \rho_g \left( \frac{Q_g}{Q_t} \right) + \rho_L \left( \frac{Q_w}{Q_t} \right) = \rho_g (f_g) + \rho_w \quad (4.3)$$

$$Q_t = Q_g + Q_w \quad (4.4)$$

$$u_t = u_w + u_g = \frac{Q_t}{2.448d^2} \quad (4.5)$$

for drill pipe flow with pipe inner diameter  $d$ ,

$$u_t = u_w + u_g = \frac{Q_t}{2.448(d_o^2 - d_i^2)} \quad (4.6)$$

for annulus flow with inner and outer diameters,  $d_i$  and  $d_o$  respectively, and

$$\rho_g = \frac{PM}{ZRT} \quad (4.7)$$

for any pressure and temperature conditions ( $P$ ,  $T$ ) with compressibility factor  $Z$  calculated from molecular weight  $M$  and the ideal gas law constant  $R$ .

The frictional pressure loss ( $\Delta P_f$ ) can be calculated as described in Figure 4. 1 and Figure 4. 2, and the acceleration pressure loss ( $\Delta P_a$ ) is ignored due to its negligible contribution. Field units are used in these equations, such as [psia] for pressure, [ $^{\circ}$ F] for temperature, [gpm] for flow rate, [ft/s] for velocity, [inch] for diameter, [ppg] for density, [lbm/lbmol] for molecular weight, and [J/mol. K] for the ideal gas law constant.

This study borrows the rheological properties of low-quality-regime foams from the experimental study of Chen et al. (2007), which defines the consistency index (K) and Power-Law exponent (n) based in liquid-phase viscosity ( $\mu_w$ ) and foam quality ( $f_g$ ) as follows:

$$K/\mu_w = e^{af_g^2 + bf_g + c} \quad (4.8)$$

$$n = -0.45f_g + 0.7633 \quad (4.9)$$

where, a, b, and c are model parameters defined as

$$a = (-0.533\mu_w^2 + 3.6735\mu_w - 13.546) \quad (4.10)$$

$$b = (0.8926\mu_w^2 - 6.5877\mu_w + 29.966) \quad (4.11)$$

$$c = (-0.3435\mu_w^2 + 2.5273\mu_w - 14.218) \quad (4.12)$$

The parameters K and  $\mu_w$  have the units of [ $\frac{\text{dyne-s}^n}{\text{cm}^2}$ ] and [cp]. Note that these equations are not used in the new model explicitly; they are rather incorporated implicitly to determine a series of pressure contour lines in the low-quality regime (see Figure 4. 2 ) through which they help determining three of the nine model parameters ( $m_L$ ,  $K_L$  and  $n_L$ ).

In addition, this study borrows the high-quality regime foam rheology from Edrisi and Kam (2013), which is originated from the experimental data of Edrisi et al. (2014). They include next three of the nine model parameters ( $m_H$ ,  $K_H$  and  $n_H$ ).

As a result, there are only three more parameters to decide (i.e.,  $u_{wRef}$ ,  $u_{gRef}$ , and  $\Delta P_{Ref}$ ), which is related to how to define the reference point ( $(u_{wRef}, u_{gRef}, \Delta P_{Ref})$  in Figure 4. 2 ) and, in turn, the

size of the transition region (Domain 3 in Figure 4. 2 ).

Once these nine parameters are determined, Figure 4. 3 through Figure 4. 5 demonstrate graphically how the frictional pressure loss can be calculated depending on which domain the velocities of interest fall into. Note again that  $(u_{wRef}, u_{gRef}, \Delta P_{Ref})$  defines the reference point,  $K_H$  and  $n_H$  define the Power-Law parameters along  $u_g = u_{gRef}$ ,  $K_L$  and  $n_L$  define the Power-Law parameters along  $u_w = u_{wRef}$ , and  $m_H$  and  $m_L$  define the slopes of average contour line slopes in the high-quality and low-quality regimes, respectively. Suppose any  $(u_w, u_g)$  is given arbitrarily, and the corresponding frictional pressure loss is to be calculated. Such an assignment can be represented by the point “a”, “b”, or “c” in Figure 4. 3 through Figure 4. 5 for Domain 1, 2, or 3, respectively.

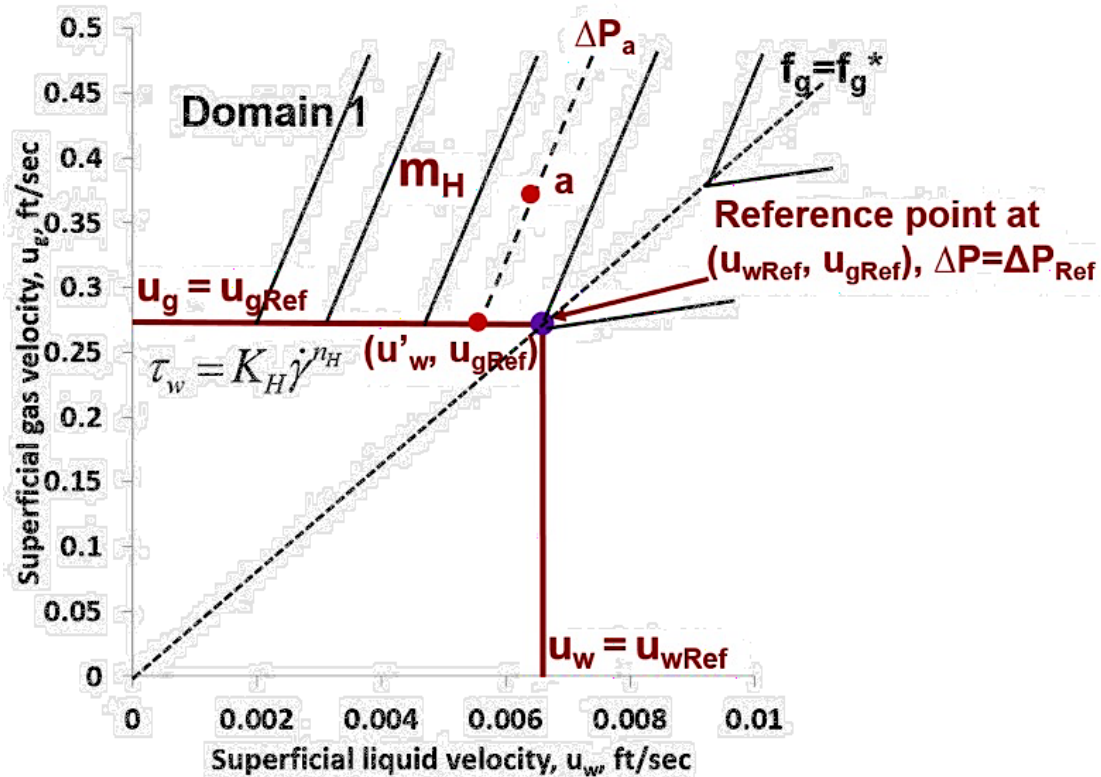


Figure 4. 3 A schematic on how to determine the frictional pressure gradient in Domain 1

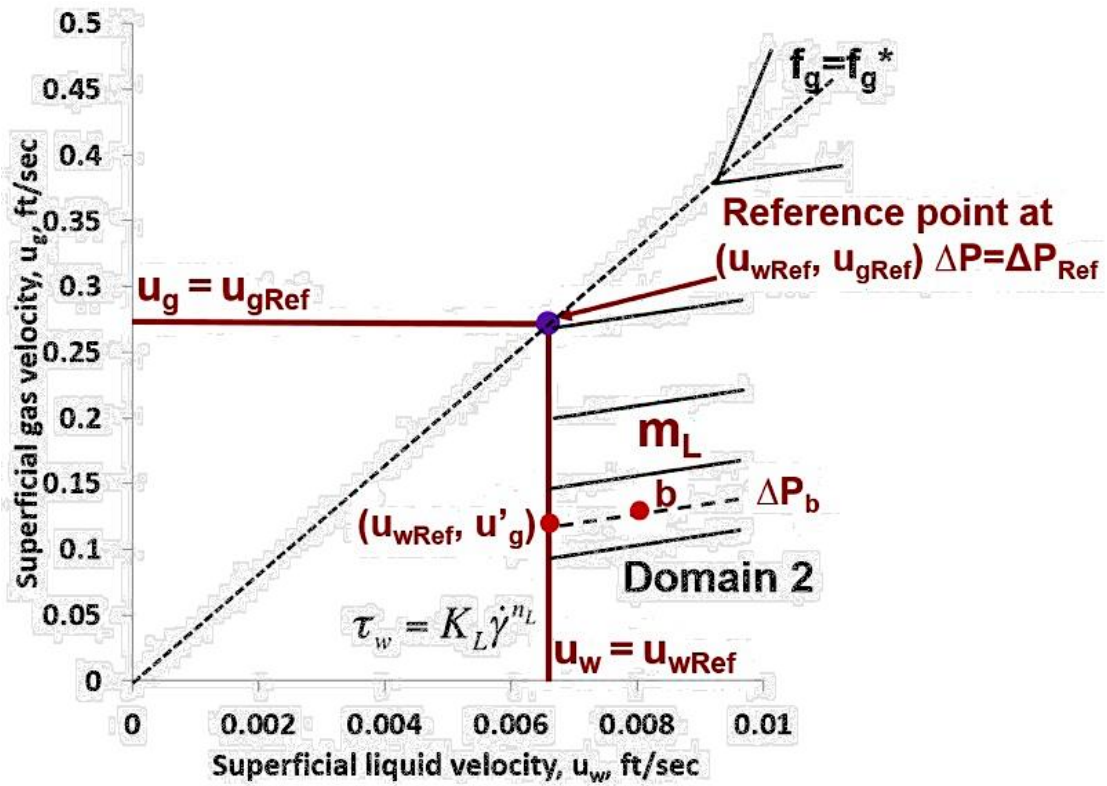


Figure 4. 4 A schematic on how to determine the frictional pressure gradient in Domain 2

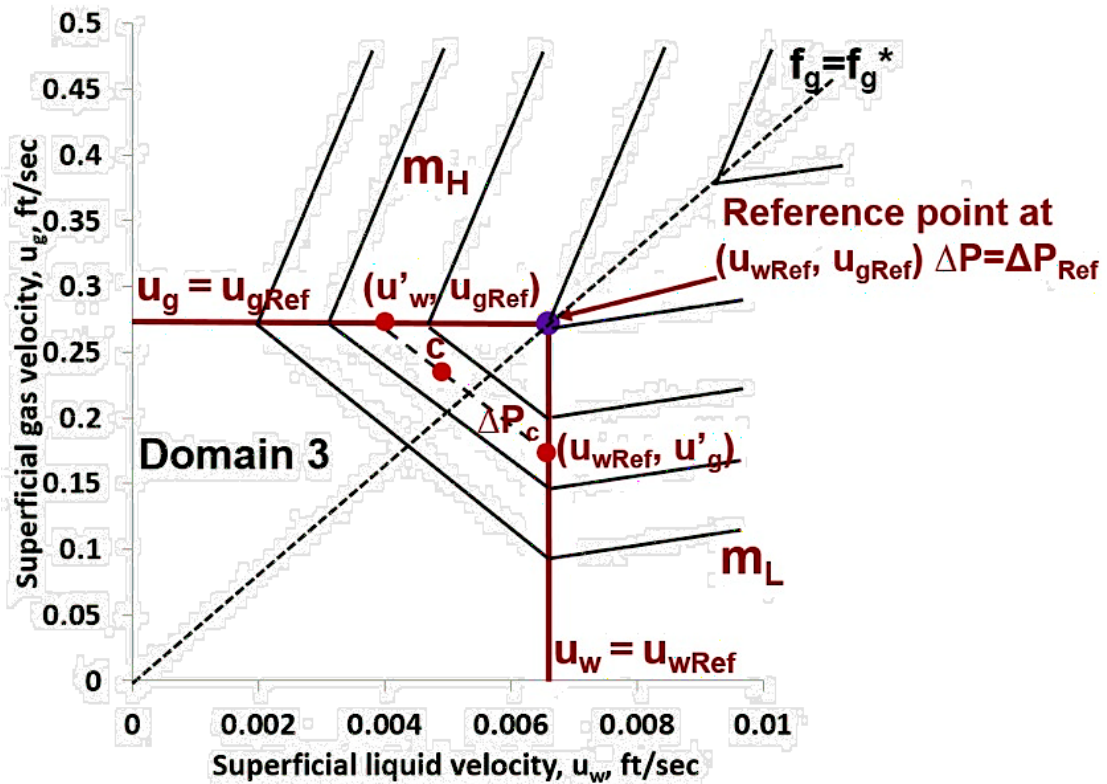


Figure 4. 5 A schematic on how to determine the frictional pressure gradient in Domain 3

The next step is to follow the average slope in the domain to reach the point  $(u'_w, u_{gRef}, \Delta P_a)$  for point “a”,  $(u_{wRef}, u'_g, \Delta P_b)$  for point “b”, and either  $(u'_w, u_{gRef}, \Delta P_c)$  or  $(u_{wRef}, u'_g, \Delta P_c)$  for point “c”. Table 4. 1 and Table 4. 2 show examples of these nine model parameters required for the modeling in this study. The Power-Law rheology model defines the relationship between shear stress ( $\tau_w$ ) and shear rate ( $\dot{\gamma}_w$ ) along the  $u_g = u_{gRef}$  line or  $u_w = u_{wRef}$  line as follows for the high-quality and low-quality regimes, respectively: i.e.,

$$\tau_w = K_H \dot{\gamma}_w^{n_H} \quad (4.13)$$

$$\tau_w = K_L \dot{\gamma}_w^{n_L} \quad (4.14)$$

The definitions of shear stress ( $\tau_w$ ) and shear rate ( $\dot{\gamma}_w$ ) are given by

$$\tau_w = 3d \frac{\Delta P_f}{\Delta L} \quad (4.15)$$

where the frictional pressure loss ( $\Delta P = \Delta P_f$ ) over the length scale of  $\Delta L$ , and

$$\dot{\gamma}_w = \frac{96u_w}{d} \quad (4.16)$$

for the high-quality regime foams and

$$\dot{\gamma}_w = \frac{96u_g}{d} \quad (4.17)$$

for the low-quality regime foams. The frictional pressure loss can be determined by using the Power-Law fluid rheology, i.e.,

$$\frac{\Delta P_a}{\Delta P_{Ref}} = \left( \frac{u'_w}{u_{wRef}} \right)^{n_H}, \text{ for point “a”} \quad (4.18)$$

$$\frac{\Delta P_b}{\Delta P_{Ref}} = \left( \frac{u'_g}{u_{gRef}} \right)^{n_L}, \text{ for point “b”} \quad (4.19)$$

or

$$\frac{\Delta P_c}{\Delta P_{Ref}} = \left( \frac{u'_w}{u_{wRef}} \right)^{n_H} = \left( \frac{u'_g}{u_{gRef}} \right)^{n_L} \text{ for point “c”}. \quad (4.20)$$



Table 4. 1 Nine input parameters for foam flow inside drill pipe

Parameters		Units	
$u_{wRef}$	Superficial liquid velocity at the reference point	1.53	ft/s
$u_{gRef}$	Superficial gas velocity at the reference point	8.7	ft/s
$\Delta P_{Ref}$	Pressure drop at the reference point (frictional)	0.05	psi over 1 ft horizontal distance
$m_H$	Average contour slope in the high-quality regime	90	Dimensionless
$m_L$	Average contour slope in the low-quality regime	2.47	Dimensionless
$K_H$	Consistency index in the high-quality regime	0.0322	$\frac{\text{dyne} - \text{s}^{0.8858}}{\text{cm}^2}$
$n_H$	Power-Law Exponent in the high-quality regime	0.8858	Dimensionless
$K_L$	Consistency index in the low-quality regime	0.0001	$\frac{\text{dyne} - \text{s}^{1.6145}}{\text{cm}^2}$
$n_L$	Power-Law Exponent in the low-quality regime	1.6145	Dimensionless

Table 4. 2 Nine input parameters for foam flow in the annulus

Parameters		Units	
$u_{wRef}$	Superficial liquid velocity at the reference point	0.46	ft/s
$u_{gRef}$	Superficial gas velocity at the reference point	2.6	ft/s
$\Delta P_{Ref}$	Pressure drop at the reference point (frictional)	0.05	psi over 1 ft horizontal distance
$m_H$	Average contour slope in the high-quality regime	90	Dimensionless
$m_L$	Average contour slope in the low-quality regime	1.9	Dimensionless
$K_H$	Consistency index in the high-quality regime	0.0518	$\frac{\text{dyne} - \text{s}^{1.1223}}{\text{cm}^2}$
$n_H$	Power-Law Exponent in the high-quality regime	1.1223	Dimensionless
$K_L$	Consistency index in the low-quality regime	0.0008	$\frac{\text{dyne} - \text{s}^{1.652}}{\text{cm}^2}$
$n_L$	Power-Law Exponent in the low-quality regime	1.652	Dimensionless

For three scenarios considered as shown in Figure 4. 6 (vertical, inclined and horizontal wells), a finite difference calculation is conducted at given gas and liquid rates. Iterations are needed to satisfy the pre-specified backpressure ( $P_b$ ) at the surface of annular section. Note that there is an additional pressure drop through the nozzles at the drill bit ( $\Delta P_{bit}$ ) between  $N^{th}$  and  $(N+1)^{th}$  nodes, i.e.,

$$\Delta P_{bit} = \frac{8.311 \times 10^{-5} \rho_m Q_t^2}{\left[0.95 n_{noz} \times \left(\frac{\pi}{4} D_{noz}^2\right)\right]^2} \quad (4.21)$$

where  $n_{noz}$  for the number of nozzles,  $D_{noz}$  for nozzle diameter in [inch],  $\rho_m$  for foam mixture density in [ppg], and  $Q_t$  for total flow rate in [gpm]. The apparent foam mixture viscosity ( $\mu_{app}$ ) for drill pipe and annulus are given by

$$\mu_{app} = 47900 \frac{\tau_w}{\dot{\gamma}_w} = 47900 \frac{3d \frac{\Delta P_f}{\Delta L}}{\frac{96u_t}{d}} \quad (4.22)$$

for flow in drill pipe and

$$\mu_{app} = 47900 \frac{\tau_w}{\dot{\gamma}_w} = 47900 \frac{3(d_o - d_i) \frac{\Delta P_f}{\Delta L}}{\frac{144u_t}{(d_o - d_i)}} \quad (4.23)$$

for flow in annulus. The units are [lbf/ft<sup>2</sup>] for shear stress ( $\tau_w$ ), [s<sup>-1</sup>] for shear rate ( $\dot{\gamma}_w$ ), [cp] for apparent viscosity ( $\mu_{app}$ ).

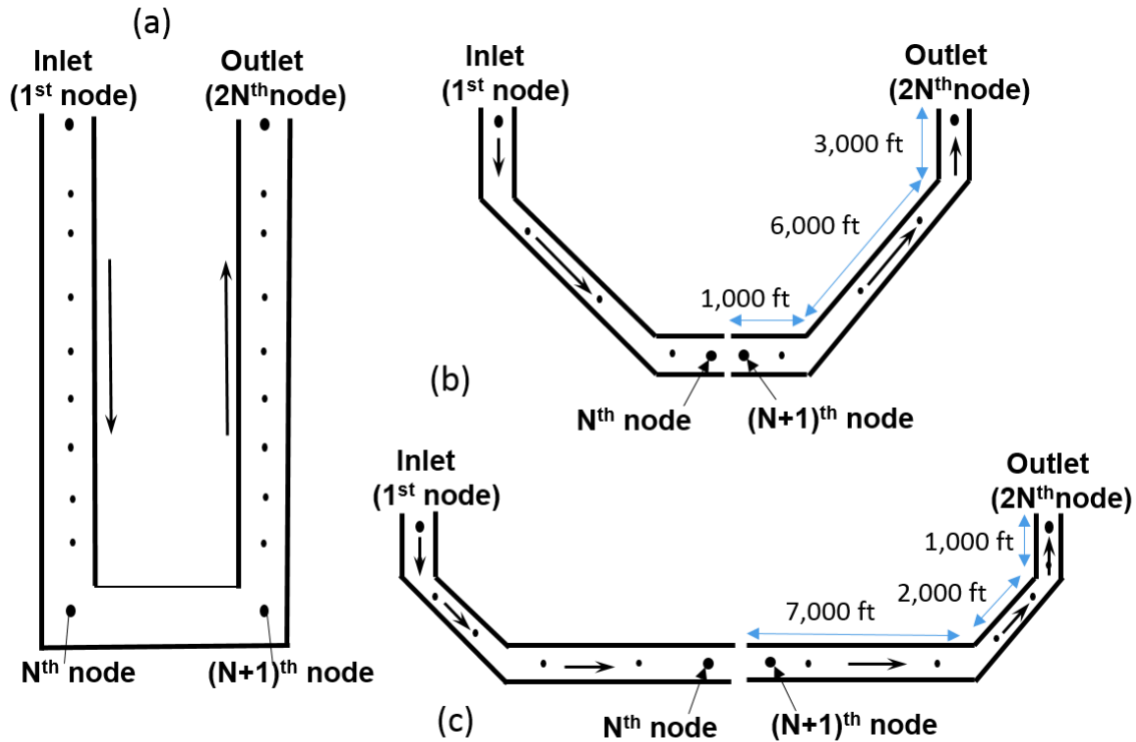


Figure 4. 6 Schematics of U-tube concept wellbore configurations: (a) vertical well (b) inclined well (c) horizontal well

Numerical calculation conducted in this study essentially takes advantage of material-balance and momentum-balance equations for the pressure drop calculations. For steady-state flow, the following outlines the algorithm for the field case shown in Table 4. 3 briefly.

1. Read input parameters as shown in Table 4. 1 , Table 4. 2 , and Table 4. 3 , including wellbore geometries and interval sizes for numerical calculations.
2. Specify the boundary conditions, that is, the outlet pressure as well as gas and liquid flow rates at the standard condition (or, mass rates equivalently).
3. Assume the inlet pressure at the 1<sup>st</sup> node.
4. Calculate foam mixture properties such as density, viscosity, Z factor, velocity, flow rate and so on.
5. Calculate the total pressure loss based on the frictional and hydrostatic components over

the interval size specified. Determine the pressure in the next node.

6. Go to the next node and repeat step 4 and 5, until it reaches the drill bit ( $N^{\text{th}}$  node).
7. Determine the pressure drop through the bit and calculate the pressure at the  $(N+1)^{\text{th}}$  node.
8. Go to the next node and repeat step 4 and 5, until it reaches surface.
9. If the surface pressure calculated is close enough to the back pressure, the steady-state solution is obtained. If not, repeat the entire calculations by using a new assumed inlet pressure.

#### 4.4 Results and Discussions

As shown in Figure 4. 6 , the well consists of three components. Following from the injection point ( $1^{\text{st}}$  node), the foam mixture travels down inside drillpipe, through the drill bit, and up along the annulus to reach the annular surface ( $2N^{\text{th}}$  node). Foam model parameters are shown in Table 4. 1 and Table 4. 2 for the flow in the drillpipe and annulus, respectively. The well configuration and related characteristics are summarized in Table 4. 3 .

Table 4. 3 Field data for foam circulation modeling

Wellbore Diameter ( $D_w$ )	8.5 (inch)	Drillpipe OD ( $D_{pout}$ )	5 (inch)
Drillpipe ID ( $D_{pin}$ )	4.276 (inch)	Wall Roughness ( $\epsilon$ )	0
Number of Nozzles ( $n_{noz}$ )	3	Diameter of Nozzles ( $D_{noz}$ )	0.375 (inch)
Inlet Liquid Rate ( $Q_w$ )	40 (gpm)	Inlet Gas Rate ( $Q_g$ )	1300 (scfm)
Outlet Back Pressure ( $P_b$ )	100 (psia)	Formation Fluid Influx ( $Q_{in}$ )	varies (gpm or scfm)
Liquid Viscosity ( $\mu_w$ )	1 (cp)	Liquid Density ( $\rho_w$ )	62.4 (lbm/ft <sup>3</sup> )
Gas Molecular Weight ( $M$ )	28.9 (lbm/lbmol)	Gas Specific Gravity ( $SG$ )	1
Temperature at the Standard Condition ( $T_{sc}$ )	70 (°F)	Pressure at the Standard Condition ( $P_{sc}$ )	14.7 (psia)
Z-factor at the Standard Condition ( $Z_{sc}$ )	1	Vertical Temperature Gradient ( $\Delta T/\Delta Z$ )	1.5 (°F/100ft)
Total Measured Length	10000 (ft)	Interval Size for Vertical Well ( $\Delta L_1$ )	400 (ft)
Interval Size for Inclined Well ( $\Delta L_2$ )	500 (ft)	Interval Size for Horizontal Well ( $\Delta L_3$ )	500 (ft)

Figure 4. 7 through Figure 4. 9 show the calculation results for vertical, inclined, and horizontal wells when there is no formation fluid influx ( $Q_{in} = 0$ ). Each figure consists of the changes in pressure, foam quality, foam density, and total velocity as a function of distance from the injection point, where the arrows represent the direction of foam flow, either down to the bottom hole along the drillpipe or up to the annular surface along the annulus. In all cases, the injection condition (in terms of gas and liquid rates) and the outlet condition (in terms of annular backpressure) require foam quality of 97 % at the annular surface.

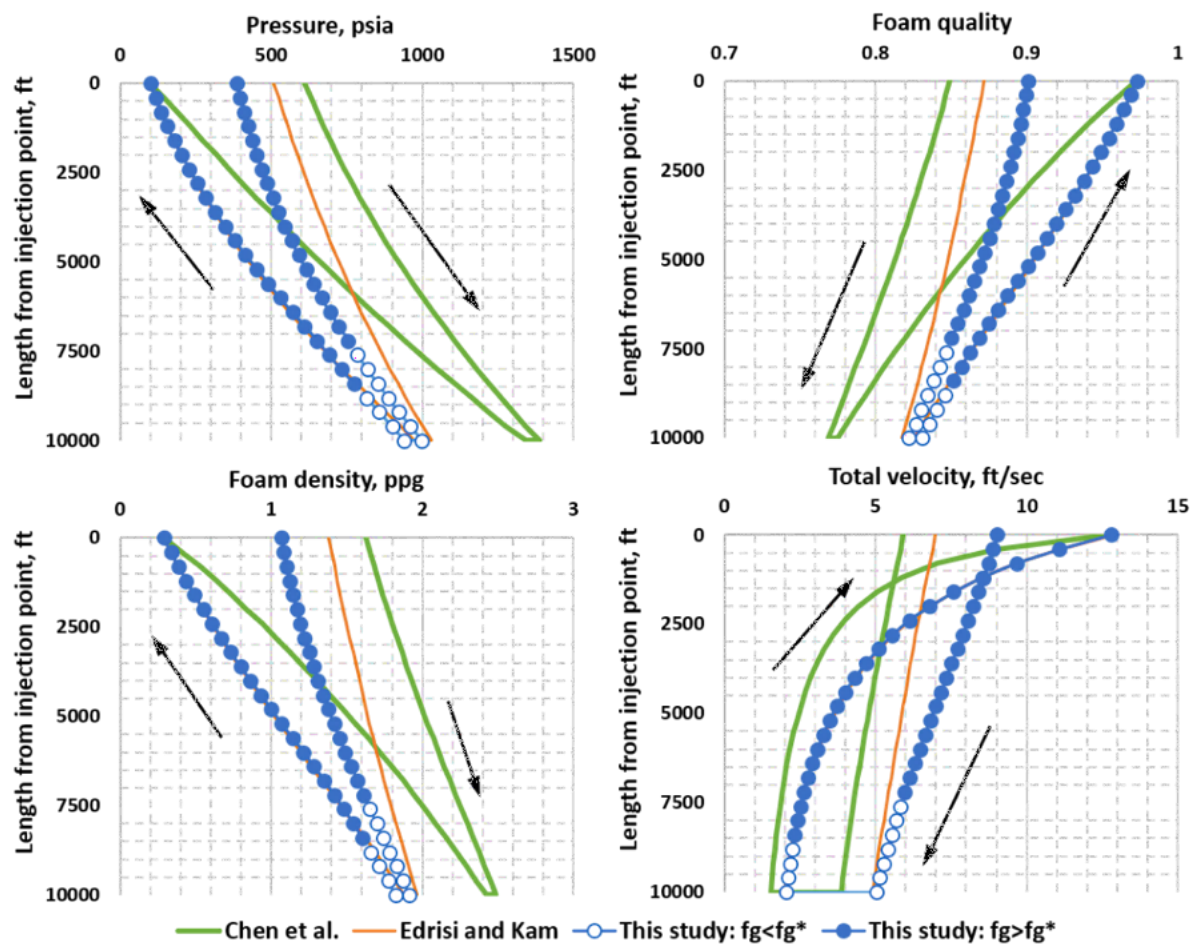


Figure 4. 7 Steady-state simulation results for the vertical well

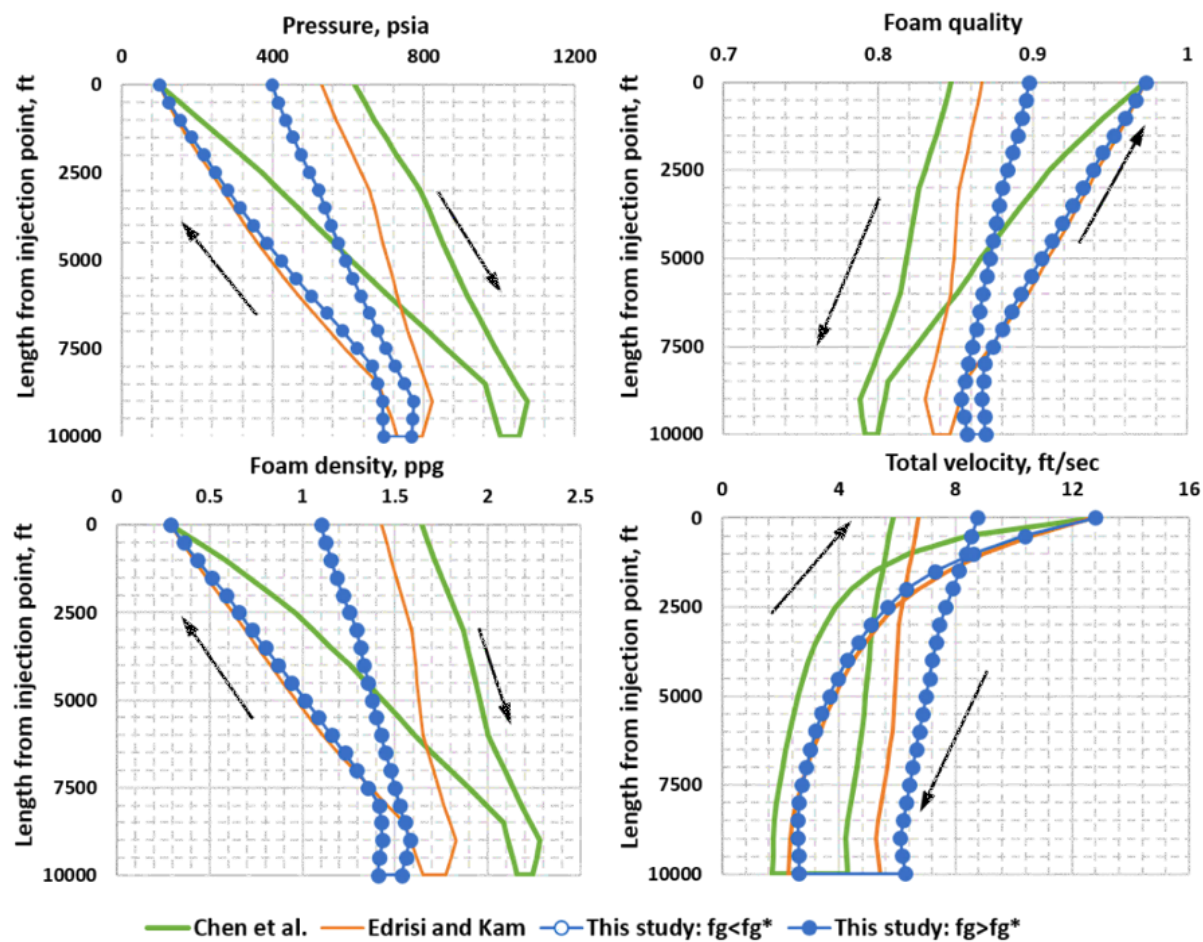


Figure 4. 8 Steady-state simulation results for the inclined well

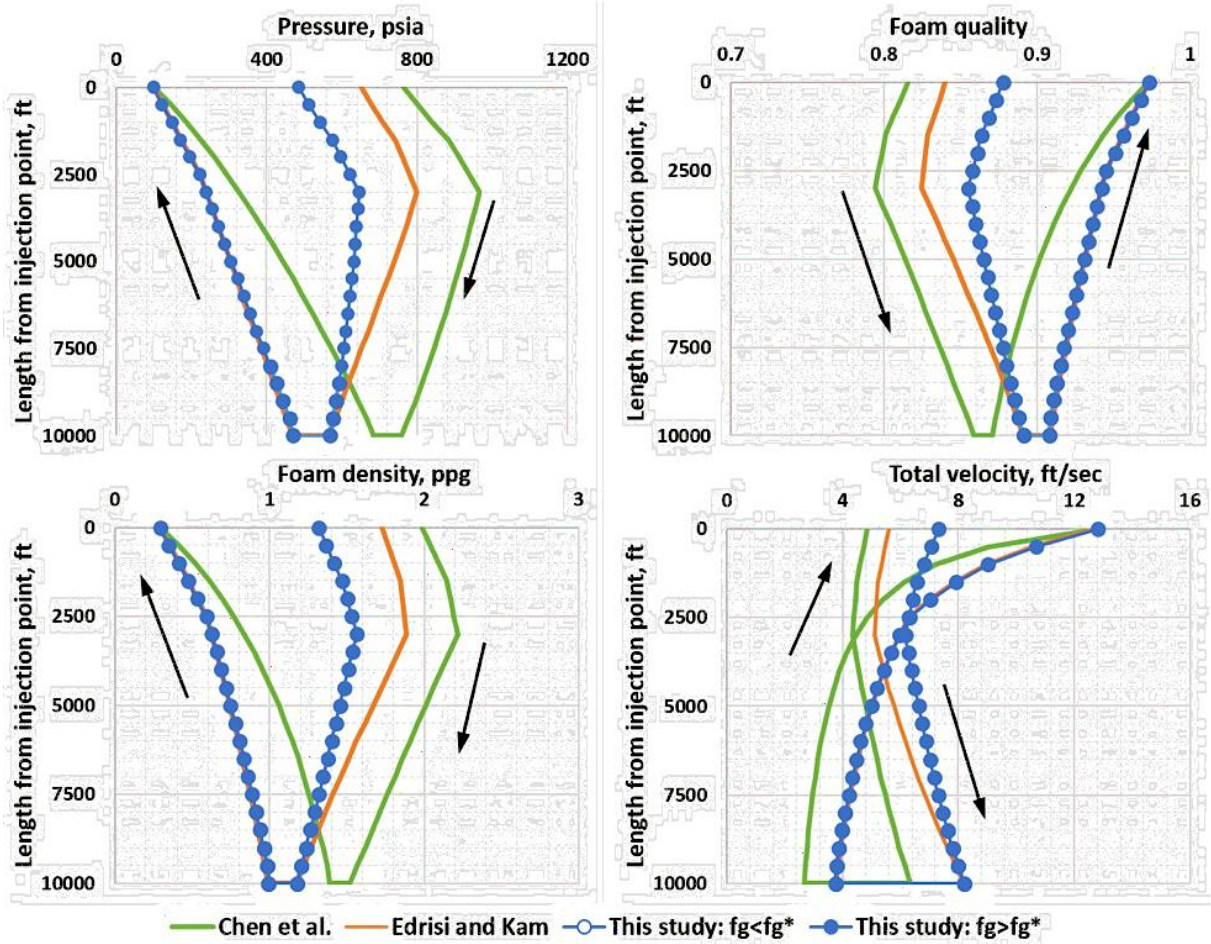


Figure 4. 9 Steady-state simulation results for the horizontal well

The results for the vertical well in Figure 4. 7 show the general trend that is consistent with what is expected (note that the length on the y axis is equivalent to vertical depth in this case). First, the pressure increases with depth primarily because of hydrostatic pressure, and the slope (meaning the pressure gradient) is steeper along the drillpipe than the annulus due to higher frictional pressure loss in annulus. There exists a pressure discontinuity at the bottom hole which reflects the pressure drop through the nozzles at the bit. The pressure at the annular surface in all cases converges into the backpressure as specified in Table 4. 3 . Second, such a pressure response is well connected to the foam quality plot. Higher pressure means lower gas volume which, in turn, means lower foam quality. Third, foam density also varies accordingly. It is high near the bottom



hole where the pressure is high and foam mixture volume is small. In fact, the foam density plot seems mirror-imaged to the foam quality plot. Last, total velocity is high near the surface and low near the bottom hole due to gas compressibility, but the effect of gas expansion is more significant near the annular surface, playing more important roles in gas velocity and thus total velocity. Once again, the total velocity at the annular surface converges into a fixed value ( $u_t = 12.8 \text{ ft/s}$  ( $3.901 \text{ m/s}$ )), as set by the injection and outlet conditions. In all, the lines are curved, which primarily reflects the fact that the mixture contains a significant portion of compressible gas phase in it.

Figure 4. 10 (a) and Figure 4. 10 (b) help to identify the paths followed by the new model, for the downward flow within drillpipe (i.e., from the top to the bottom of the vertical line in Figure 4. 10 (a)) and for the upward flow in the annulus (i.e., from the bottom to the top of the vertical line in Figure 4. 10 (b)) on the top of contour plots created by using the input parameters in Table 4. 1 and Table 4. 2 respectively.

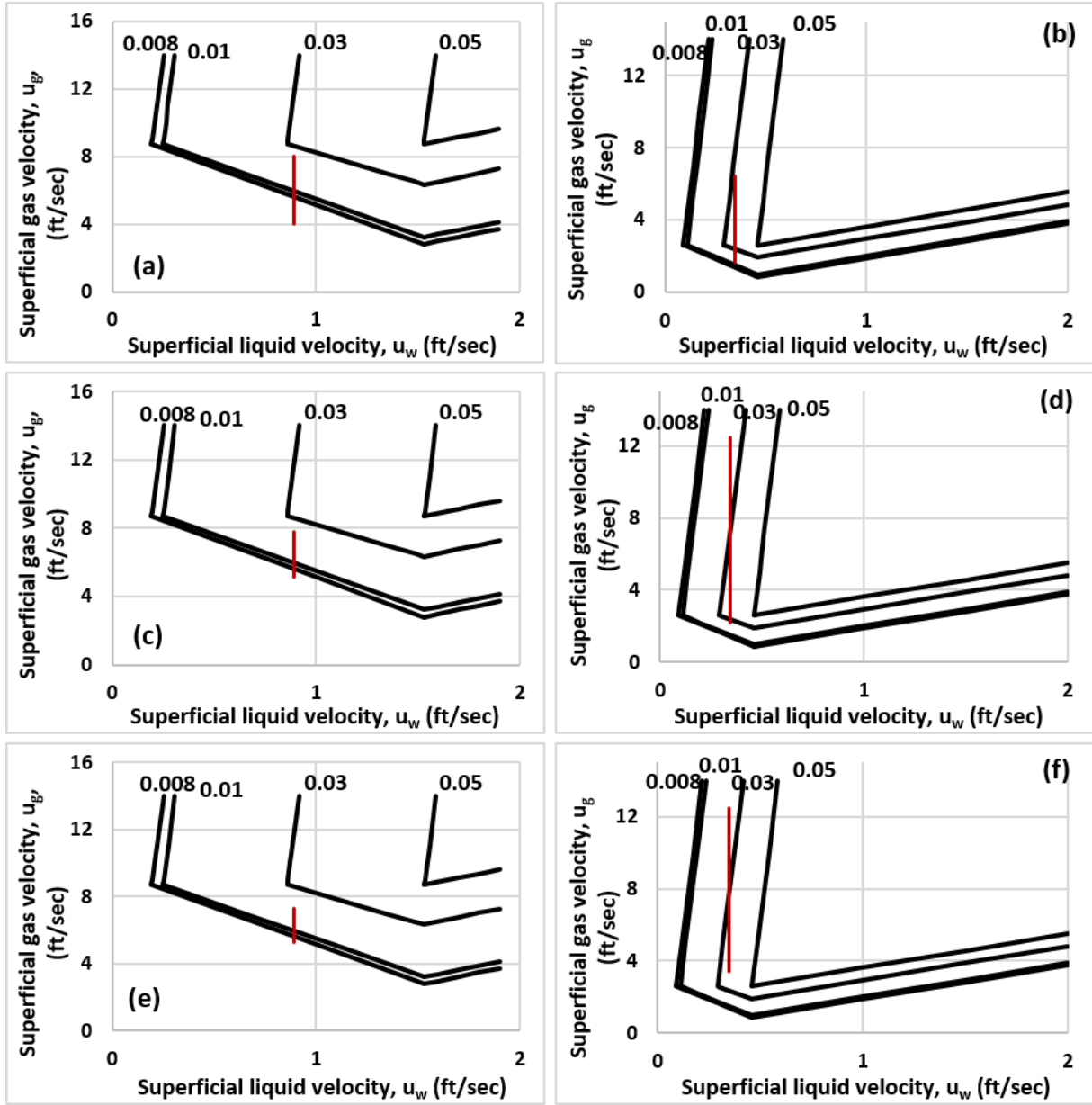


Figure 4.10 Simulated paths along the drill pipe (left) and annulus (right): (a)(b) vertical well, (c)(d) inclined well, (e)(f) horizontal well

The three methods compared in Figure 4.7 show a couple of interesting aspects. First, Chen et al.'s model (2009) based only on the low-quality regime foams over-predicts the change in frictional pressure loss and, as a result, over-predicts the changes in all responses such as pressure, foam quality, foam density, and total velocity. Second, Edrisi and Kam's model (2013), which has both high-quality and low-quality regimes but with no transition region in between, captures the

trend reasonably well but under-predicts the changes because of wider range of low-quality-regime foams. Note that the results from the model used in this study have filled symbols for  $f_g > f_g^*$  and open symbols for  $f_g < f_g^*$ , which makes it possible to keep track of the change in domains, once analyzed together with Figure 4. 10 (a) and Figure 4. 10 (b). (Note that  $f_g^* = 85\%$  in both drillpipe and annulus as shown in the foam quality plot in Figure 4. 7.)

In contrast to the vertical well (Figure 4. 7), the results for the inclined and horizontal wells are shown in Figure 4. 8 and Figure 4. 9, respectively. The overall responses are similar to the case of vertical well, but the less contribution from the hydrostatic pressure loss leaves a clear signature to the inclined and horizontal sections of the trajectories. As indicated by Figure 4. 8 and Figure 4. 9, Figure 4. 10 confirms that, in both inclined and horizontal wells, the paths downward (Figure 4. 10 (c) and Figure 4. 10 (e)) stay within the transition region (Domain 3), while the paths upward (Figure 4. 10 (d) and Figure 4. 10 (f)) mostly stay within the high-quality regime (Domain 1). Because of lacking the transition region, Edrisi and Kam's model (2013) deviates from the results in this study. Chen et al.'s model deviates significantly more because it is based only on foam rheology in the low-quality regime.

Table 4. 4 summarizes the calculation results for all three scenarios in terms of inlet pressure as well as pressure, foam quality, density, and mixture velocity at the bottom hole conditions. It clearly shows that foam modeling techniques based only on fine-textured foam rheology (or, the low-quality regime foam rheology) cannot predict the results accurately. Even the two-flow-regime model without transition region can lead to a significant level of errors.

Table 4. 4 Comparison of three different foam simulation methods

Vertical well case			
	This study	Chen et al. (2009)	Edrisi and Kam (2013)
Inlet Pressure, psia	395	611 (35%)	509 (22%)
BH Pressure, psia	996	1341 (26%)	973 (2%)
BH Foam Quality, %	82	77 (6%)	83 (1%)
BH Density, ppg	1.91	2.43 (21%)	1.88 (2%)
BH mixture Velocity, ft/s	1.95	1.54 (26%)	1.99 (2%)
Inclined well case			
	This study	Chen et al. (2009)	Edrisi and Kam (2013)
Inlet Pressure, psia	402	618 (54%)	529 (32%)
BH Pressure, psia	712	1003 (41%)	731 (3%)
BH Foam Quality, %	87	80 (8%)	85 (2%)
BH Density, ppg	1.44	2.16 (5%)	1.65 (15%)
BH mixture Velocity, ft/s	2.59	1.73 (33%)	2.25 (13%)
Horizontal well case			
	This study	Chen et al. (2009)	Edrisi and Kam (2013)
Inlet Pressure, psia	485	764 (57%)	651 (34%)
BH Pressure, psia	471	685 (45%)	469 (0.4%)
BH Foam Quality, %	91	87 (4%)	91 (0%)
BH Density, ppg	1	1.39 (39%)	1 (0%)
BH mixture Velocity, ft/s	3.75	2.68 (28%)	3.76 (0.3%)

Two more cases are investigated in this study, repeating the same calculations for three scenarios as shown in Figure 4. 7 through Figure 4. 10 – the first with influx of formation water ( $Q_{in} = 4$  gpm ( $0.00025 \text{ m}^3/\text{s}$ ); Figure 4. 11 through Figure 4. 14 ) and the second with influx of formation gas ( $Q_{in} = 500$  scfm ( $0.235 \text{ m}^3/\text{s}$ ); Figure 4. 15 through Figure 4. 18 ). The influx of formation water (which is a tenth of liquid circulation rate) dilutes the concentration of chemicals (such as surfactants and polymers) in the aqueous phase, and thus may change the foam model parameters (e.g., Table 4. 1 and Table 4. 2 ) and steady-state pressure contours (e.g., Figure 4. 10 ). This study assumes, however, that such an effect is negligible, only focusing on the change in flowrates and foam quality primarily.

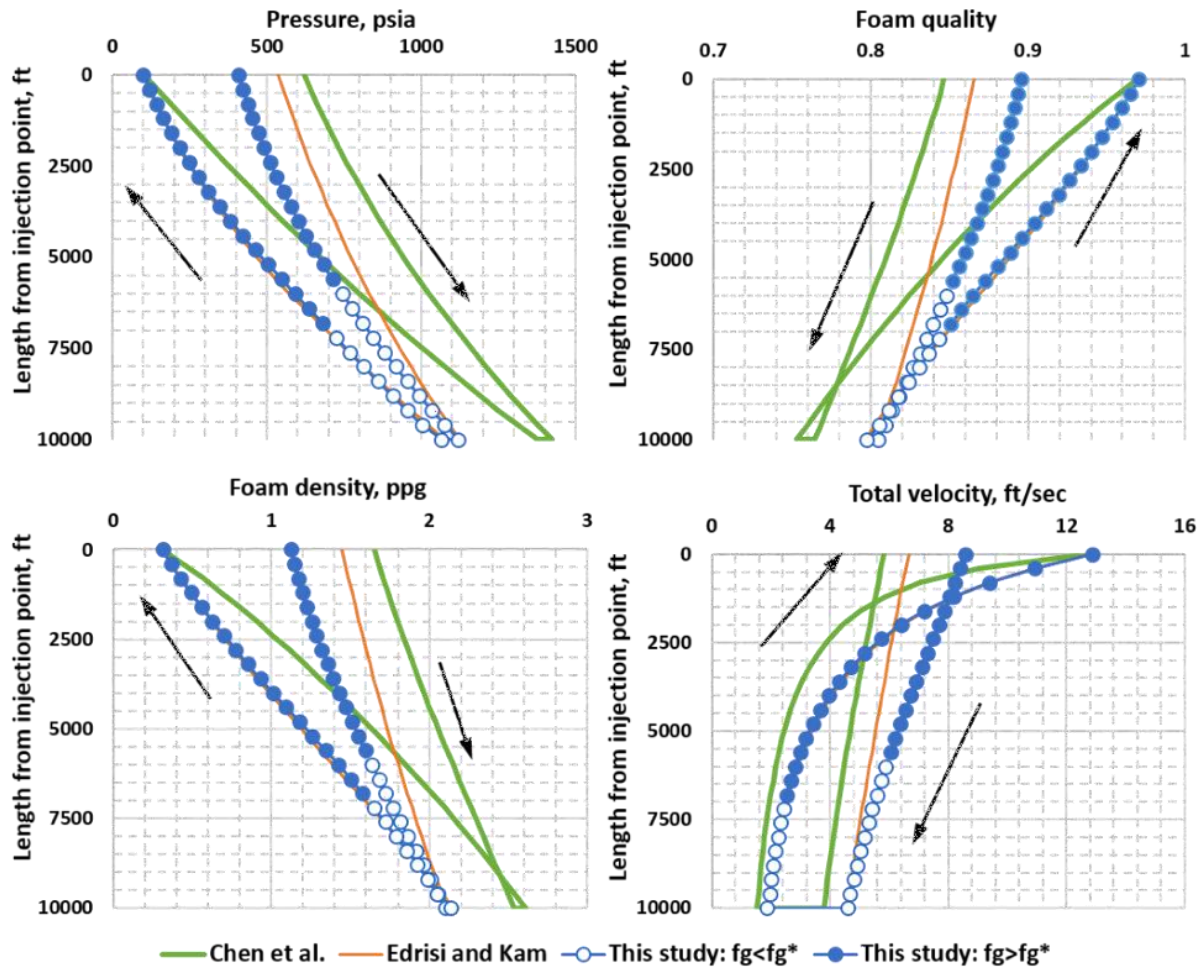


Figure 4. 11 Steady-state simulation results for the vertical well with formation water influx

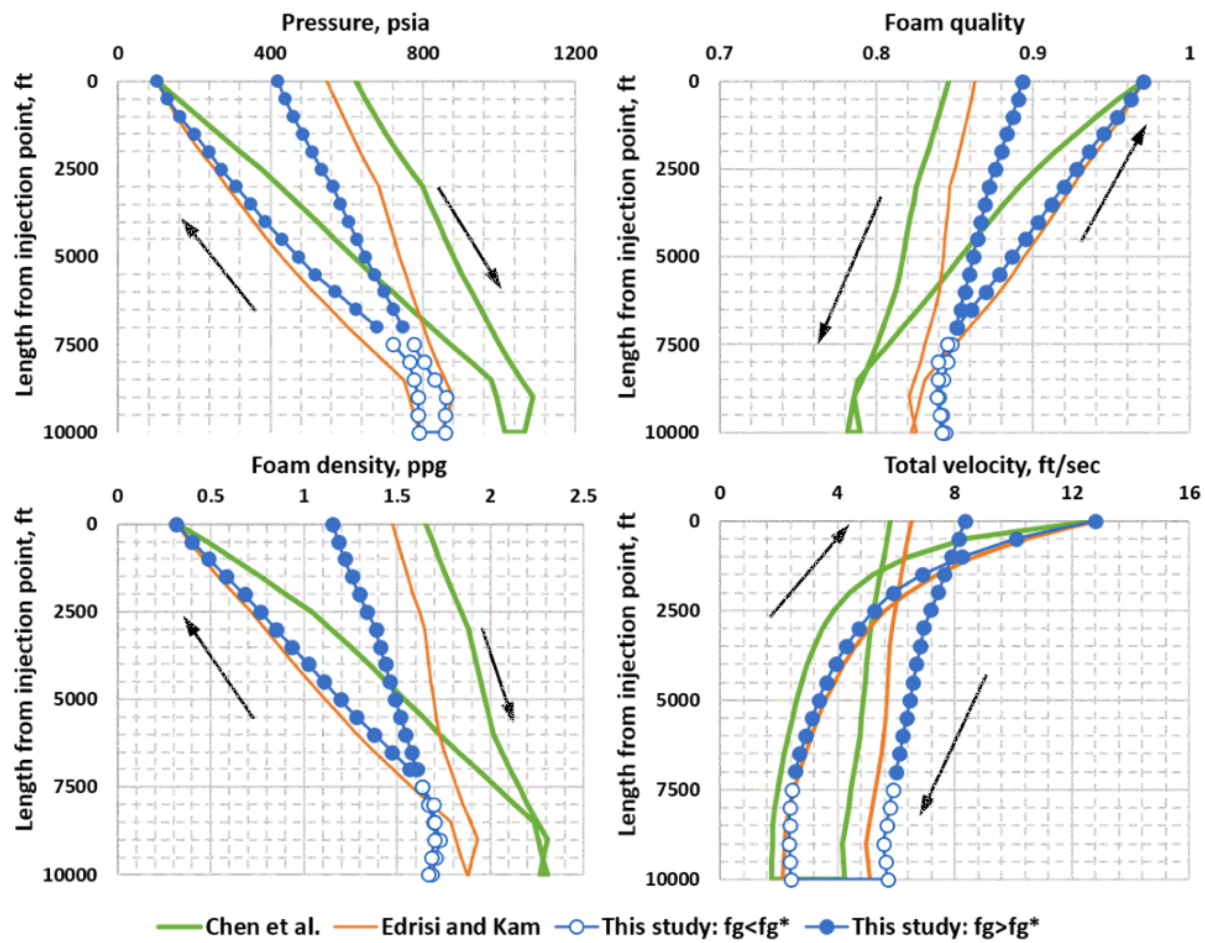


Figure 4. 12 Steady-state simulation results for the inclined well with formation water influx

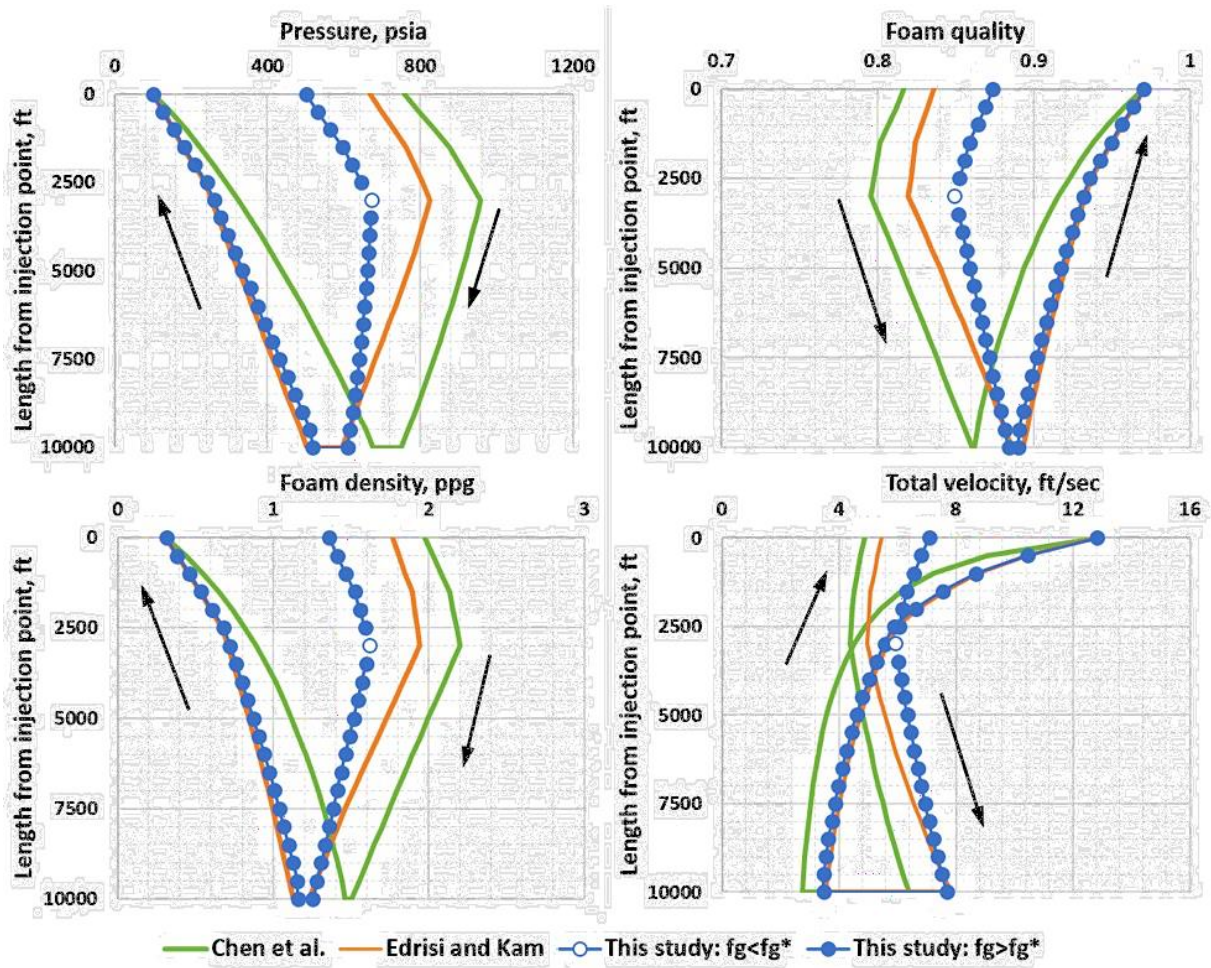


Figure 4. 13 Steady-state simulation results for the horizontal well with formation water influx



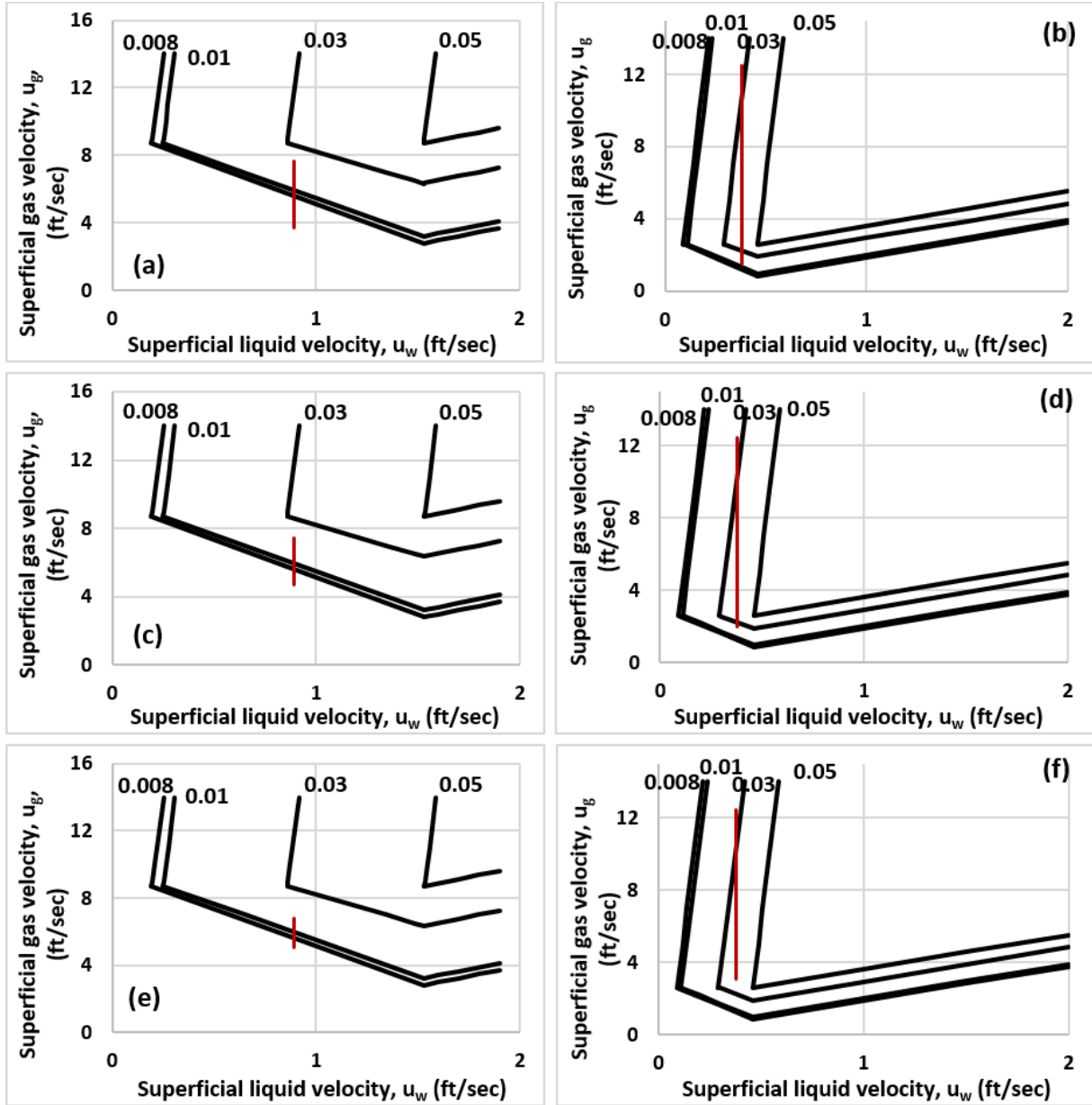


Figure 4. 14 Simulated paths with formation water influx along the drillpipe (left) and annulus (right): (a)(b) vertical well, (c)(d) inclined well, (e)(f) horizontal well

When there is a formation liquid influx at the bottom hole (Figure 4. 11 through Figure 4. 14), the increased liquid rate in the annulus causes an additional hydrostatic pressure loss, which distorts other responses to keep the same backpressure. Overall, there is a significant shift in liquid rate, foam quality, and total velocity in the annulus. Foam quality in the annular surface becomes slightly lower than 97%. When there is a formation gas influx at the bottom hole (Figure 4. 15



through Figure 4. 18 ), the opposite occurs: an increase in gas rate and foam quality, but a decrease in hydrostatic pressure loss. In many field applications, the process requires the bottom hole pressure to be maintained at a certain level. In such a case, Figure 4. 11 through Figure 4. 18 are believed to provide a useful guideline.

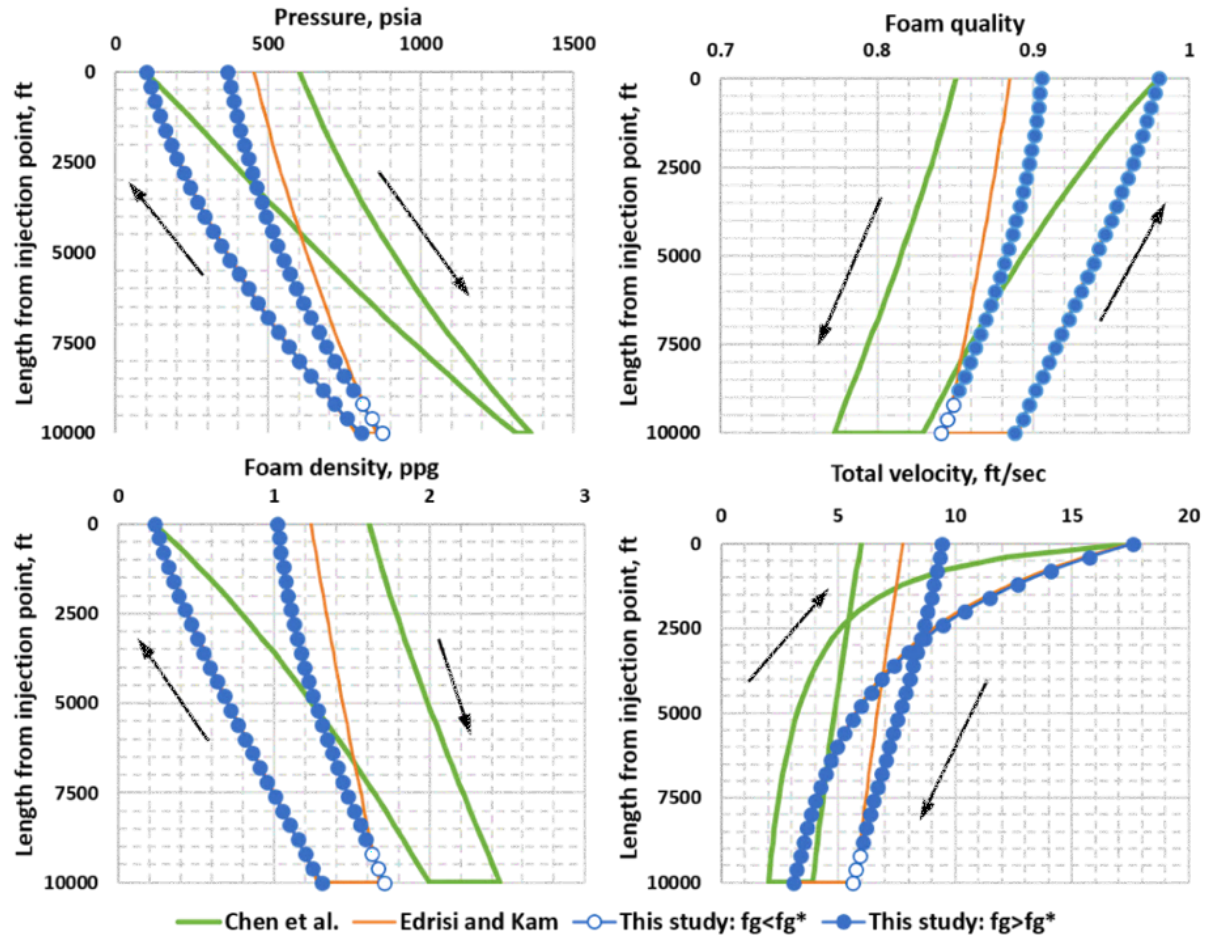


Figure 4. 15 Steady-state simulation results for the vertical well with formation gas influx

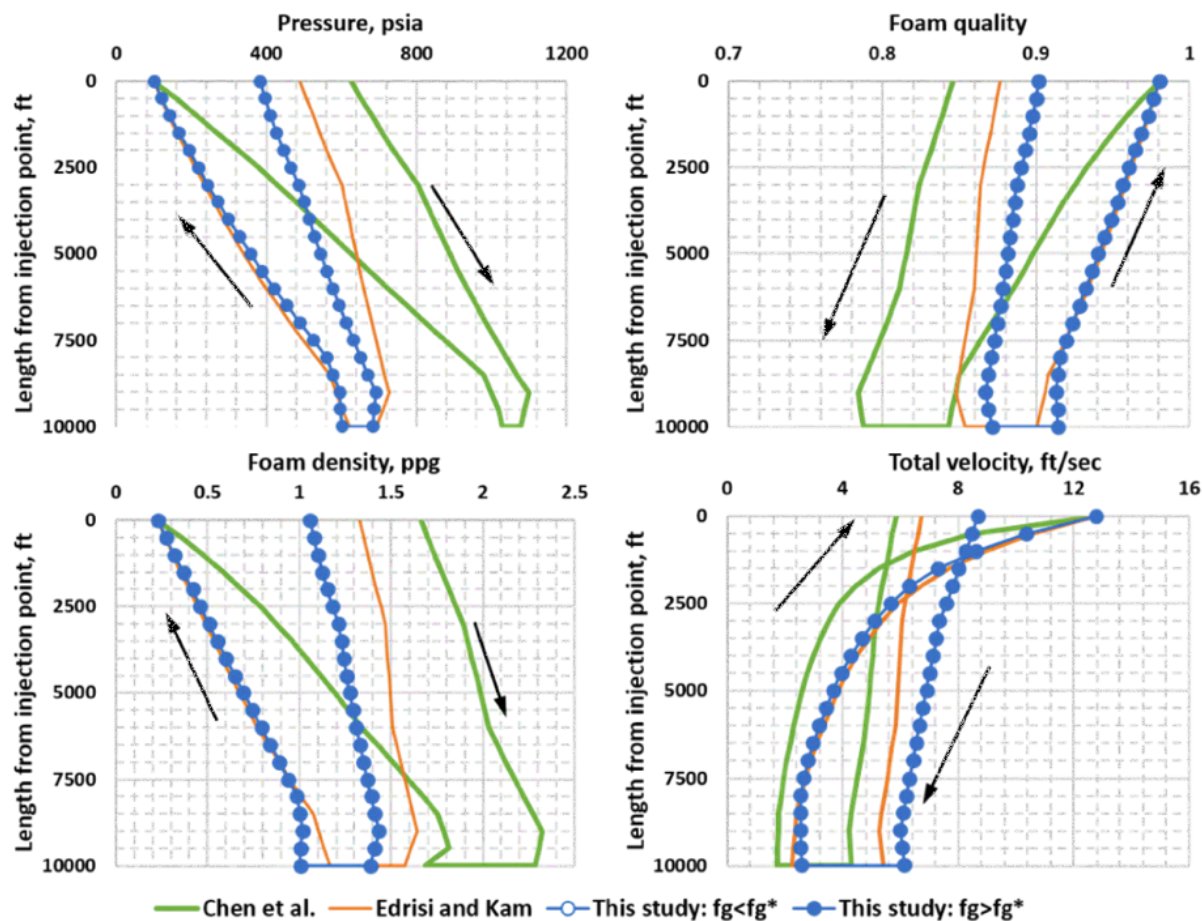


Figure 4. 16 Steady-state simulation results for the inclined well with formation gas influx

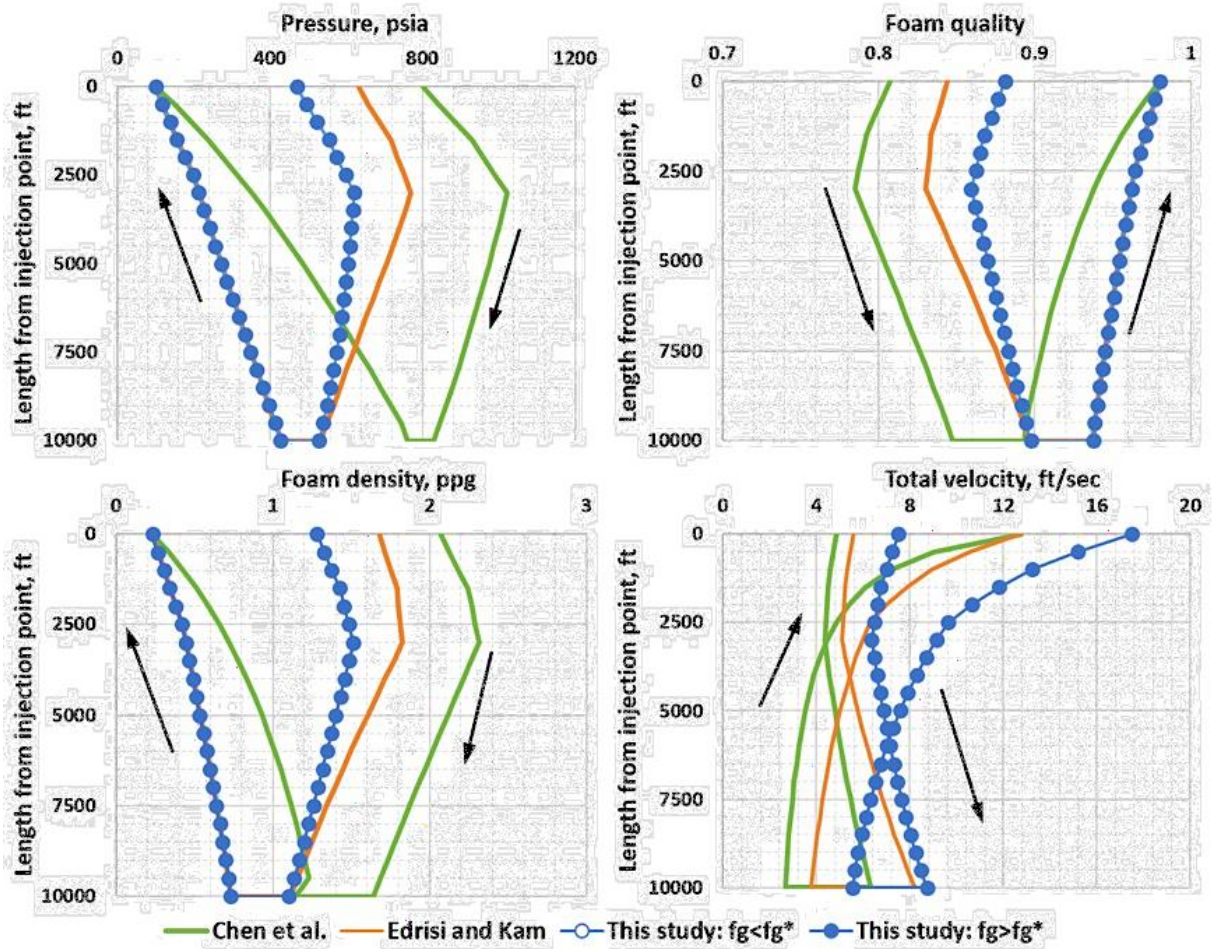


Figure 4. 17 Steady-state simulation results for the horizontal well with formation gas influx

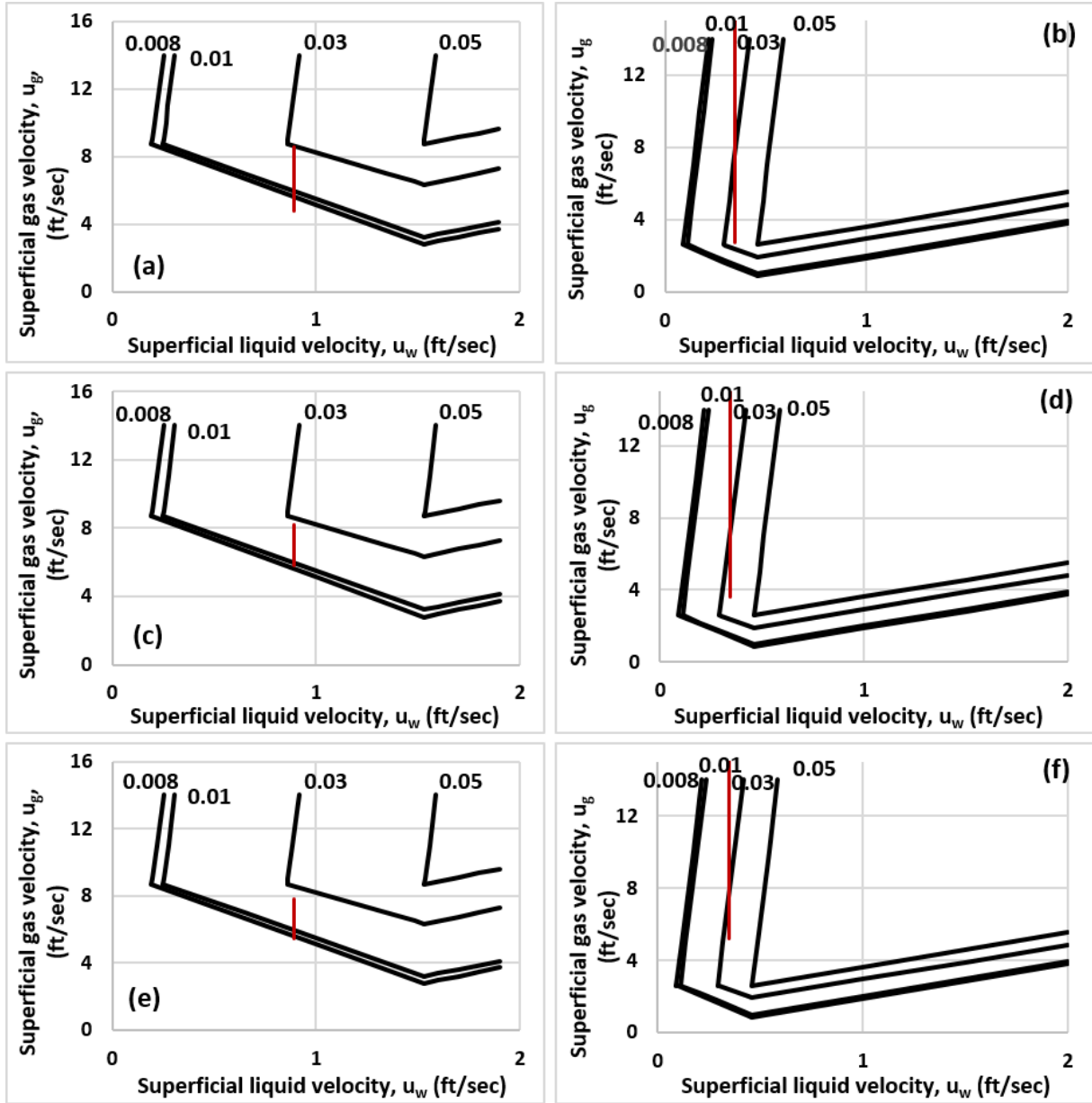


Figure 4.18 Simulated paths with formation gas influx along the drillpipe (left) and annulus (right): (a)(b) vertical well, (c)(d) inclined well, (e)(f) horizontal well

Some investigators find the use of apparent foam viscosity ( $\mu_{app}$ ) more convenient to understand foam rheological properties. The results of this study can also be plotted in that manner. Examples are shown in Figure 4.19 through Figure 4.21, apparent foam viscosity as a function of depth, which results from the vertical wells with no fluid influx, with water influx, and with gas influx (Figure 4.7, Figure 4.11, and Figure 4.15, respectively). Although complicated, they

show consistently how important it is to take two flow regimes and the transition region in between to accurately model foam-associated drilling and well cleanup processes.

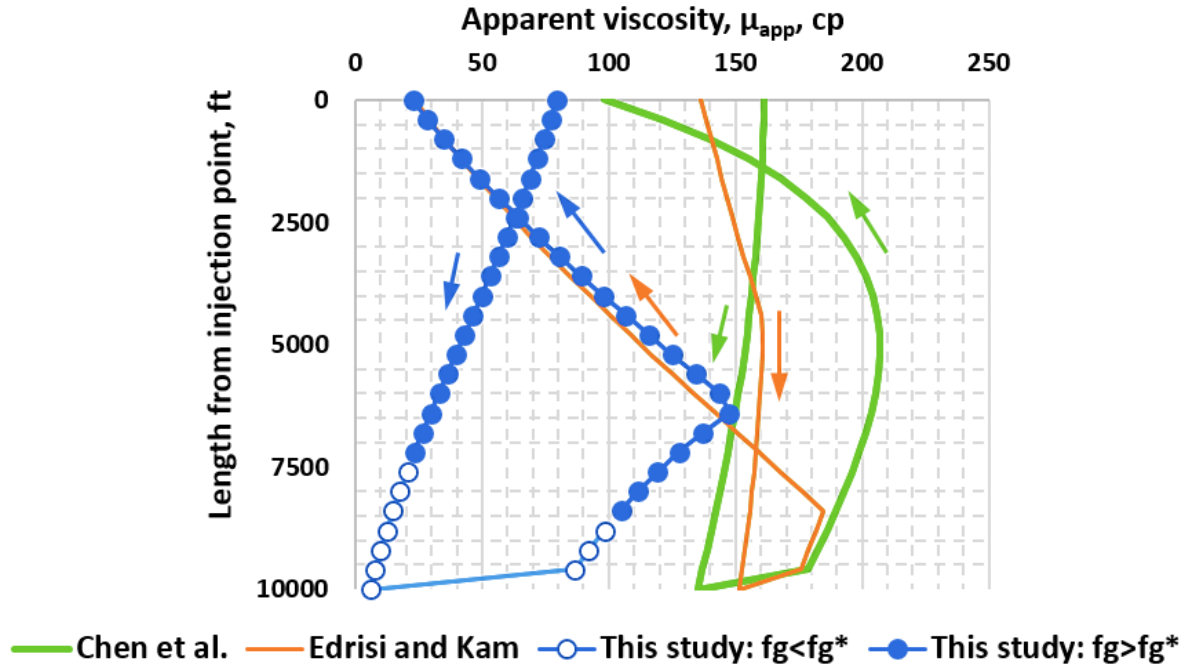


Figure 4. 19 Steady-state simulation results of apparent viscosity for the vertical well without influx



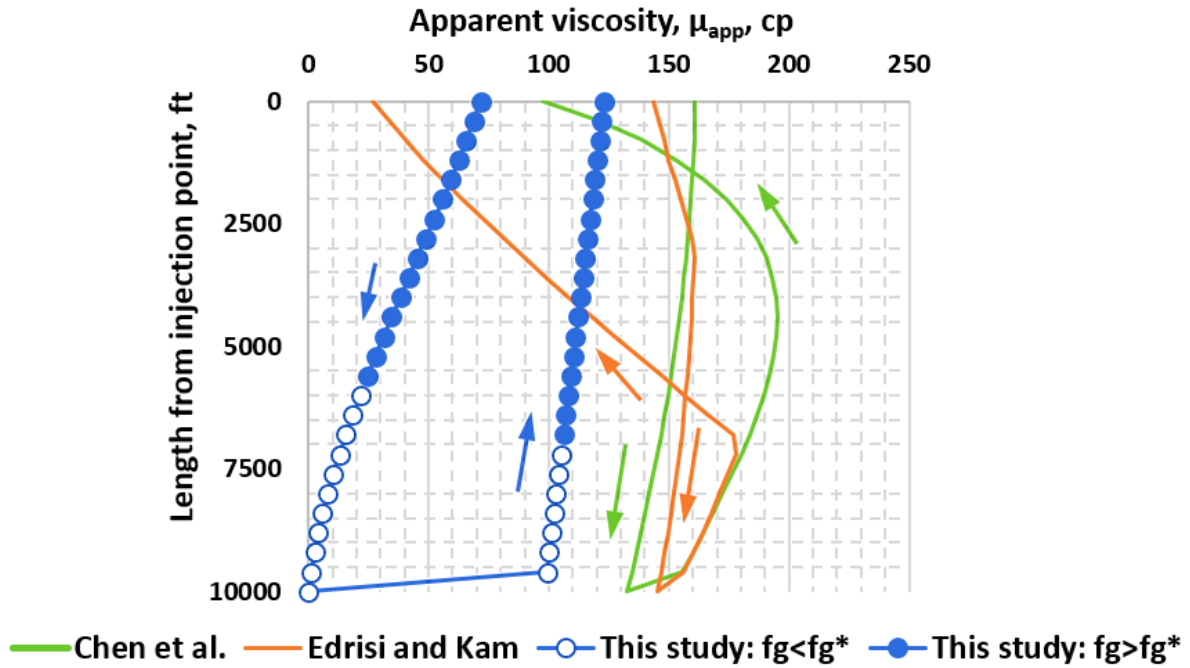


Figure 4. 20 Steady-state simulation results of apparent viscosity for the vertical well with formation water influx

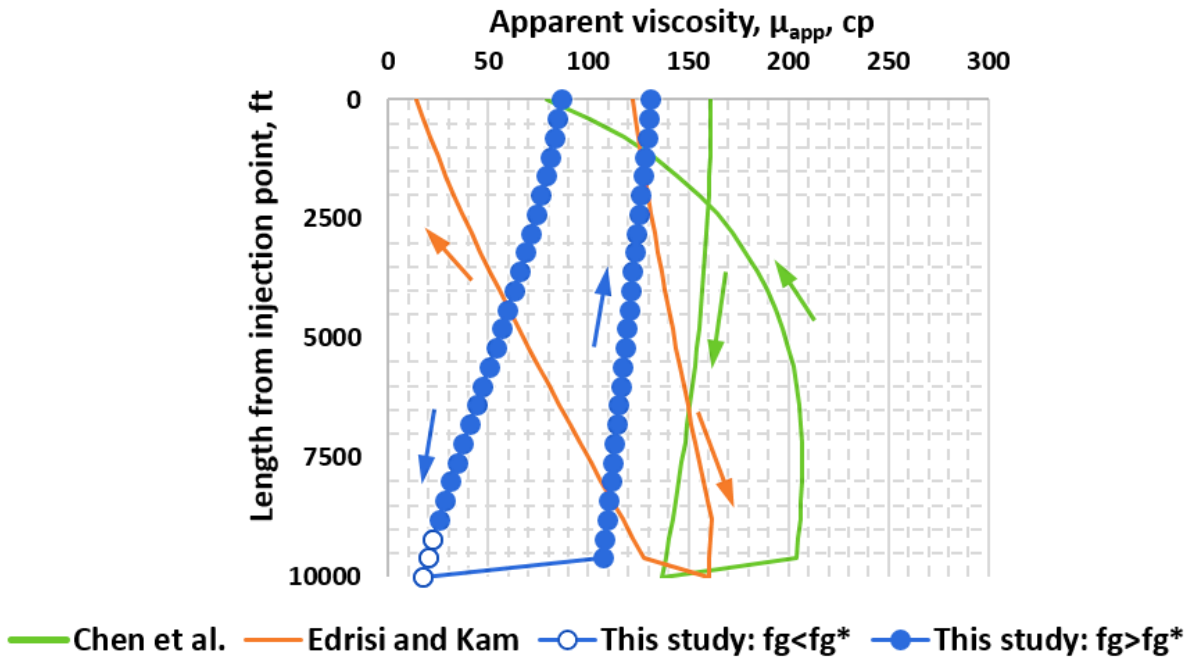


Figure 4. 21 Steady-state simulation results of apparent viscosity for the vertical well with formation gas influx

## 4.5 Conclusions

This study investigates how a new foam model, recently developed by Wang et al. (2017), can improve the prediction of foam-associated drilling and well cleanup processes in three different well scenarios (vertical, inclined, and horizontal wells), with and without formation fluid influx. The new model has nine model parameters and can capture two different rheological properties for dry foams (or, the high-quality regime foams) and wet foams (or, the low-quality regime foams) with a transition region in between. The comparison is made with a foam model based only on fine-textured foam rheology (or, the low-quality regime foams) (Chen et al., 2009) and a foam model that accounts for two foam flow regimes with some limitations (Edrisi and Kam, 2014).

The results show that the new model has unique advantages in accurately predicting foam properties and reliably guiding field applications. Ignoring coarsening foam texture in the high-quality regime can result in significant errors, as much as 40 – 60 %, in the scenarios tested. Even for a model with two flow regimes built in, not incorporating a transition region and two independent foam rheological properties may also lead to a meaningful level of errors in terms of injection pressure and bottom hole conditions.

## CHAPTER 5. NUMERICAL MODELING AND SIMULATION OF FOAM-ASSISTED MUD CAP DRILLING PROCESSES

### 5.1 Introduction

In challenging situations with low-pressure and depleted reservoirs as well as vuggy or fractured carbonates, over-balanced circulation is difficult because the margin between fracture pressure and pore pressure is too narrow or unable to achieve. This often does not allow the conventional drilling techniques to be applied to reach the targets. In order to drill to the target depth, Equivalent Mud Weight (EMW) must stay within the drilling window for drilling to progress. Managed Pressure Drilling (MPD) can help these harsh conditions because of its improved accessibility.

MPD is an adaptive drilling process used to precisely control the annular pressure profile throughout the wellbore (Kuroda et al., 2017). It aims to ascertain the downhole pressure environments and to manage the annular hydraulic pressure profile accordingly. There are typically three different categories of MPD methods. The first is Constant Bottom Hole Pressure Drilling (CBHP) that keeps the bottom hole pressure constant by applying backpressure on the annulus. This method is typically effective in formations with narrow drilling windows. Second, Mud Cap Drilling (MCD) is a method where the bottom hole pressure is maintained in balance with the reservoir pressure. MCD is particularly effective in fractured and/or vugular formations where total losses are encountered. In MCD, losses are allowed, but the fluid lost into the formation is designed to be an inexpensive sacrificial fluid. MCD could result in formation damage and require a large volume of sacrificial fluids, however. Third example is Dual Gradient Drilling (DGD), often used in Deepwater wells, where mud in the marine riser creates the bottom hole pressure in excess of the fracture pressure. In onshore shale-gas drilling, this method involves simultaneous use of higher Mud Weight (MW) in shale and lower MW in the upper sands. This



prevents influxes into shales without fracturing the overlying weak sand zones (Ridley et al., 2013; Safipour et al., 2017).

#### 5.1.1 Pressurized Mud Cap Drilling

In general, when drilling fractured pay zones extensively, MCD (especially, Pressurized Mud Cap Drilling (PMCD)) is preferred over other MPD methods. For example, PMCD method can be found in highly fractured and cavern reservoirs such as Austin Chalk (Colbert and Medley, 2002), offshore Malaysian carbonate reservoir (Idris et al., 2018, Hamizan et al., 2014), and offshore Kalimantan (Benny et al., 2013), as well as in High Pressure High Temperature (HPHT) gas wells in offshore Abu Ahabi (Al-Awadhi et al., 2014) and Gulf of Mexico (GoM) (Fossli and Sangesland, 2006). It is shown to have many advantages in the literature, including reduced loss treatment cost, better well control, less Non Productive Time (NPT), and higher Rate of Penetration (ROP).

Figure 5. 1 shows an example of PMCD where drilling mud, or sea water for offshore case, is used as a sacrificial drilling fluid (SAC) into the drillpipe and exerts the bottom hole pressure high enough to prevent the formation fluids from entering. At the same time, a viscous mudcap fluid, often called Light Annular Mud (LAM) is injected down the annulus, this capmud is maintained in annulus with near, or slightly lower, hydrostatic pressure than reservoir pressure. In the case of offshore PMCD method, backpressure is applied by the Rotating Control Device (RCD) system as shown in Figure 5. 2 . This mud in annulus works as a primary barrier to avoid upward gas migration in the event of gas kick. If the gas influx starts to invade into the annulus and accumulates, it has to be pumped and pushed back to the formation typically at a pre-determined rate, the operation of which is called bullheading. During the operation, there is no fluid return to the surface. While the use of choke valve is crucial, RCD plays a key role in offshore drilling. The

RCD is a typical setup installed to switch from conventional drilling to unconventional drilling such as closed-loop-circulation, PMCD and Early Kick Detection (EKD) drilling techniques (Kuroda et al., 2017).

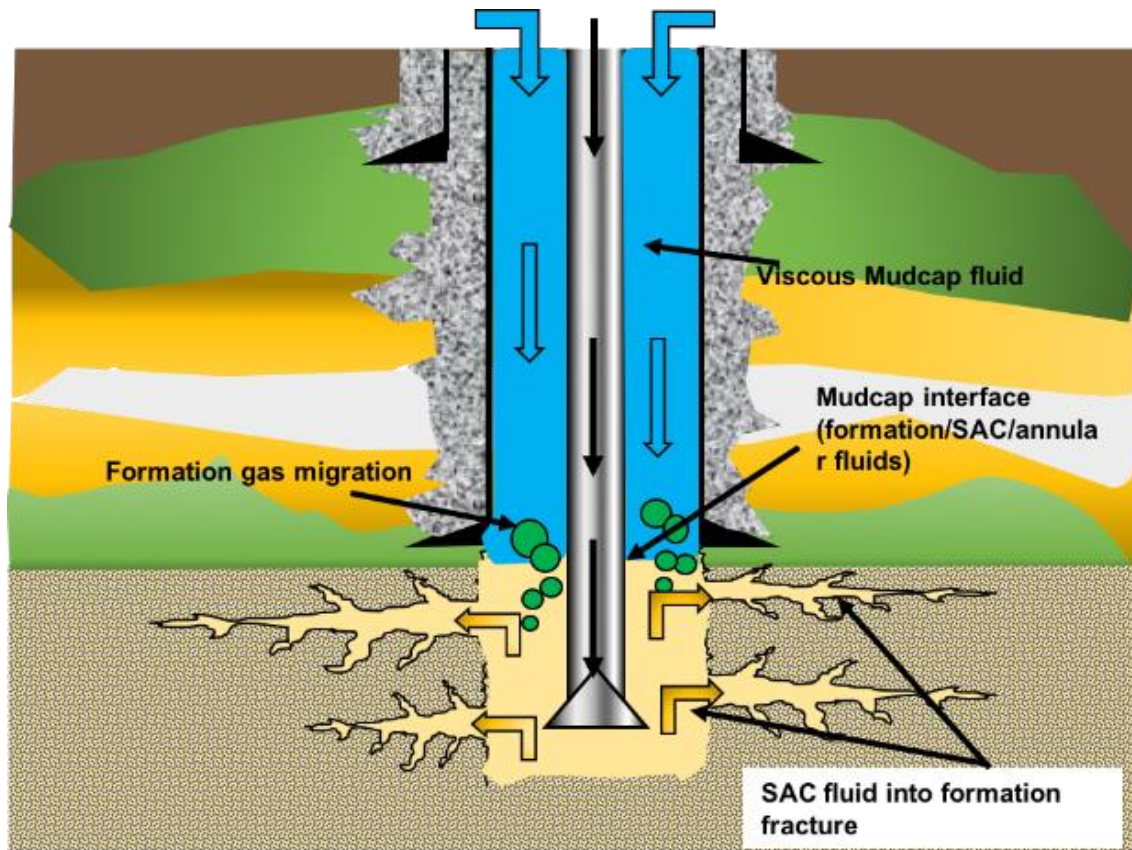


Figure 5. 1 A schematic of fluid flow in a typical PMCD operation for bullheading

This RCD can seal the annulus around drill pipe during drilling and reciprocating by installing a bearing assembly. As Figure 5. 2 shows, with the RCD installation, the return fluid is directly diverted to the RCD flowline instead of the rig diverter. Besides of the RCD flow line, three other lines are usually connected up to the RCD – an injection line, a fill-up line, and a bleed-off line. Each line has its own purpose (Benny et al., 2013), for instance, if total loss is encountered and zero return is confirmed, the RCD return line valve closes to generate certain back pressure and the injection line must be open up to mud pump or cementing pump to inject SAC and LAM. If there is no return and some back pressure is observed, it means PMCD condition is achieved. If

the back pressure has reached a pre-specified value, the injection line can be viewed as performing bullheading or fill-up jobs successfully in the annulus during PMCD (Dipura et al., 2018). Compared to the underbalanced operations which require installation of fluid separation equipment, PMCD needs less equipment on surface facilities.

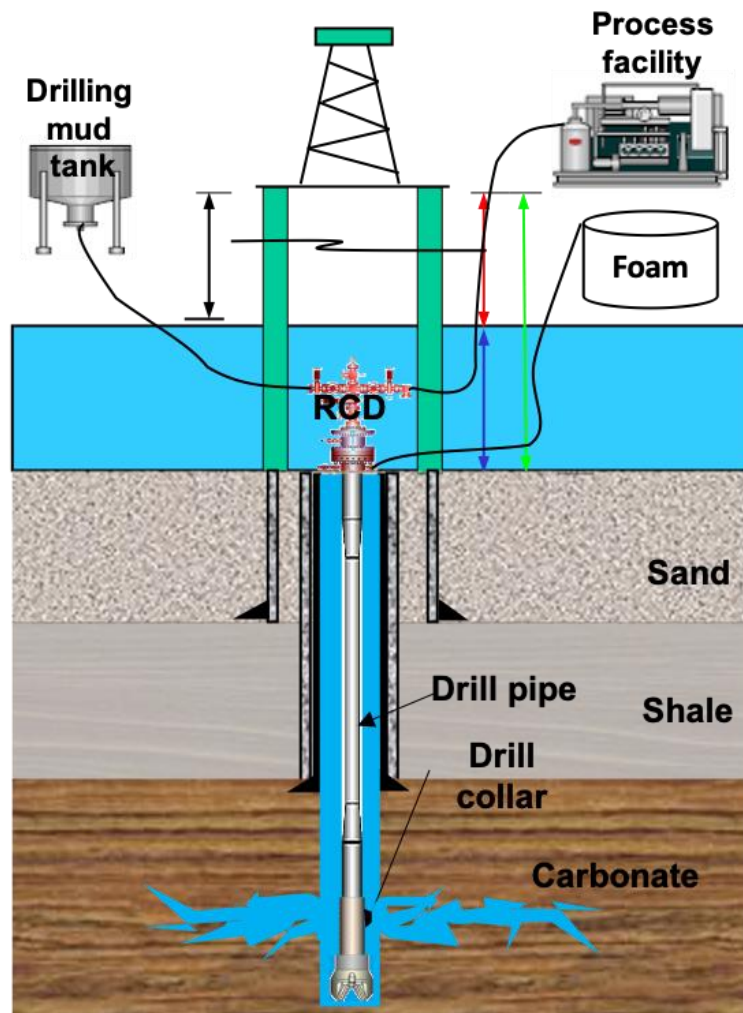


Figure 5. 2 Offshore drilling schematic with RCD

PMCD is a good choice when drilling through fractured formations where the size of surface working area is limited. There are some disadvantages of PMCD compared to other MPD methods, however. They include, for example, a large required volume of water or brine (because there are no returns), a possibility of severe formation damage (because drilling fluid and drilled cuttings

are injected into the formation), lacking information on formation evaluation and fracture penetration identification (because there are no returns to surface to evaluate mud log samples), and potential differential sticking and uncontrollable operating conditions. In order to successfully operate with PMCD, an injection test should be carried out prior to continued drilling with PMCD method.

### 5.1.2 Pressurized Mud Cap Drilling for Well Control

The reservoir is controlled by the hydrostatic pressure due to the column of annular fluid with the addition of surface backpressure. When the hydrostatic pressure is not maintained properly, it may trigger formation gas to start flowing into the annulus and rise to the surface. Understanding how quickly the gas phase rises is an important aspect of PMCD.

### 5.1.3 Bubble-Rise Velocity

The calculation of the annular fluid velocity to stop gas migration is very significant to safely control the well and force formation fluids back into the formation. Davies and Taylor (1950) developed a correlation to describe the rising velocity of bubbles, large enough to almost fill the pipe. The derived equation for the bubble-slip velocity (or, bubble-rise velocity;  $u_s$ ) in vertical pipes as shown in Equation (5.1):

$$u_s = 0.35 \sqrt{g(\rho_l - \rho_g)D / \rho_l} \quad (5.1)$$

where  $\rho_l$  and  $\rho_g$  are the liquid and gas densities, respectively,  $D$  is the pipe diameter and  $g$  is the acceleration of gravity. For a 200-mm (7.8 inch) diameter pipe with water, this predicts a bubble-slip velocity of about 0.5 m/s (1.6 ft/s) (Johnson and White, 1991).

In order to determine the factors affecting bubble rise through liquids in vertical annuli, Rader et al. (1975) conducted various experiments considering parameters of annular geometry, gas and

liquid densities and viscosities, rate of gas expansion, liquid velocity, bubble length, interfacial tension between gas and liquid, and inclination angle. The results showed that the eccentricity of the annulus had little impact on bubble-rise velocity. They also concluded that changing either gas or liquid density would not significantly affect bubble-rise velocity, as long as the gas density was small compared with the liquid density. They also observed that the bubble-rise velocity was affected by rapid bubble expansion or compression due to sudden annular back pressure change. It was found that as long as the rate of expansion or compression of the bubble was small when compared with its upward velocity, the velocity of the trailing edge of the bubble remained almost constant.

In addition, the experimental data (Rader et al., 1975) showed that the bubble-rise velocity was independent of bubble length, in good agreement with theories (Davies and Taylor, 1950) and experiments (Griffith and Walli, 1961). The capillary effect of interfacial tension became significant for smaller tubes (less than 0.5 inch (0.0127 m)), while the effect of interfacial tension decreased as the size of the annulus increases. Those tests in the small 0.58 inch (0.0147 m) OD/0.44 inch (0.0112 m) ID, 0.58 inch (0.0147 m) OD/0.32 inch (0.0081 m) ID, and 0.58 inch (0.0147 m) OD/0.20 inch (0.0051 m) ID annular models with various interfacial tension values indicated no significant variations in bubble-rise velocity.

Hasan and Kabir (1992) proposed an equation for the slip velocity of a Taylor bubble ( $u_s$ ) in an annulus geometry, as shown in Equation (5.2):

$$u_s = \left(0.35 + 0.1 \frac{D_i}{D_e}\right) \sqrt{g D_e (\rho_l - \rho_g) / \rho_l} \quad (5.2)$$

where  $D_i$  is the inner diameter of the outer pipe and  $D_e$  is the outer diameter of the inner pipe forming the annulus space. For PMCD process, Equation (5.2) is considered the more suitable formula for the bubble-rise velocity calculation.

#### 5.1.4 Bullheading

After the first detection of gas kick into the annulus, the well should shut in immediately for safety issues, and the surface could raise annular pressure to compensate the reduction in hydrostatic pressure. The surface pressure at the top of casing at the time of shut-in is called Shut-in Casing Pressure (SICP), the drill pipe pressure at the time of shut-in is Shut-in Drill Pipe Pressure (SIDPP). Between well shut-in and the start of bullheading operation, it takes a certain response time ( $t_{resp}$ ) to initiate well control by injecting the LAM (Lighter Annular Mud) into the annulus. During this response time, the bottom hole pressure is balanced with the formation pressure causing no more fluid influx, whereas the gas kick migrates up freely and the annular pressure keeps increasing due to gas expansion.

During the bullheading operation, the primary way to control the well is to fill up the annulus with LAM at a rate which exceeds the upward gas migration rate. When drilling a pre-salt carbonate reservoir in Brazil, Kuehn (2015) presented a method to determine the minimum LAM injection rate and the minimum volume required to ensure the gas kick back to formation. The LAM injection rate ( $Q_{LAM\_in}$ ) must be greater than the gas rate ( $Q_g$ ) (that is related to the gas velocity ( $u_g$ )) with a safety factor to avoid gas migration, as shown in Equation (5.3):

$$Q_{LAM\_in} = Q_g SF - Q_{LAM\_loss} = u_g \pi \frac{(D_e^2 - D_i^2)}{4} SF - Q_{LAM\_loss} \quad (5.3)$$

where SF is the safety factor ( $SF \geq 1$ ) and  $Q_{LAM\_loss}$  is the rate of LAM lost to the formation during PMCD operation.

#### 5.1.5 Foam Modeling

Foam, as a mixture of gas and surfactant solutions, has been widely applied to numerous onshore and offshore wells. Drilling and cleaning up wellbore with foam fluid can bring many benefits, including minimizing water usage and formation damage, avoiding lost circulation,

extending drill bit life, lowering treatment costs, and improving cutting and solid transport efficiency. There are also several reasons for selecting foam (or, foamed mud) as capmud in PMCD. First of all, it fulfills the requirements causing non- to negligible-damage to the rock matrix. In addition, the mud weight of foam capmud can be adjusted quite easily and quickly by controlling foam quality (or gas fraction,  $f_g$ , equivalently), while the non-Newtonian behavior such as yield stress and shear thinning/thickening makes foam versatile rheologically. Because economically viable, capable of suspending rock cuttings and highly viscous, foam has been regarded as a useful means of mitigating the gas migration. (Rojas et al., 2002, Chen et al., 2006, Nugroho et al., 2017).

A clear understanding of foam rheology is very important to predict various operations associated with foam flow in wellbore and annulus conditions. A series of recent foam experimental studies in a range of pipe sizes, inclinations, surfactant formulations and concentrations, and polymer-added surfactants (Bogdanovic et al., 2009; Gajbhiye and Kam, 2011, 2012; Edrisi et al., 2014) presented the concept of a threshold foam quality,  $f_g^*$ , above which bubbles are unstable and bubble stability is very sensitive to foam quality (so-called high-quality regime;  $f_g > f_g^*$ ), and below which bubbles are stable with relatively uniform bubble sizes (so-called low-quality regime;  $f_g < f_g^*$ ). Edrisi and Kam (2013) proposed a foam model to capture the presence of these two foam flow regimes by using 5 model parameters, borrowing the experimentally-measured rheology of unstable foams in the high-quality regime from Edrisi et al. (2014) and that of stable foams in the low-quality regime from Chen et al. (2007). For example, Chen et al. (2007) proposed a relationship between Power-Law parameters (the consistency index  $K$  and Power-Law exponent  $n$ ) and foam quality,  $f_g$ , at a pre-specified liquid-phase viscosity  $\mu_w$ , as shown in Equations (5.4) through (5.8):

$$K/\mu_w = e^{af_g^2+bf_g+c} \quad (5.4)$$

$$n = -0.45f_g + 0.7633 \quad (5.5)$$

where, a, b, and c are model parameters defined as

$$a = (-0.533\mu_w^2 + 3.6735\mu_w - 13.546) \quad (5.6)$$

$$b = (0.8926\mu_w^2 - 6.5877\mu_w + 29.966) \quad , \text{ and} \quad (5.7)$$

$$c = (-0.3435\mu_w^2 + 2.5273\mu_w - 14.218) \quad (5.8)$$

where K and  $\mu_w$  have the units of  $[\frac{\text{dyne-s}^n}{\text{cm}^2}]$  and [cp].

Wang et al. (2017) further improved Edrisi and Kam's model (Edrisi and Kam, 2013) with the concept of two regimes by using 9 model parameters, overcoming the major limitation of coupled foam rheology along the  $f_g^*$  line. The model from Wang et al. (2017) was applied to foam circulation scenarios, and the results in terms of pressure, foam-quality, foam-density and mixture-velocity profile were compared with previous models of Chen et al. (2009) and Edrisi and Kam (2015), as shown in Wang et al. (2018).

## 5.2 Objectives

Although using foams to bullhead a gas kick has been accepted as a novel and reliable technique when drilling a well with total fluid loss or sour gas migration problems, it is yet to be clear exactly what happens as foam capmud is injected during the process, primarily because of complicated foam properties as well as interactions between different types of fluids in the annulus. Therefore, the objective of this study is to model and simulate the bullheading process of gas kick using a foam-assisted pressurized mud cap drilling technique for well control. More precisely, the process of interest is the propagation of foam mixture in the annulus, during which gas fraction and foam rheological properties change with time and vertical locations, to suppress gas kick



containing hydrocarbon or toxic gas down to the bottom hole and flow back into the fractured formations.

Three scenarios are considered in this study: (i) injected foams not in contact with formation gas during the process because of relatively quick response after gas kick (i.e., a smaller response time,  $t_{resp}$ ) as Base Scenario, (ii) injected foams in contact with formation gas because of relatively slow response after gas kick (i.e., a larger  $t_{resp}$ ), but foam stability not affected by the gas kick keeping the formation gas right below foam front, as Scenario 1, and (iii) the same as (ii) but losing foam stability at the interface between foam front and formation gas, as Scenario 2. This study borrows the model and model parameters from Wang et al. (2017, 2018) in order to accommodate two distinct rheological properties represented by high-quality and low-quality regimes and calculate the frictional pressure loss during foam flow.

Because of the focus made on modeling and simulating bullheading process based on the complexity of foam capmud, this study simplifies its calculations by making the following major assumptions: gas is compressible but liquid is not; there is no mass transfer between different phases; the formation gas influx exists as a single gas bubble in the well (so-called a single bubble model), therefore there is no two-phase flow regime concept between drilling mud and formation gas; the formation fluid has only gas phase with a pre-specified amount of influx; the temperature is constant along the well, but the pressure changes with time ( $t$ ) and vertical distance ( $z$ ) due to hydrostatic and frictional pressure losses; frictional pressure loss from drilling mud and formation gas is negligible compared to that from foam, among many (more details are shown below with model description). It should be noted that these assumptions are made not because of their insignificance but because of the primary focus of this study on foams. Each of these topics can be investigated as a separate topic in the future.

### 5.3 Methodology

#### 5.3.1 Modeling of Foam-Assisted Mudcap Drilling

In order to bullhead a gas kick, foam mixture as capmud is continuously injected down to the annulus at a pre-specified total injection flow rate ( $Q_t$ ) (i.e., a sum of gas and water rates ( $Q_g$  at the standard condition (or  $Q_{gsc}$ ) and  $Q_w$ , respectively);  $Q_t = Q_g + Q_w$ ) and injection foam quality  $f_g$  (i.e.,  $f_g = Q_g / (Q_g + Q_w)$ ). During the process, the system is balanced by keeping the bottom hole pressure equal to the formation pressure.

Figure 5. 3 illustrates the Base Scenario bullheading process. At time  $t = t_1$ , the well is shut-in, the bottom hole pressure is balanced with the formation pressure, and no more gas enters the wellbore after a gas kick occurs initially. The gas kick volume,  $V_{gk}$ , has a value of  $V_{gkbtm}$  at the bottom hole, as an input parameter. Up until foam injection is initiated at  $t = t_2$ , there is a time interval required to respond to the kick, so-called response time ( $t_{resp}$ ), during which the gas kick migrates upward freely at a pre-specified bubble-rising velocity of  $u_{br}$  (in other words,  $t_2 = t_1 + t_{resp}$ ). The longer the response time, the more upward the gas kick migrates and the thicker the gas-occupied segment due to gas expansion.

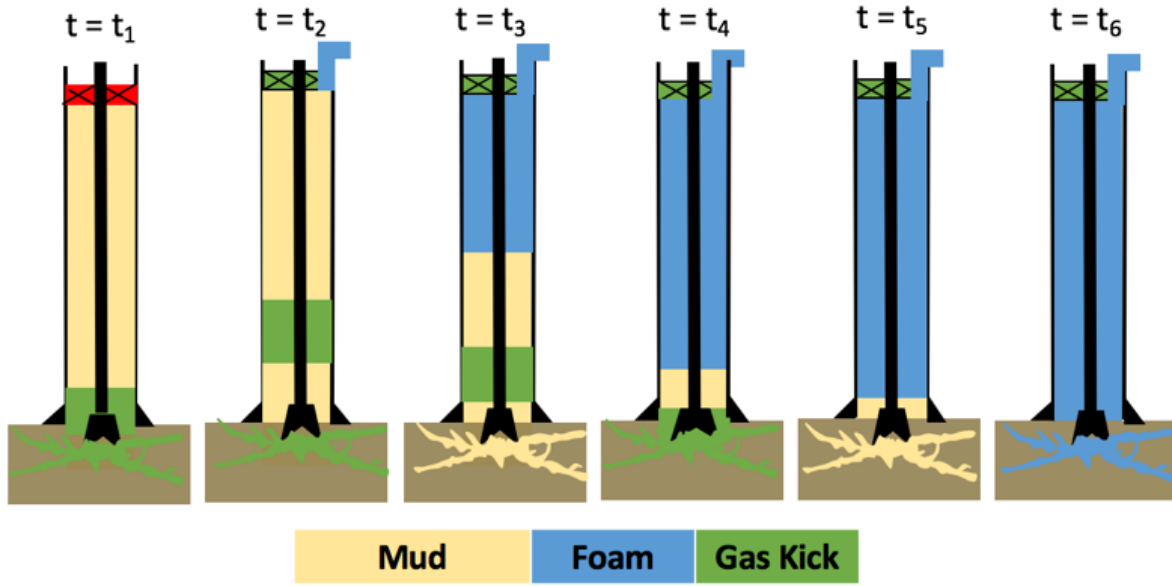


Figure 5. 3 Foam-assisted bullheading process when foam is not in contact with formation gas

At time  $t = t_3$ , a certain amount of foam is already injected continuously during the time period of  $t_3 - t_2$ . Note that although the total injection flow rate ( $Q_t$ ) is maintained, the actual  $Q_t$  value decreases with time, as the injection pressure ( $P_{inj}$ ) builds up and  $Q_g$  decreases due to gas compression. This implies that the foam frontal velocity (i.e., the downward velocity of foam front,  $u_{ff}$ ) also slows down with time. Even though the injected foam pushes drilling mud downward, the formation gas does not necessarily move in the same direction – for example, the formation gas migrates downward only if  $u_{ff} > u_{br}$ , while the formation gas can still migrate upward, even with foam injection, if  $u_{ff} < u_{br}$ .

The system reaches  $t = t_4$ ,  $t_5$ , and  $t_6$ , subsequently afterwards, as foam successfully pushes drilling mud below the formation gas back into the formation, then the formation gas ( $t = t_4$ ), drilling mud between foam and formation gas ( $t = t_5$ ), and finally reaching a steady state with full of foam in the annulus ( $t = t_6$ ). The injection pressure ( $P_{inj}$ ) increases continuously from  $t_1$  through  $t_6$ , after which it stays at the maximum value.

If the response time ( $t_{resp}$ ) is large, the gas kick can rise further upward and may contact the front of foam moving downward during the process. The problem becomes more complex, if it happens, due to the coarsening effect at the interface between gas kick and foam front. This study investigates such cases as well, assuming that foam stability at the interface is not affected by the formation gas (Scenario 1) and that foam becomes unstable and turns into gas and water of the same fraction as soon as it contacts the formation gas and the coalescence wave propagates upward at a constant wave velocity of  $u_{fc}$  (Scenario 2). Scenarios 1 and 2 are two extreme cases, of course, with the reality somewhere in between (i.e., foam coarsening at the interface does occur to a certain extent, which depends on the nature of interactions between foam and formation gas).

Figure 5. 4 shows an example of Scenario 1 where  $t_{resp}$  is relatively larger than Base Scenario. Note that the process in Scenario 1 is the same as that in Base Scenario, but at  $t = t_4$ , the foam front contacts the gas kick below which the drilling mud is positioned. For  $t > t_4$ , the position of the foam front is determined by the injection rate and the gas phase is displaced and located right below the foam front. The process is continued to push the drilling mud ( $t = t_4$ ) and then formation gas ( $t = t_5$ ) into the formation, until it reaches the steady state with the well finally filled with foams ( $t = t_6$ ).

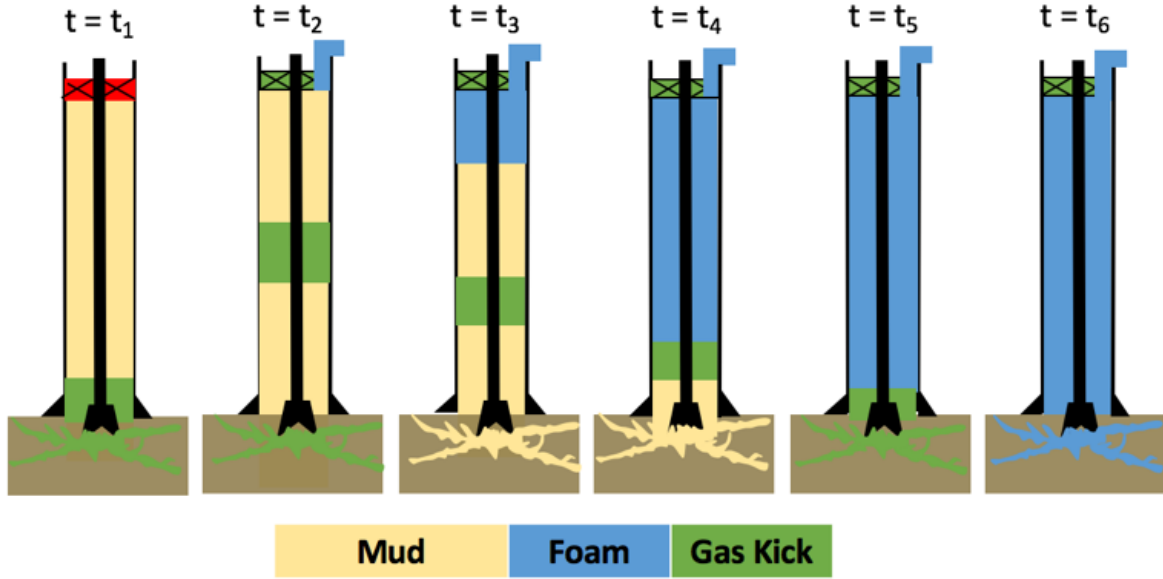


Figure 5. 4 Foam-assisted bullheading process when foam is in contact with formation gas but remains stable

Similarly, Figure 5. 5 shows an example of Scenario 2. While up to  $t = t_4$  it is the same as Scenario 1, after  $t = t_4$  foam mixture breaks down to gas and liquid, forming wet gas, at the interface between foam and formation gas. As a result, the foam front contacts the gas kick at  $t = t_4$  from which the wet gas segment grows upward from the interface at the pre-specified foam coalescence wave velocity of  $u_{fc}$ . The foam injected from the surface then pushes the drilling mud ( $t = t_5$ ), formation gas ( $t = t_6$ ) and wet gas ( $t = t_7$ ) into the formation, until it reaches the steady-state condition ( $t = t_8$ ). It must be noted that the final steady state of the well fully occupied by foams at  $t = t_8$  can be achieved only when the foam front velocity is greater than the foam coalescence velocity (i.e.,  $u_{ff} > u_{fc}$ ). (If  $u_{ff} = u_{fc}$ , the foam front stays at the same position below which the well is occupied by wet gas at steady state, while if  $u_{ff} < u_{fc}$ , the front moves back upward such that the steady state is obtained with wet gas only eventually.)

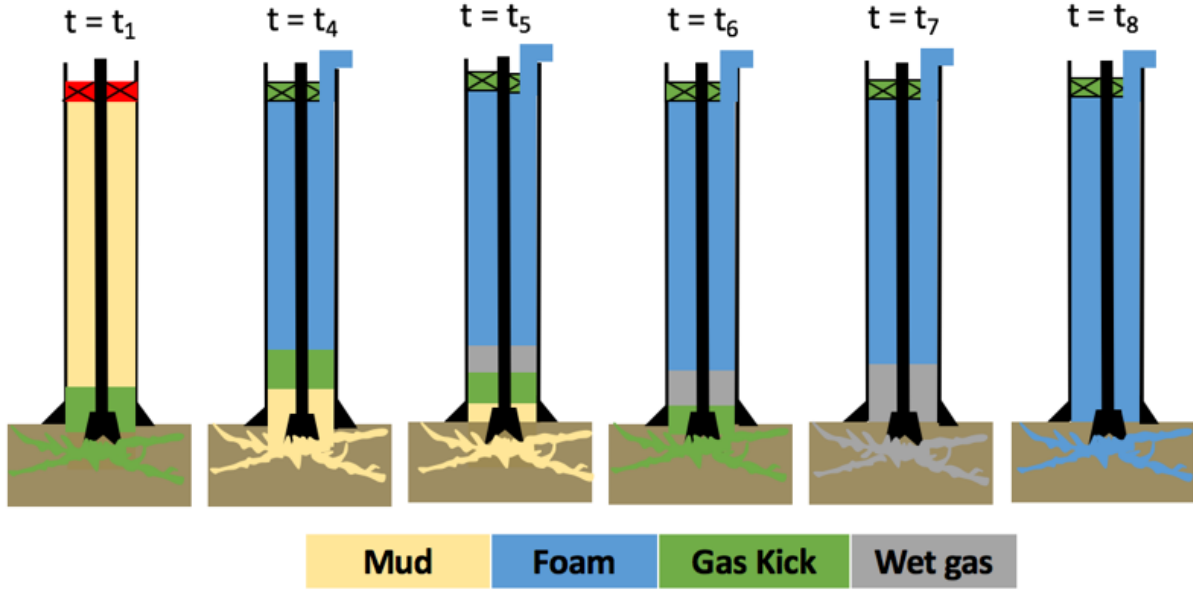


Figure 5. 5 Foam-assisted bullheading process when foam is in contact with formation gas and becomes unstable

The surface pressure at the top of the annulus ( $P_s$ , also called annular pressure or injection pressure during foam injection) is expressed as follows by using formation pore pressure ( $P_p$ ) and hydrostatic, frictional and accelerational pressure losses ( $\Delta P_h$ ,  $\Delta P_f$ ,  $\Delta P_{acc}$ , respectively) :

$$P_s = P_p - \Delta P_h - \Delta P_f - \Delta P_{acc} \quad (5.9)$$

where  $\Delta P_h = 0.052\rho_j H$  (5.10)

and  $\Delta P_{acc} = \rho_j(u_1^2 - u_2^2)/\Delta z$  (5.11)

Note that  $\rho_j$  is the density of phase j, H is the height of the column with phase j,  $u_1$  and  $u_2$  are the average fluid velocities of two adjacent vertical locations over the distance of  $\Delta z$ .

For multiphase mixture with gas and water, the mixture density ( $\rho_m$ ) and total mixture velocity ( $u_t$ ) are defined as follows:

$$\rho_m = f_g \rho_g + (1 - f_g) \rho_w \quad (5.12)$$

$$u_t = Q_t / A = (Q_g + Q_w) / A = u_g + u_w \quad (5.13)$$

where  $f_g$  is the gas fraction,  $\rho_g, \rho_w$  are the densities of gas and water,  $Q_t$  is the total injection rate,  $Q_g, Q_w$  are the injection rates of gas and water,  $A$  is the cross section flow area, and  $u_g, u_w$  are the superficial velocities of gas and water.

This study assumes that  $\Delta P_{acc}$  is negligible compared to  $\Delta P_h$  and  $\Delta P_f$ . In addition, it further assumes that  $\Delta P_f$  of formation gas and drilling mud is negligible compared to  $\Delta P_f$  of foam mixture, because foams are more viscous than mud or gas by a few orders of magnitude difference. Wang et al. (2017) is used to determine  $\Delta P_f$  for the segment occupied by foams in the annulus.

### 5.3.2 Foam Rheological Model

Foam may be generated either at the injection point (known as in-situ generation) or by passing through a porous medium or coiled tubing generator. When foam (or foamed mud) is injected during mudcap drilling, the hydrostatic pressure can be reduced due to lower mixture density, and the viscosity can be improved significantly due to liquid films (or, lamellae) separating bubbles. The density and viscosity can be adjusted further depending on the need, by controlling total flowrate ( $Q_t$ ), foam quality ( $f_g$ ), surfactant compositions and concentrations, chemical additives, and so on. Because the gas phase in the foam mixture is compressible, total flowrate ( $Q_t$ ) and foam quality ( $f_g$ ) are sensitive to the surrounding pressure and temperature conditions.

Briefly describing, Figure 5. 6 shows an example of the steady-state pressure contours showing the high-quality and low-quality regimes. Shown together is the bubble size distribution – fine-textured foams in the low-quality regime, indicated by point “a” and point “b”, and repetitions of fine-textured foams and free gas in the high-quality regime, indicated by point “c” and point “d”, separated by the threshold foam quality,  $f_g = f_g^*$ . The region represented by a rectangular box at relatively lower flow rates (i.e., connecting  $(0, 0)$ ,  $(u_{wRef}, 0)$ ,  $(0, u_{gRef})$  and  $(u_{wRef},$

$u_{gRef})$ ) is a transition region (between the two flow regimes) where the foam characteristics are not fully developed.

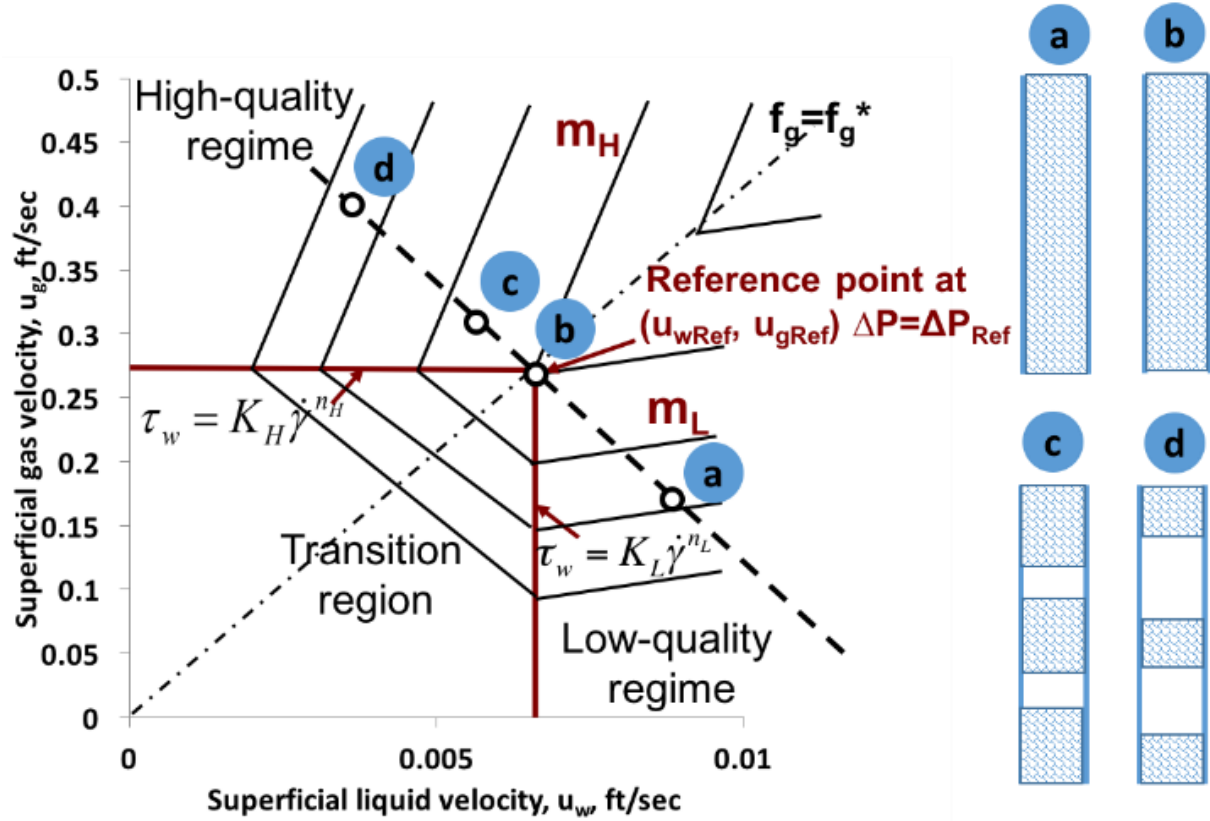


Figure 5. 6 Foam model that has both dry and wet rheological behaviors

This study uses Wang et al.'s model (2017) with 9 model parameters as shown in Table 5. 1 for foam flow in annulus. More precisely, 3 parameters are employed to define the reference point ( $u_{wRef}$ ,  $u_{gRef}$ ,  $\Delta P_{Ref}$ ), 2 parameters to define the Power-Law model in the high-quality regime ( $K_H$  and  $n_H$  along  $u_g = u_{gRef}$ ), 2 parameters to define the Power-Law model in the low-quality regime ( $K_L$  and  $n_L$  along  $u_w = u_{wRef}$ ), and 2 parameters to define the average slopes of contour lines in both regimes ( $m_H$  and  $m_L$ ). Wang et al. (2018) has more details on how the model can be used for actual hydraulics calculations, similar to this study.



Table 5. 1 Nine foam model parameters used for frictional pressure loss in this study

Parameters			Units
$u_{wRef}$	Superficial liquid velocity at the reference point	0.46	ft/s
$u_{gRef}$	Superficial gas velocity at the reference point	2.6	ft/s
$\Delta P_{Ref}$	Pressure gradient at the reference point (frictional)	0.05	psi over 1 ft horizontal distance
$m_H$	Average contour slope in the high-quality regime	90	Dimensionless
$m_L$	Average contour slope in the low-quality regime	1.9	Dimensionless
$K_H$	Consistency index in the high-quality regime	0.0518	$\frac{\text{dyne} - \text{s}^{1.1223}}{\text{cm}^2}$
$n_H$	Power-Law Exponent in the high-quality regime	1.1223	Dimensionless
$K_L$	Consistency index in the low-quality regime	0.0008	$\frac{\text{dyne} - \text{s}^{1.652}}{\text{cm}^2}$
$n_L$	Power-Law Exponent in the low-quality regime	1.652	Dimensionless

### 5.3.3 Foam-Assisted Well Control Workflow

This study uses a finite difference calculation method along the annulus. Iterations are needed to satisfy the pre-specified formation pressure  $P_p$  at the bottom hole by assuming a new total injection flow rate ( $Q_t$ ) in each iteration (This specifies injection foam quality ( $f_g$ ) at the annular surface).

Table 5. 2 lists all the input data required for the simulation work. As discussed above, the Base Scenario has a relatively short response time ( $t_{resp}$ ) of 20 minutes, while Scenario 1 and 2 have a longer response time ( $t_{resp}$ ) of 50 minutes. In Scenario 2, foam coalescence wave velocity ( $u_{fc}$ ) is taken as half of the foam frontal velocity ( $u_{ff}$ ) to account for destabilizing foam, turning into wet gas of the same gas and liquid fractions.

Table 5. 2 Input data for foam PMCD well control process

Surface Conditions	Surface pressure, psia	$P_s$	14.7
	Surface temperature, °F	$T_s$	70
Operation Conditions	Responding time between shut in and foam injection, min	$t_{resp}$	20, 50
	Injection pressure, psia	$P_{inj}$	Variable
	Injection temperature, °F	$T_{inj}$	70
	Injection liquid rate, gpm	$Q_w$	53.2
	Injection gas rate, scfm	$Q_{gsc}$	12800
Well Data	Total Vertical Depth, ft	TVD	10000
	Annulus outer diameter, inch	$D_o$	8.5
	Pipe size, inch	$d_o, d_i$	5 x 4.276
	Temperature gradient, °F/ft	$T_{gra}$	0 (isothermal)
Fluid Data	Mud Weight, ppg	MW	13
	Formation gas kick volume at BH condition, bbl	$V_{gkbtm}$	20
	Formation gas kick specific gravity (Methane)	$SG_{gk}$	0.6
	Bubble rising velocity, ft/s	$u_{br}$	2
Formation Data	Formation pressure, psia	$P_p$	8000
Foam	Foam coalescence wave velocity, ft/s	$u_{fc}$	$0.5 \times u_{ff}$
	Surfactant solution + Nitrogen ( $SG_{n2}=0.9723$ )		

Numerical calculation conducted in this study essentially solves material balance equations for drilling mud, formation gas, and injected foams. The following outlines the workflow for the Base Scenario numerical calculations briefly that can be extended to other scenarios appropriately:

1. Right after well shut-in ( $t = t_1$ ), calculate the top of the formation gas ( $z_{gktop}$ ) based on the input gas kick volume ( $V_{gkbtm}$ ). Note that the bottom of the formation gas coincides with the bottom hole ( $z_{gkbtm} = \text{TVD}$ ). Also note that the shut-in drillpipe pressure (SIDPP) and the shut-in casing pressure (SICP) can be calculated by using U-tube concept and the formation pore pressure ( $P_p$ ) provided.
2. At the onset of foam injection ( $t = t_2$ ), the bottom of the formation gas is determined by the

bubble-rising velocity ( $u_{br}$ ), i.e.,  $z_{gkbtm} = TVD - u_{br} \times t_{resp}$ . Using the pressure at  $z = z_{gkbtm}$ , a new formation gas volume ( $V_{gk}$ ) can be calculated together with the new top of the formation gas ( $z_{gktop}$ ). This requires the compressibility factor ( $Z$ ) of the formation gas. The annular surface pressure, or injection pressure ( $P_{inj}$ ), can then be calculated from the hydrostatic pressure gradients of drilling mud and formation gas.

3. For  $t > t_2$ , the calculation is conducted with a pre-determined time step size of  $\Delta t$  ( $\Delta t = 1$  min, typically). At an assumed value of  $P_{inj}$ , determine the depth of foam front ( $z = z_{ff}$ ) and calculate the hydrostatic and frictional pressure losses ( $\Delta P_h$  and  $\Delta P_f$ ) (Note that the segment occupied by foams is modelled with a number of (typically, tens of) grid blocks). The new location of formation gas can be calculated similar to step 2. When the calculated pressure at the bottom hole is not close enough to the input formation pore pressure ( $P_p$ ), the calculations are repeated with a new value of  $P_{inj}$ .

4. Repeat step 3 at new time  $t$  until the steady-state is obtained.

## 5.4 Results and Discussions

By using 9 foam model parameters listed in Table 5.1, the pressure contours as a function of gas and liquid velocities (or, total velocity and foam quality, equivalently) can be generated to calculate the frictional pressure loss for foam flow in the annulus. Figure 5.7 shows the results with parameter values. The reference gas and liquid velocities show  $f_g^* = 0.85$  that separates the two flow regimes. In the following section, the details of simulation results for each of scenarios are presented.

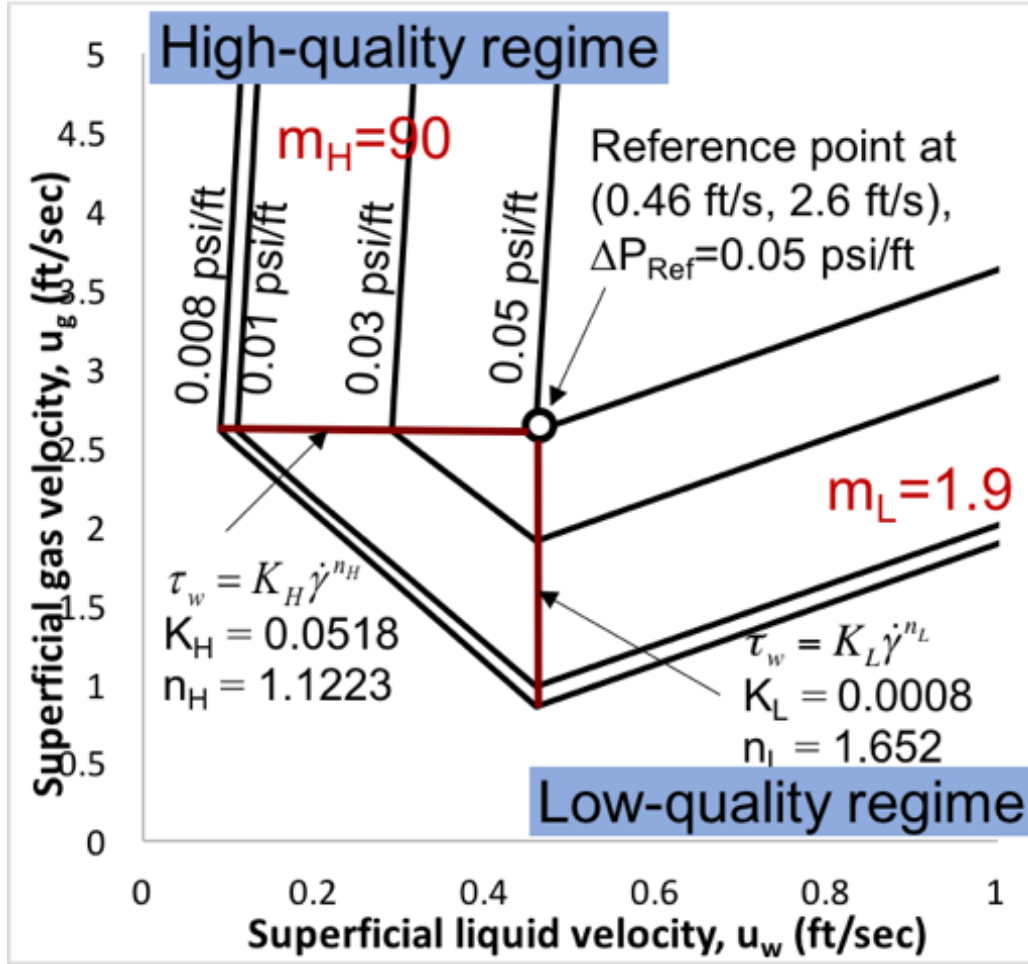


Figure 5. 7 Foam flow regime map for foam flowing in annulus

#### 5.4.1 Results of Base Scenario

Figure 5. 8 shows how the fluid column in the annulus changes with time during bullheading process. Note that the time  $t = t_2 = 0$  min represents the onset of foam injection into the annulus and the response time ( $t_{resp}$ ) from the well shut-in to foam injection, that is  $t_{resp} = t_2 - t_1$ , is 20 mins during which the gas kick migrates upward to show the top and bottom of the formation gas at  $z_{gk\text{top}} = 7053$  ft (2149.7 m) and  $z_{gk\text{btm}} = 7600$  ft (2316.5 m), respectively. The results show that foams injected from the top progressively displace the formation gas through the drilling mud in between, bullheading the formation gas completely after about 40 mins of foam injection and

finally reaching the steady state (with the annulus fully occupied by foams) after around 75 mins. During the process the bottom hole pressure is the same as the formation pressure, and the downward foam front velocity ( $u_{ff}$ ) is faster than the velocity of formation gas bullheaded by the bubble rising velocity ( $u_{br}$ ).

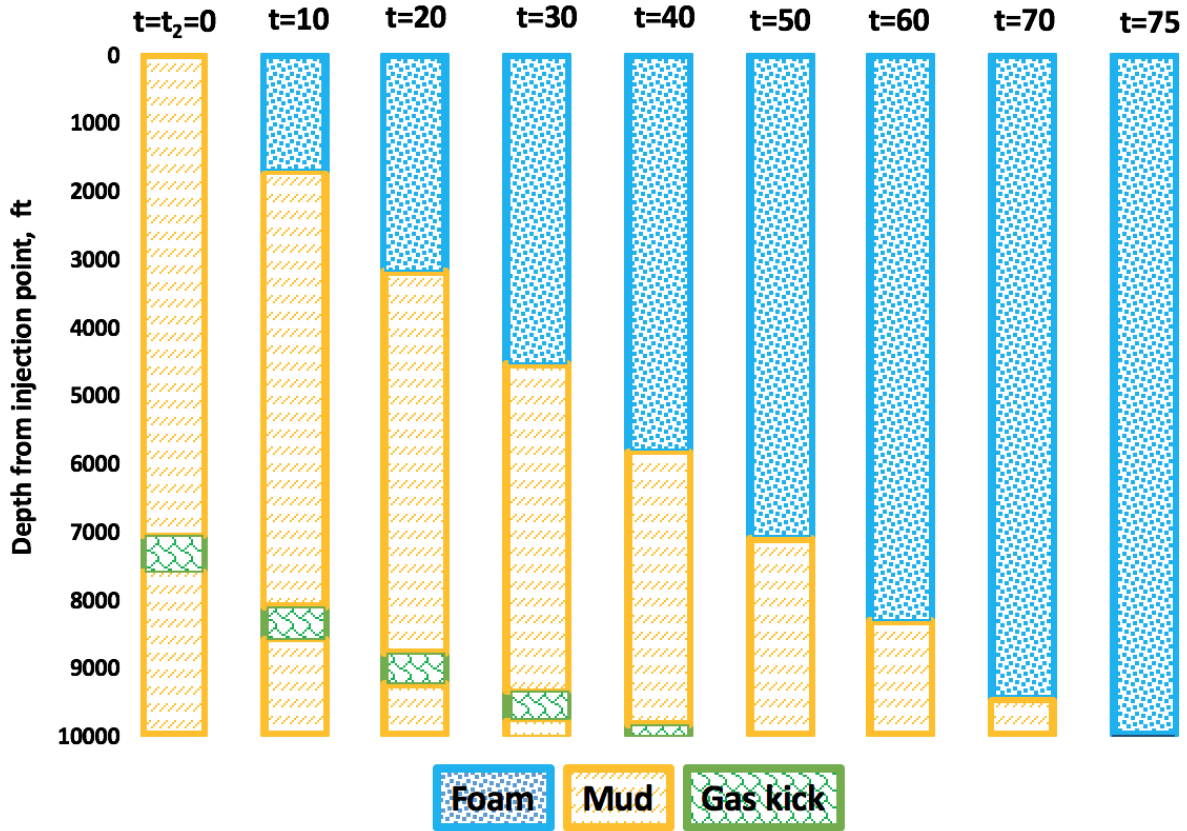


Figure 5. 8 Base Scenario results showing vertical locations of different fluid zones with time [min]

Figure 5. 9 and Figure 5. 10 present the pressure profile as a function of time during this process, all together in one plot as well as multiple plots at different times. At the time of well shut-in ( $t = t_1$ ), the gas kick is accumulated at the bottom hole with the input gas kick volume ( $V_{gkbtm}$ ) making  $z_{gktop} = 9564$  ft (2915.1 m) and  $z_{gkbtm} = 10,000$  ft (3048 m). Because of the lower hydrostatic pressure of gas, the pressure gradient (or, slope) within the formation gas is much less

than that in the drilling mud. From  $t = t_2 = 0$  mins, foams are injected (again, as represented by the low pressure gradient near the surface) such that the annulus is filled with foams, drilling mud, formation gas and drilling mud from the top. Note that the filled and open symbols within the foam zone represent foams in the high-quality regime ( $f_g > f_g^*$ ) and low-quality regime ( $f_g < f_g^*$ ), respectively (note that  $f_g^* = 85\%$  and the injection  $f_g = 90\%$  at the time of initial foam injection). As foam migrates downward, it pushes fluids back into the formation step by step as reflected by the pressure gradient. As the injection pressure increases with time during the process, the gas phase in the foam zone is compressed further and there is more chance for foams to stay in the low-quality regime at later time and at deeper location.

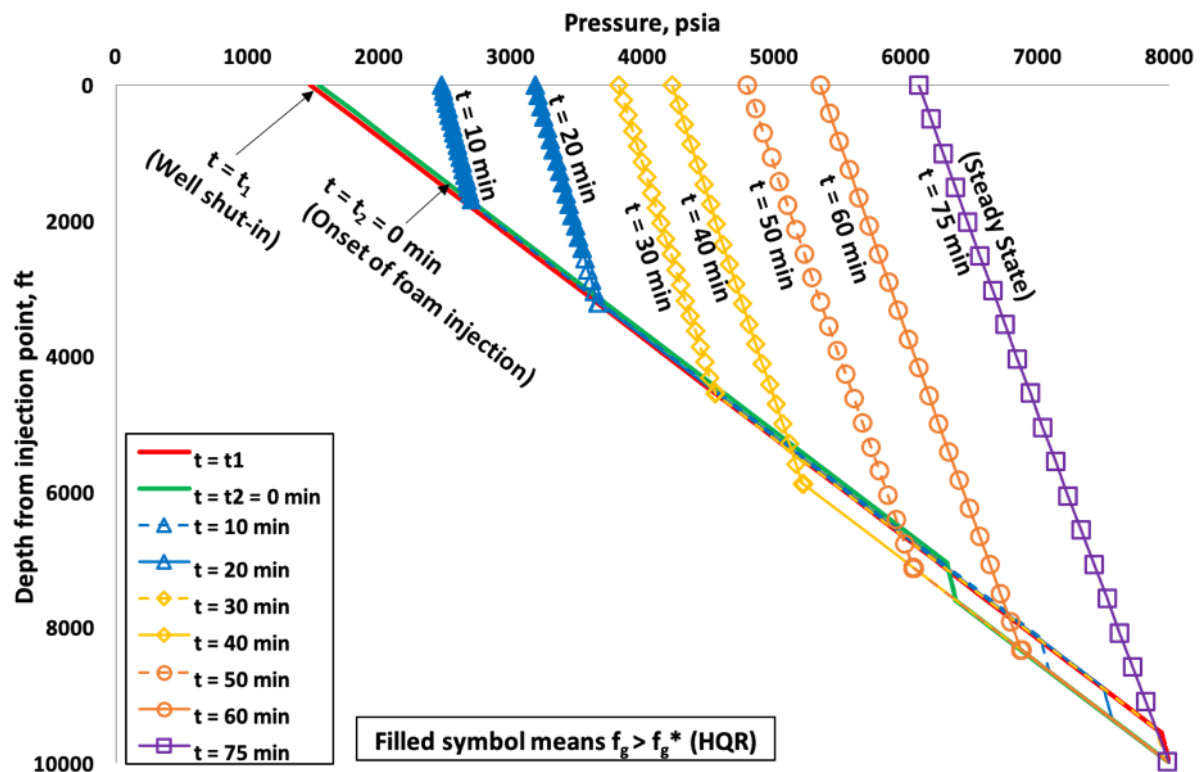


Figure 5. 9 Base Scenario results showing pressure profile changing with time

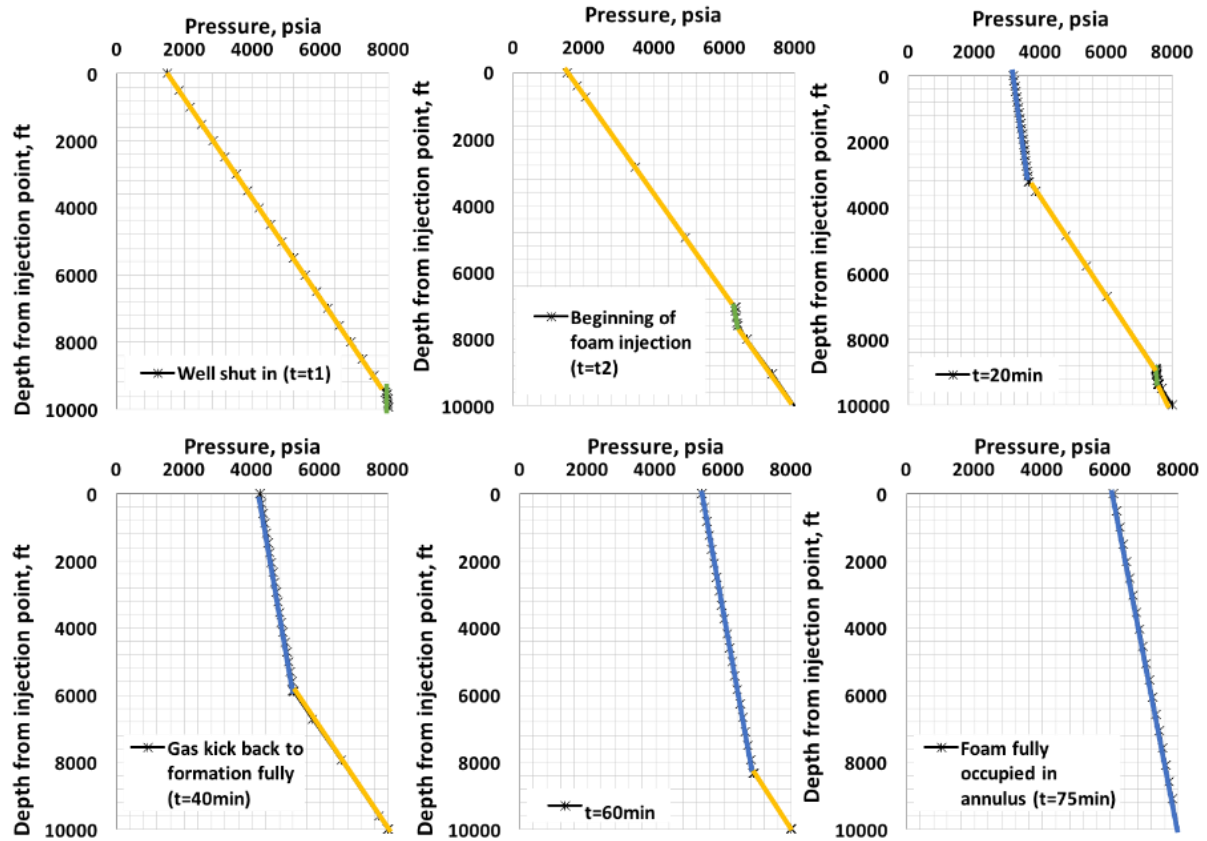


Figure 5. 10 Base Scenario results showing pressure profile at different times

Figure 5. 11 , Figure 5. 12 and Figure 5. 13 show the position of foam front ( $z_{ff}$ ), foam quality ( $f_g$ ), foam density ( $\rho_m$ ) and foam velocity ( $u_t$ ) as a function of time during the process. The results show that even though the mass rate at the injection point remains the same, foam is compressed further with time, and thus foam density increases and foam velocity decreases.

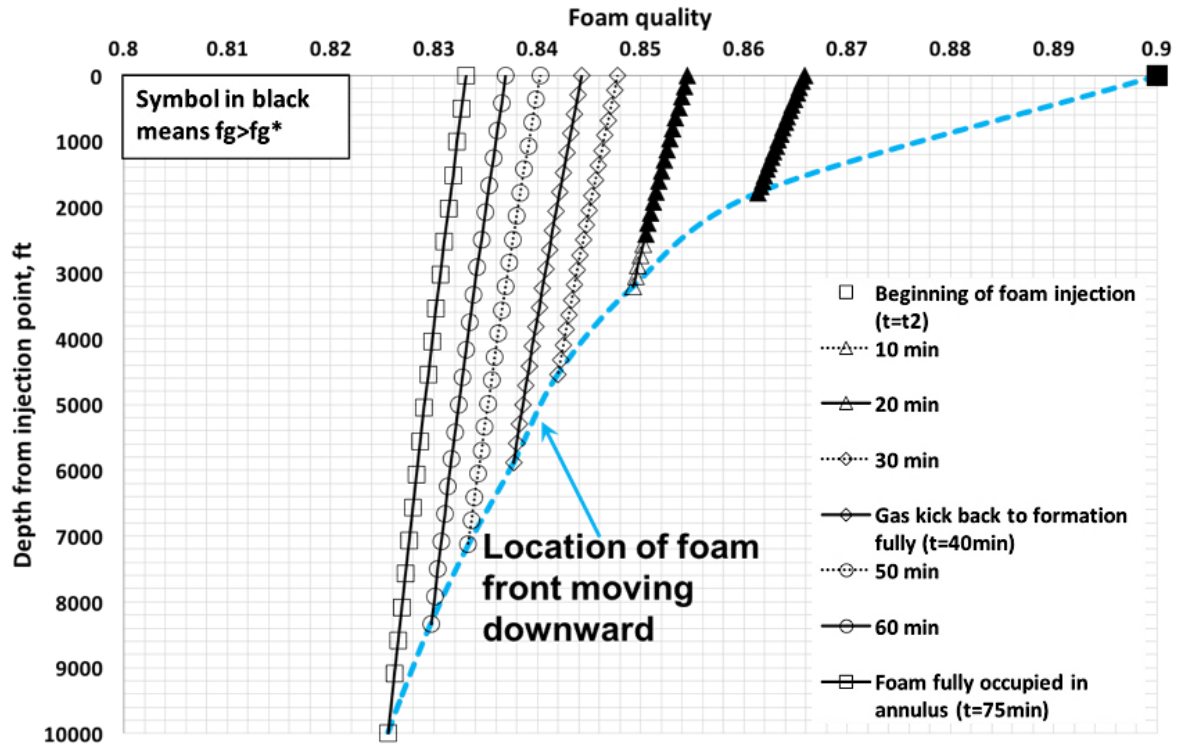


Figure 5. 11 Base Scenario results showing foam quality profile with time

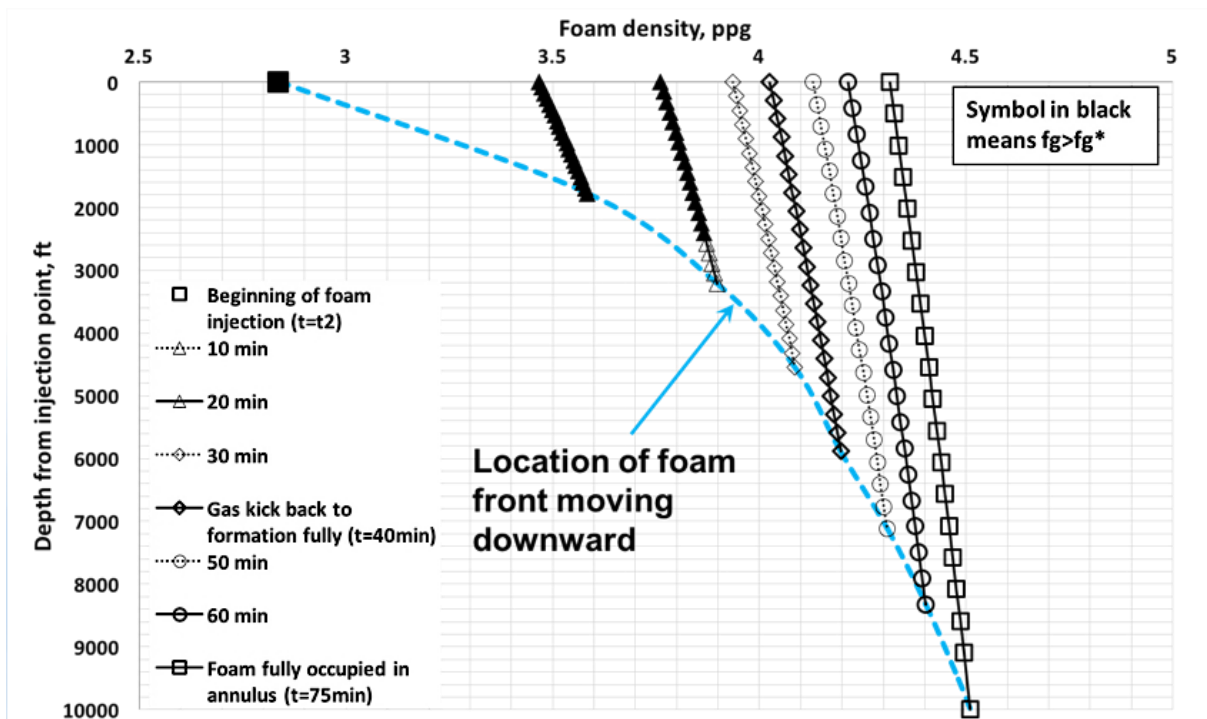


Figure 5. 12 Base Scenario results showing foam density profile with time



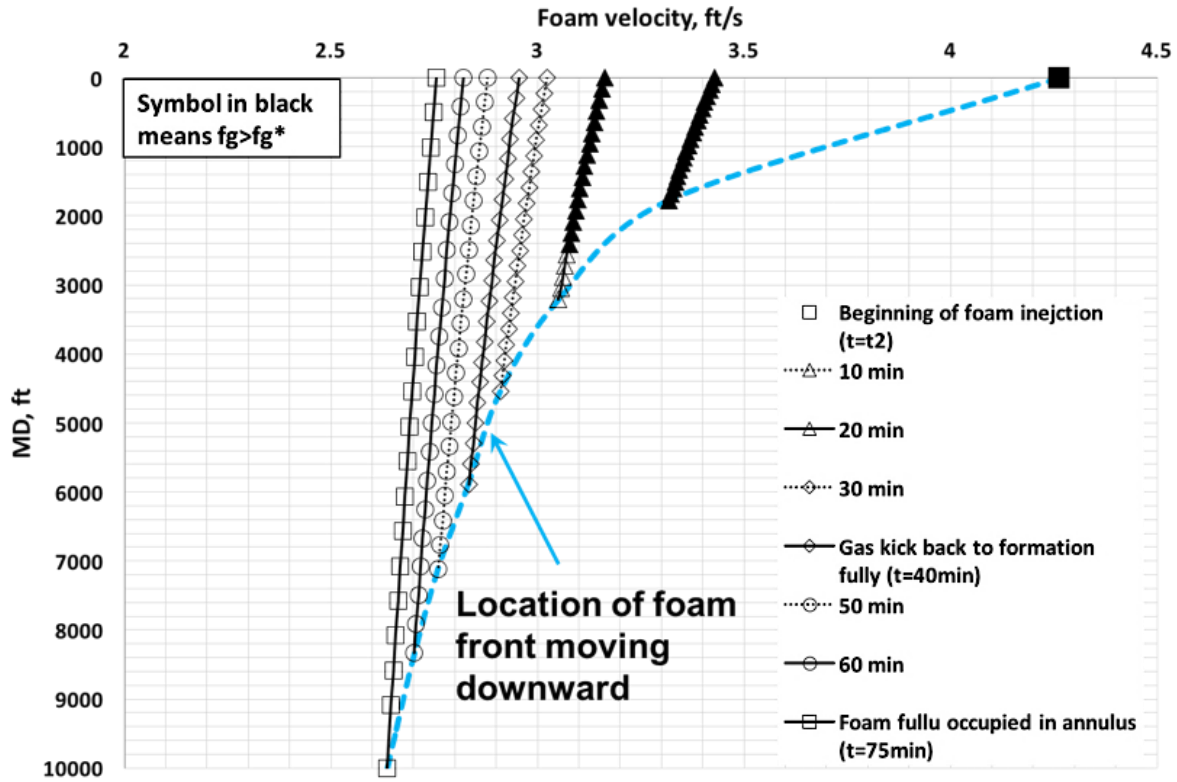


Figure 5. 13 Base Scenario results showing foam velocity profile with time

The results in Figure 5. 9 through Figure 5. 13 can be used to determine the injection pressure at the annular surface ( $P_{inj}$ ) as shown in Figure 5. 14 , with the annular pressure at the time of well shut-in ( $t = t_1$ ) noted as a reference (note that  $t_{resp} = t_2 - t_1 = 20$  mins). At the time of foam injection ( $t = t_2 = 0$  min),  $P_{inj}$  increases by about 65 psi (448159 Pa) due to gas migration and expansion. The annular pressure  $P_{inj}$  keeps increasing until  $t = 32$  mins because the injected foams continuously push drilling mud below the formation gas into the formation. The same trend is continued after  $t = 40$  mins (i.e., displacing drilling mud on the top of the formation gas) and, in between ( $32 \text{ mins} < t < 40 \text{ mins}$ ), the pressure increase is moderate when the injected foam bullheads the formation gas through the drilling mud. After  $t = 75$  mins, the surface annular pressure is maintained constant after reaching the steady state condition.

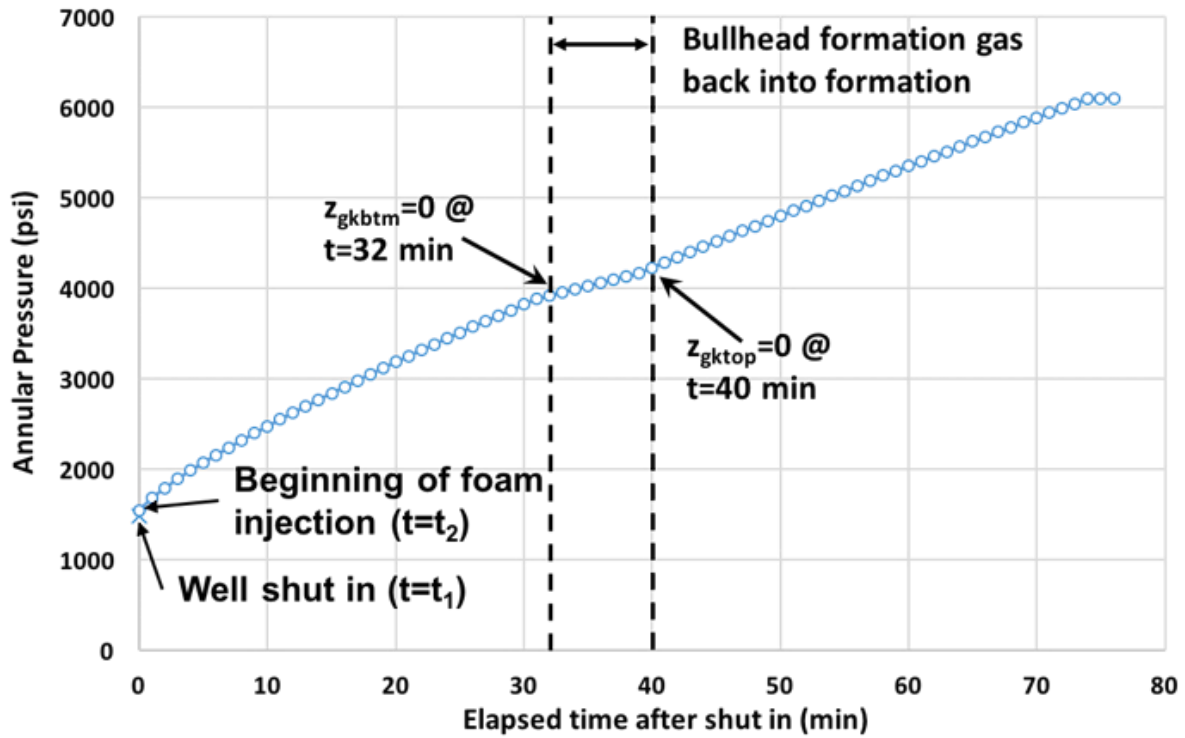


Figure 5. 14 Base Scenario results showing injection pressure at the annular surface with time

#### 5.4.2 Results of Scenario 1

Scenario 1 considers the case with a larger response time ( $t_{resp}$ ) of 50 mins where the formation gas rises further upward and becomes in contact with the injected foam during the process, as shown in Figure 5. 15 . At  $t = t_2 = 0$ , the gas kick zone migrates up and occupies the annulus from  $z_{gktop} = 3116$  ft (949.7 m) to  $z_{gkbtm} = 4000$  ft (1219.2 m). With foam injection, the foam front makes a contact with the formation gas at  $t = 44.54$  mins after displacing the mud in between. At  $t = 74.23$  mins, the system reaches a steady state after displacing the drilling mud and formation gas completely.

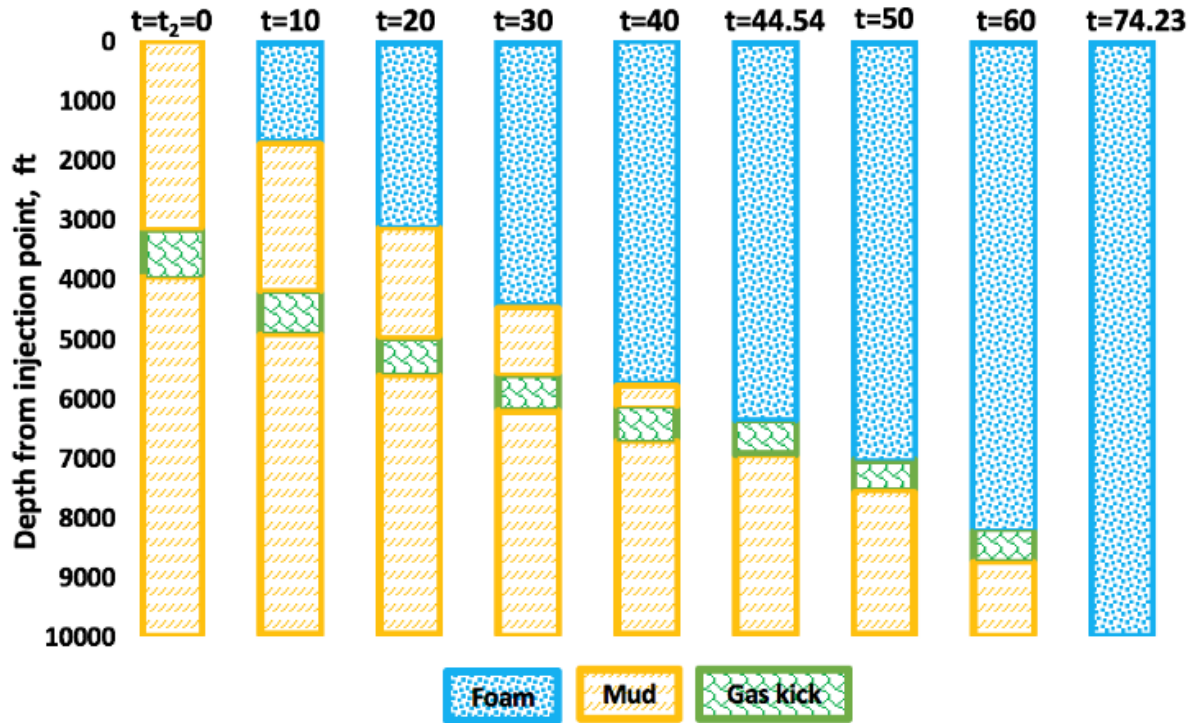


Figure 5. 15 Scenario 1 results showing vertical locations of different fluid zones with time [min]

Similar to the Base Scenario, Figure 5. 16 and Figure 5. 17 show the pressure profiles with time, while Figure 5. 18 through Figure 5. 20 show the position of foam front ( $z_{ff}$ ), foam quality ( $f_g$ ), foam density ( $\rho_m$ ) and foam velocity ( $u_t$ ) as a function of time during the process. Overall, there are no significant differences between Base Scenario and Scenario 1 except for the fact that there is no mud between the injection foam and formation gas after  $t = 44.56$  mins.

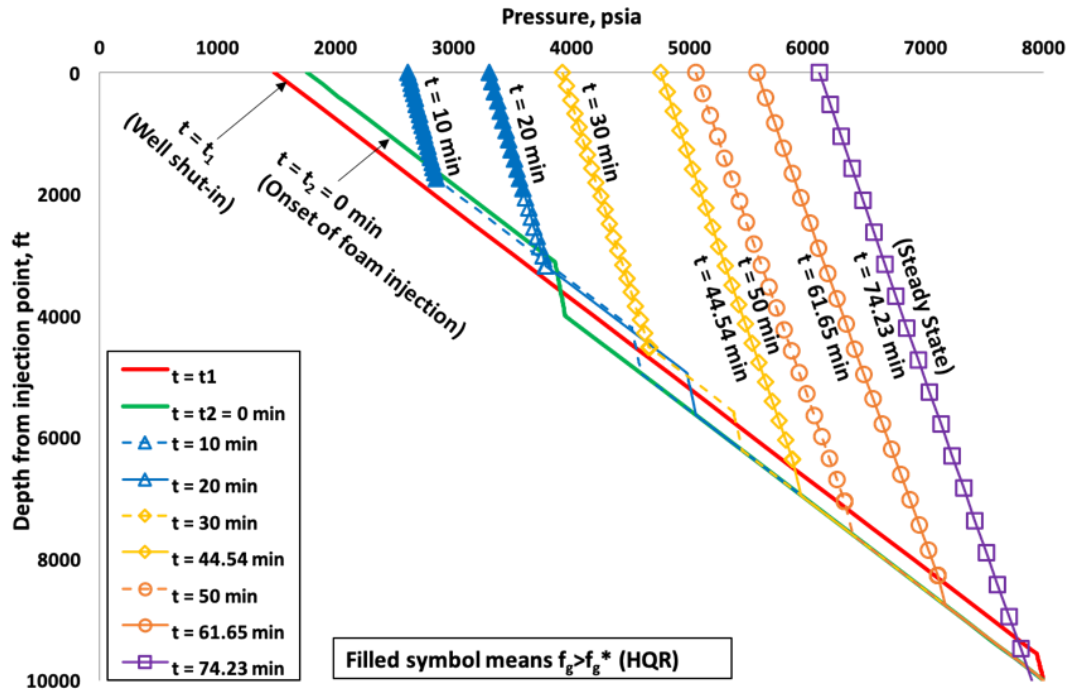


Figure 5. 16 Scenario 1 results showing pressure profile changing with time

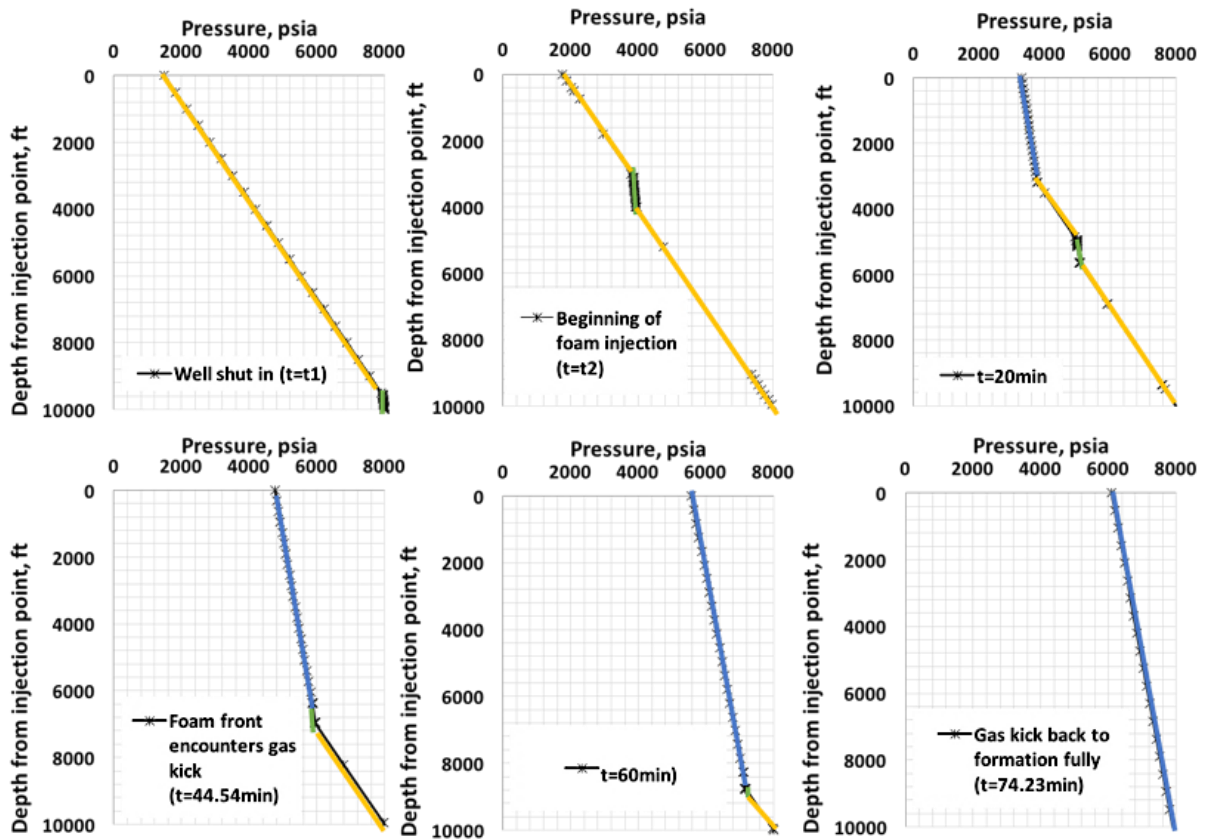


Figure 5. 17 Scenario 1 results showing pressure profile at different times

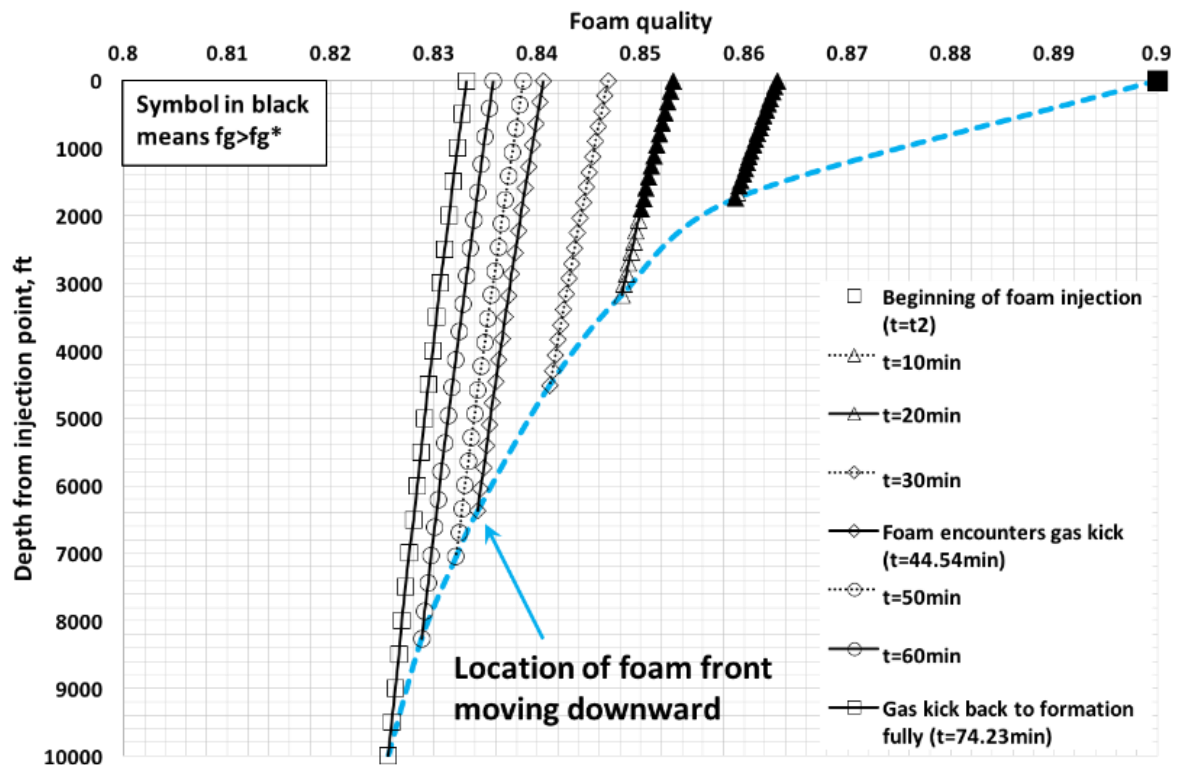


Figure 5. 18 Scenario 1 results showing foam quality profile with time

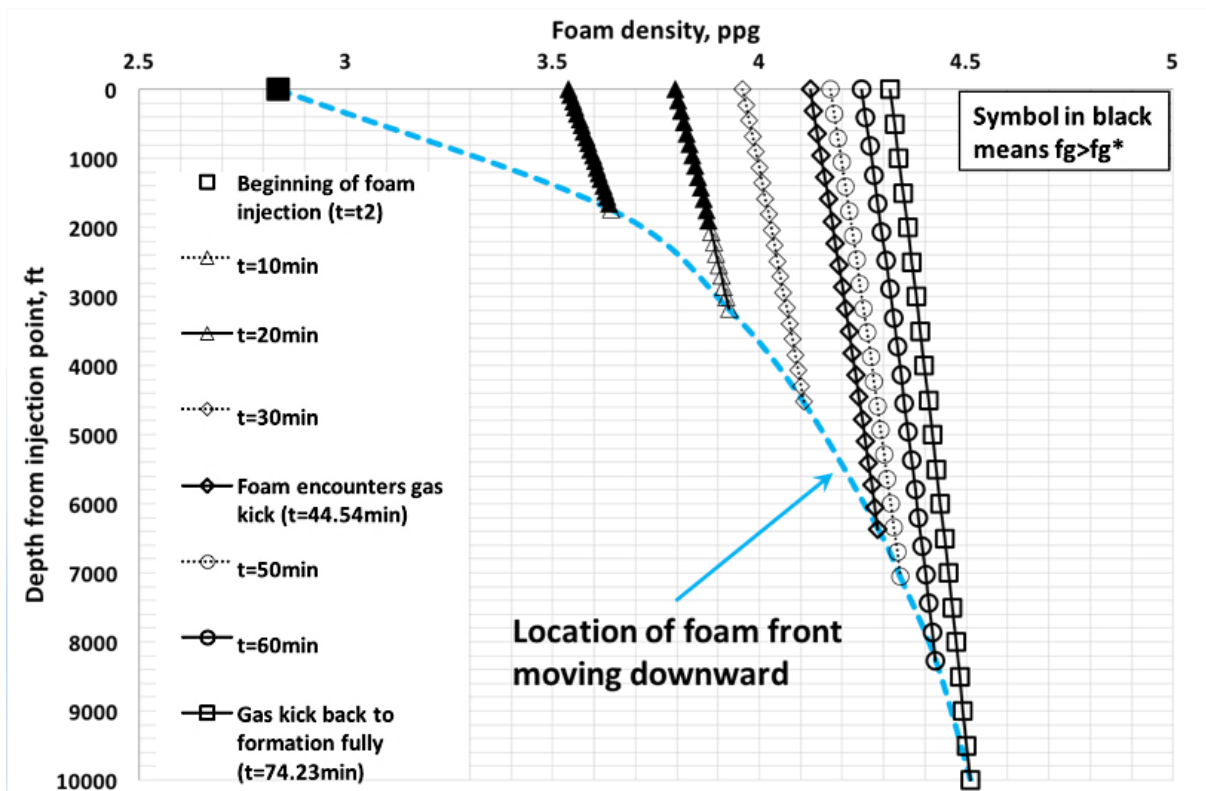


Figure 5. 19 Scenario 1 results showing foam density profile with time

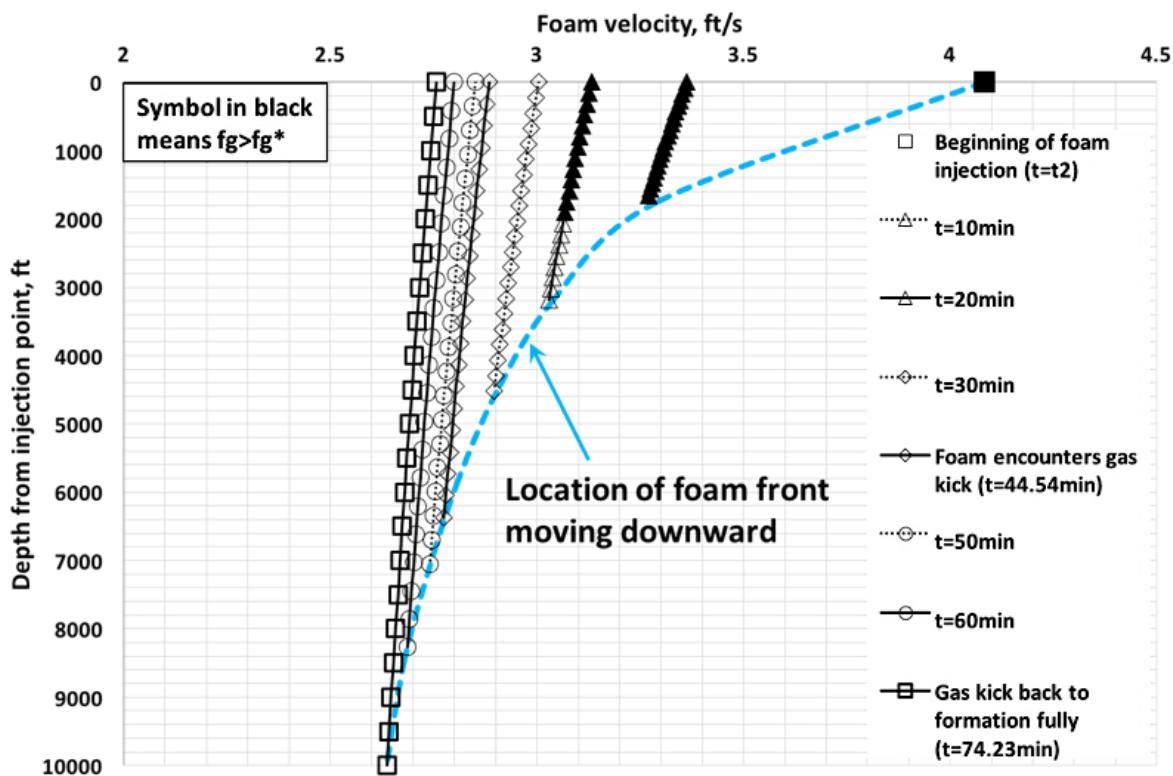


Figure 5. 20 Scenario 1 results showing foam velocity profile with time

The results in Figure 5. 16 through Figure 5. 20 can be used to determine the history of injection pressure as shown in Figure 5. 21 . The results show only two different events – foam displaces the drilling mud until  $t = 71$  mins and the formation gas afterwards to reach the steady state ( $t = 74.43$  mins). They are easily distinguished by two different slopes.

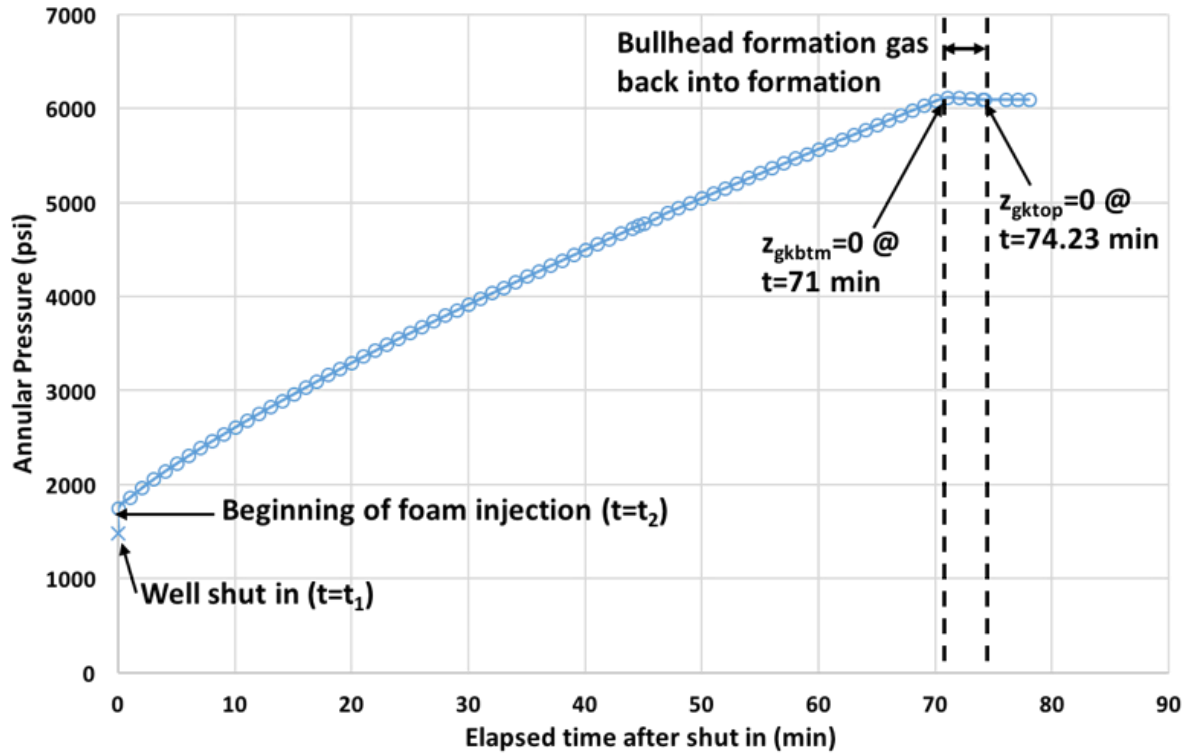


Figure 5. 21 Scenario 1 results showing injection pressure at the annular surface with time

#### 5.4.3 Results of Scenario 2

Scenario 2 considers the case when the injected foam becomes in contact with the formation gas, and foam becomes unstable at the interface. The destabilizing foam at the interface due to foam coalescence is factored in based on the wave velocity of foam coalescence ( $u_{fc}$ ). As shown in Figure 5. 22 through Figure 5. 27 , the results are identical to Scenario 1 (Figure 5. 15 ) until  $t = 44.54$  mins, after which there is a zone with the wet gas (after foams turning into gas and water of the same fraction) that grows with time. As a result, foam displaces drilling mud, formation gas,



and wet gas into the formation to reach the steady state at  $t = 122$  mins. As shown in Figure 5. 22 through Figure 5. 27 , foam front velocity ( $u_{ff}$ ) slows down significantly once the wet gas is formed and located between the injected foams and formation gas. This steady state with foam can only be obtained when  $u_{ff} > u_{fc}$ . If  $u_{ff} = u_{fc}$ , foam front stays at the same depth while the wet gas occupies the hole below. On the contrary, if  $u_{ff} < u_{fc}$ , foam becomes coarsening continuously (with such a wave propagating upward) and the hole is filled with wet gas once the steady state is reached.

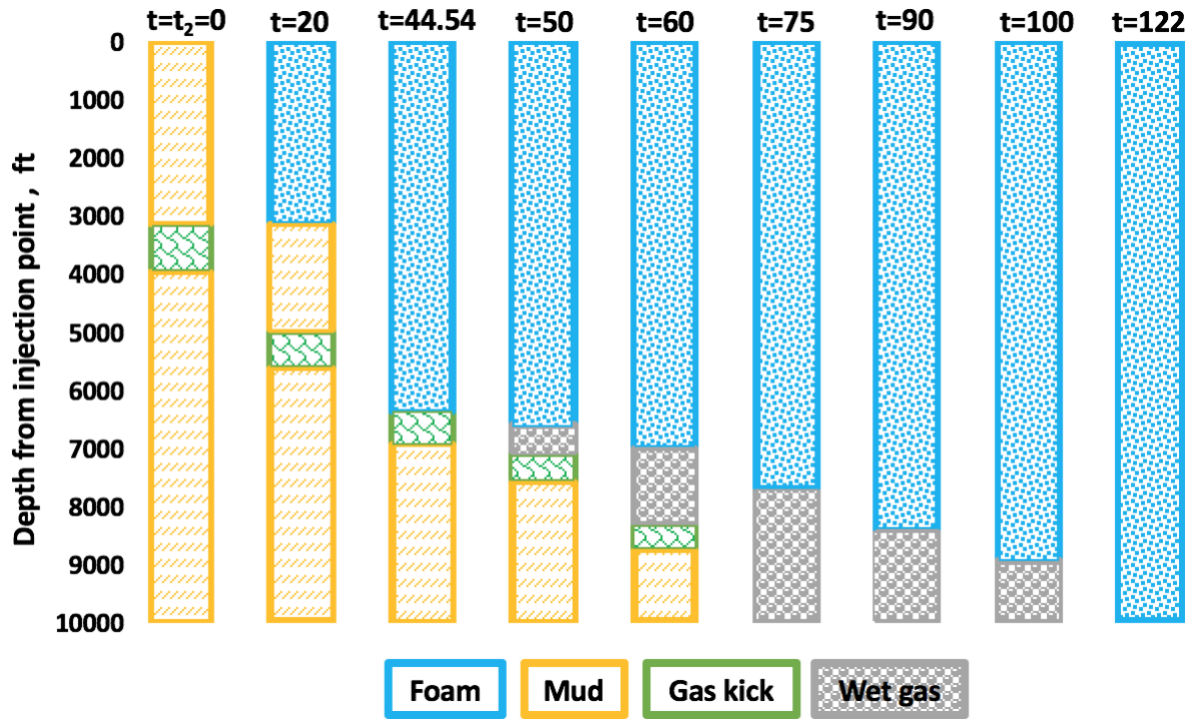


Figure 5. 22 Scenario 2 results showing vertical locations of different fluid zones with time [min]



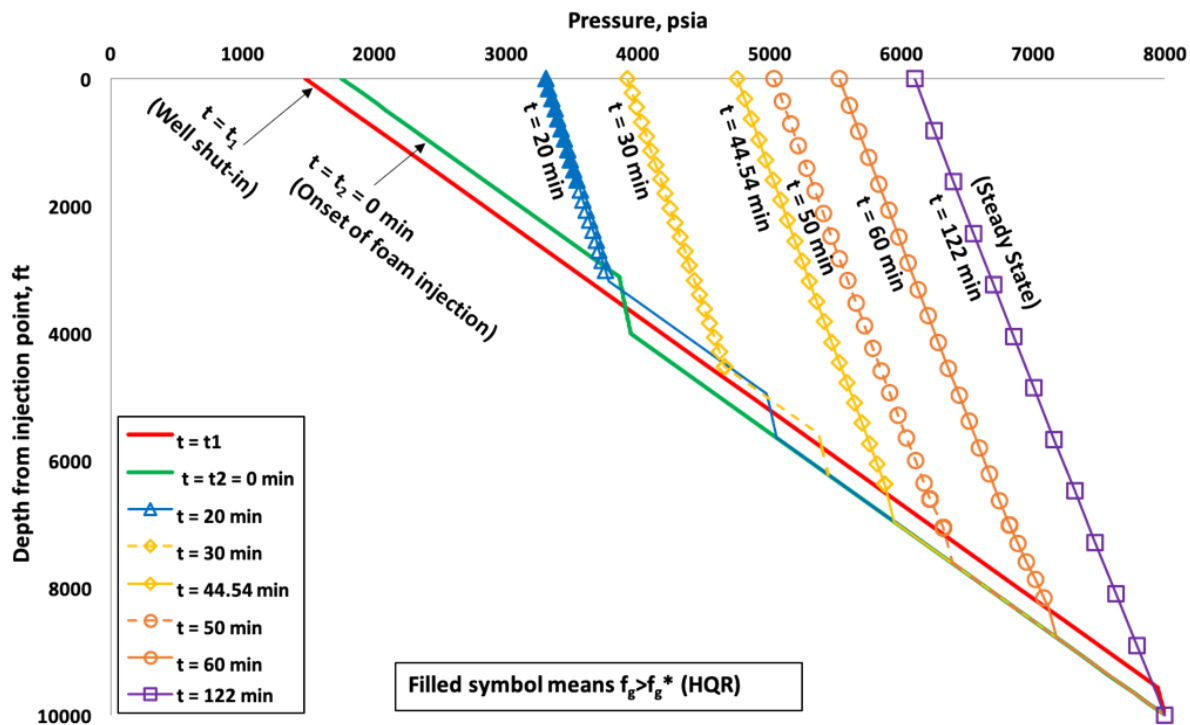


Figure 5. 23 Scenario 2 results showing pressure profile changing with time

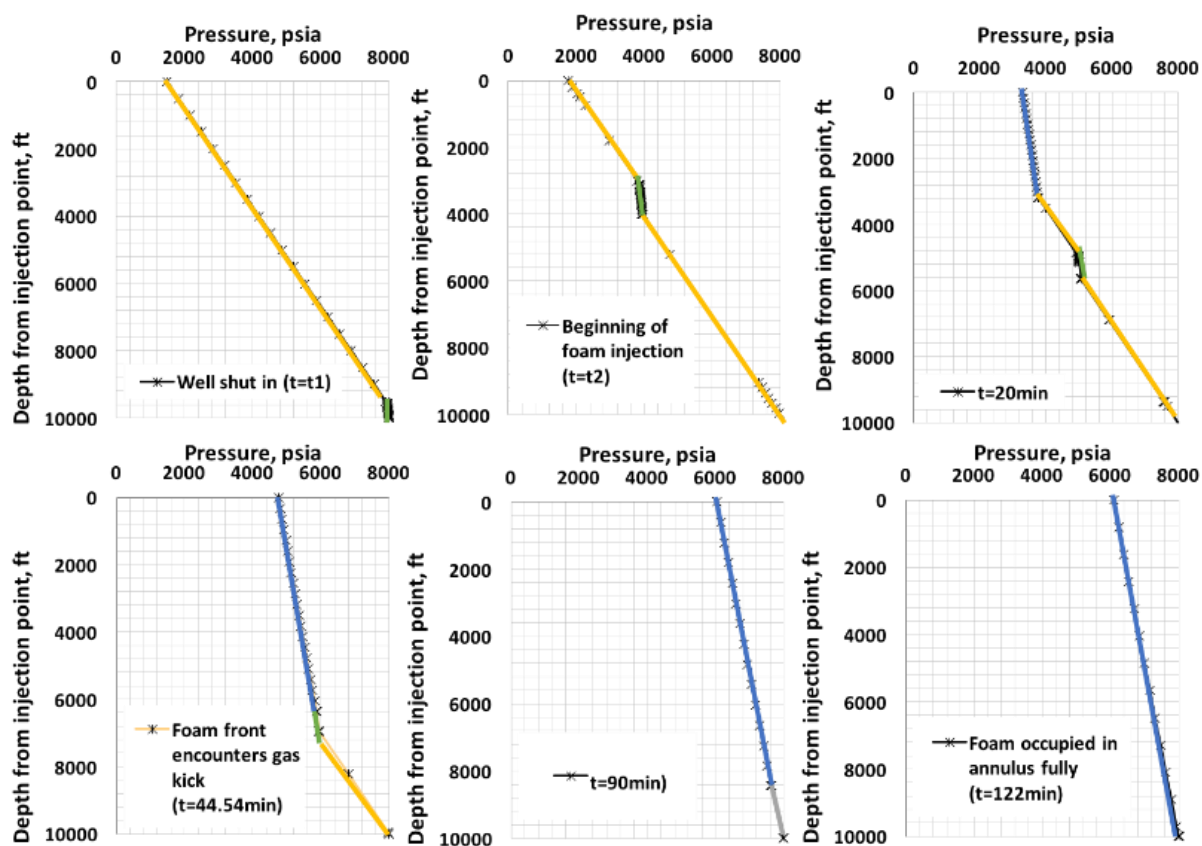


Figure 5. 24 Scenario 2 results showing pressure profile at different times

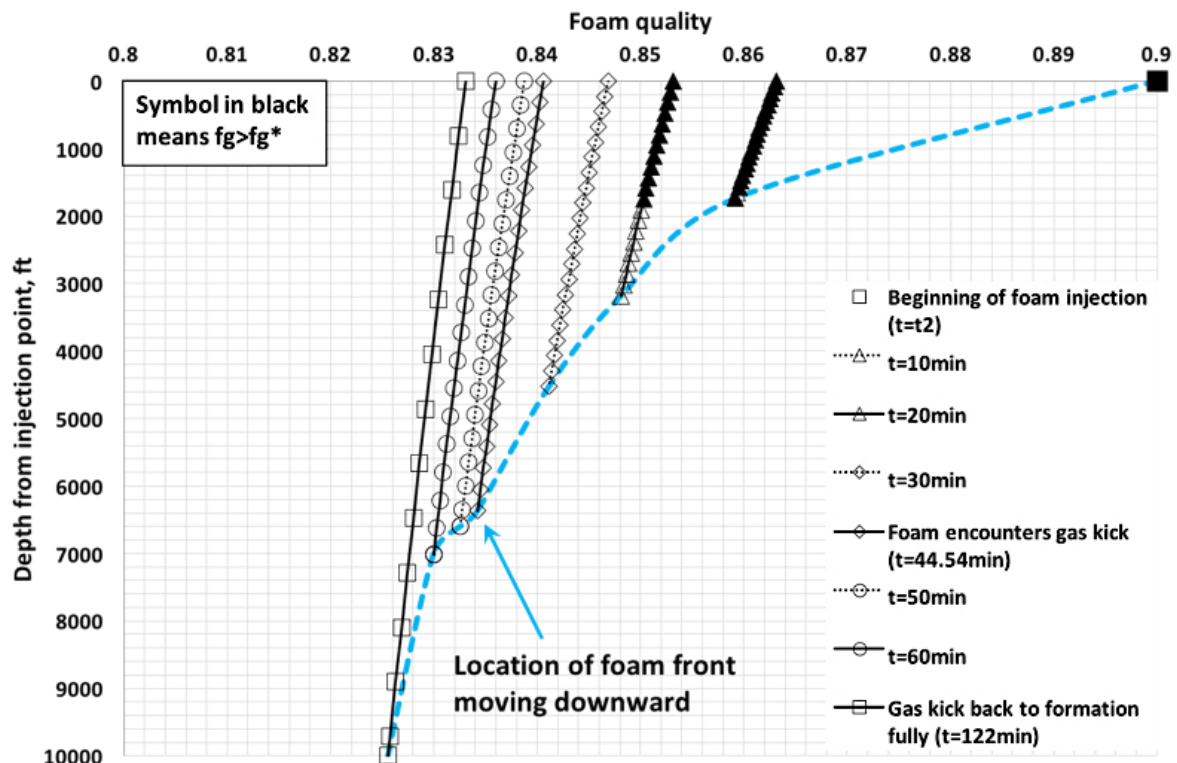


Figure 5. 25 Scenario 2 results showing foam quality profile with time

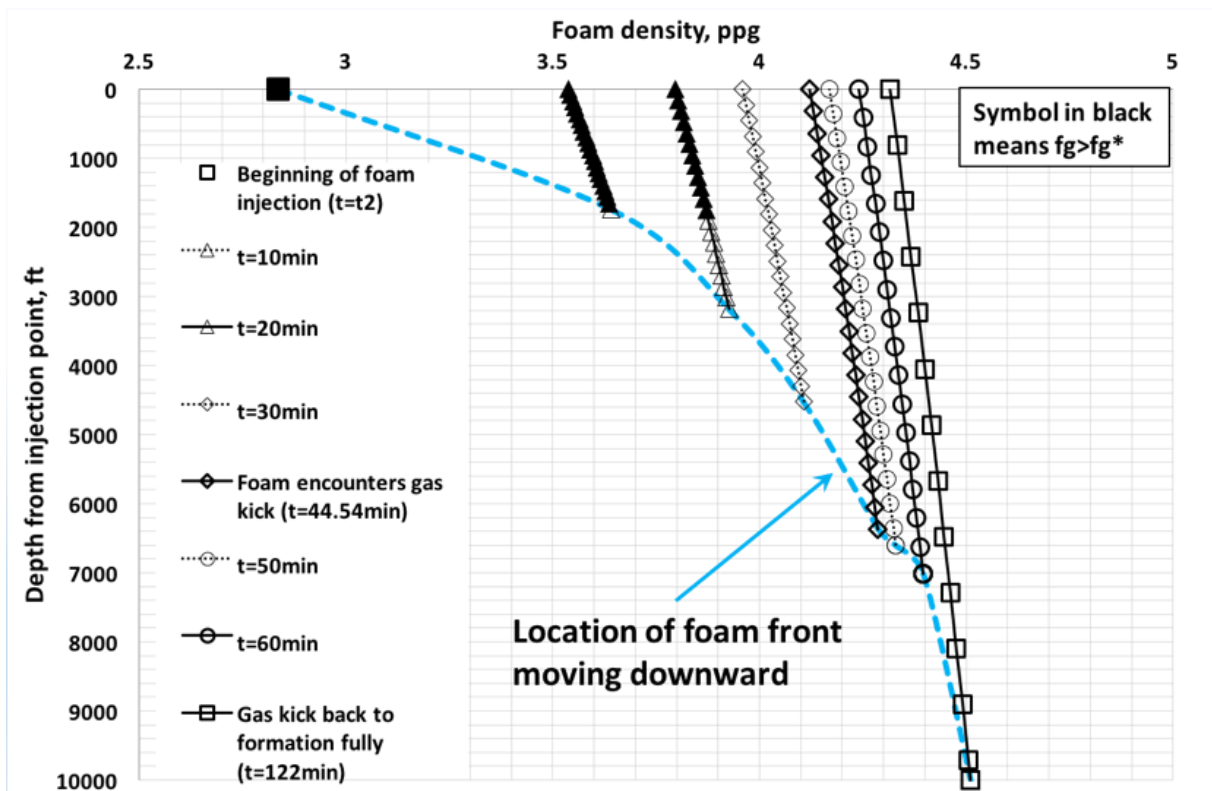


Figure 5. 26 Scenario 2 results showing foam density profile with time

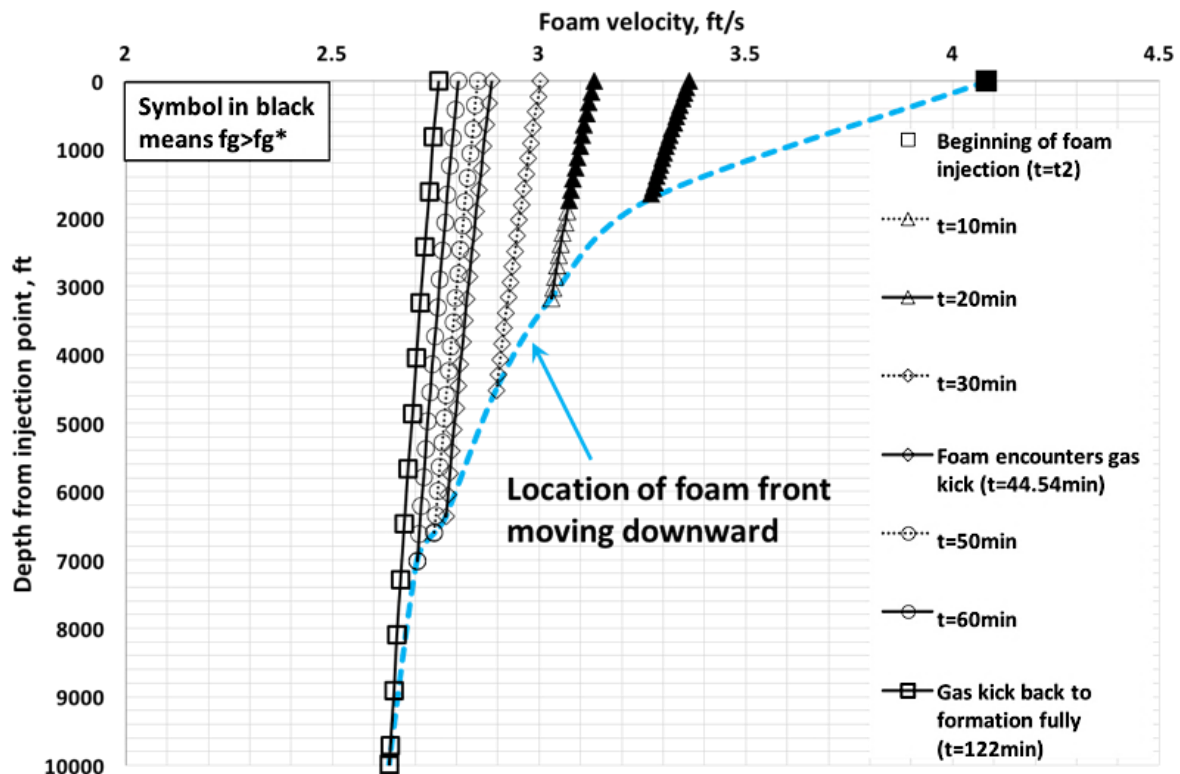


Figure 5. 27 Scenario 2 results showing foam velocity profile with time

Figure 5. 28 shows the history of injection pressure. Scenario 2 essentially shows that, with foams breaking at the interface and forming wet gas, the bullheading process takes longer (74.23 mins in Scenario 1 vs. 122 mins in Scenario 2) and the injection pressure becomes higher (6098 psia (42044246 Pa) in Scenario 1 vs. 6120 psia (42195931 Pa) in Scenario 2). This implies the stability of foams, when in contact with the formation gas, is an issue of paramount importance, affecting the maximum injection pressure as well as the operation time for bullheading process. There are additional factors that can be taken into consideration such as surfactant formulation and concentration, formation gas composition with possible presence of oil, mud composition and additives, colloidal and interfacial chemistry and so on. It is believed that Scenario 1 and Scenario 2 provide two extreme cases and, as a result, the reality can be found somewhere in between.

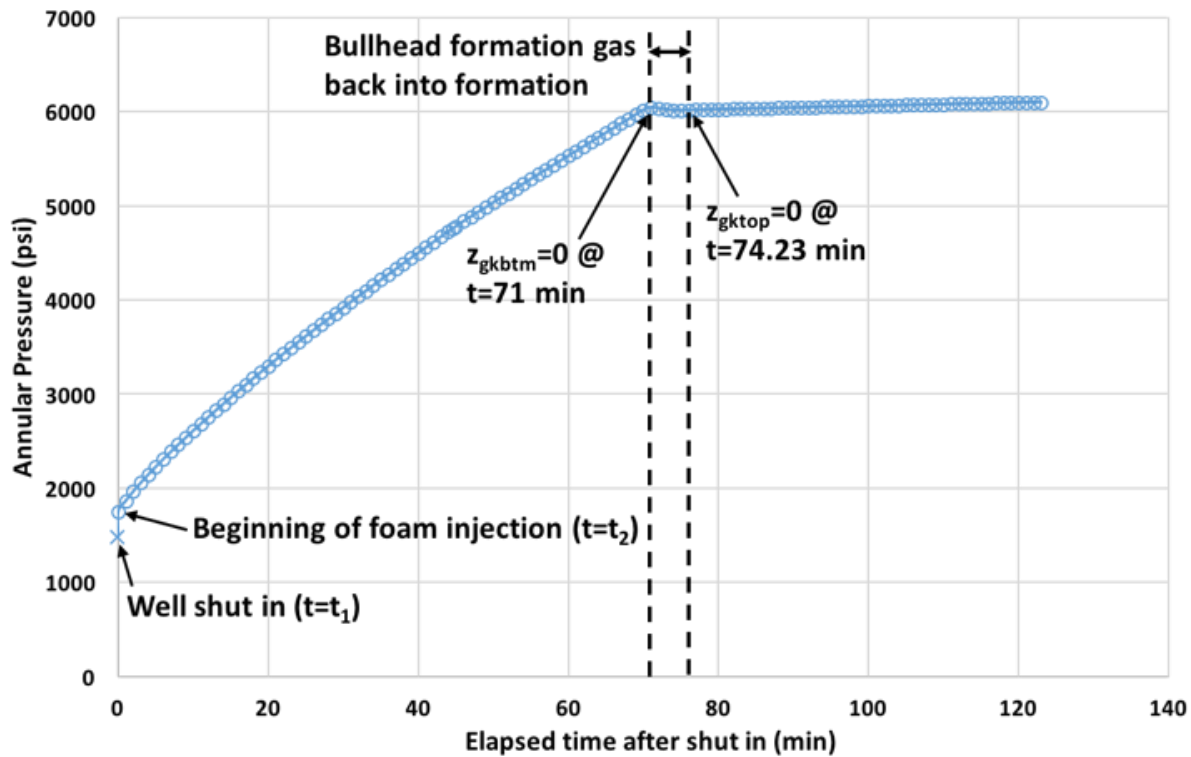


Figure 5. 28 Scenario 2 results showing injection pressure at the annular surface with time

It should be noted that if more accurate simulation results are needed, some of the assumptions made in this study should be revisited. For example, one may improve the model by adding mass

exchange between different fluids, making gas rising velocity varying with depth, gas properties and surrounding conditions (pressure, temperature), accounting for eccentricity of the annulus geometry, describing the gas phase as a mixture of formation gas and drilling mud, allowing the deviation of well trajectory and open-/cased-hole segments, among many.

It is important to point out that the two major outcomes (maximal injection pressure and overall operation time) we calculated in this study are based on the finest foam texture flow available. Any deviation from the finest foam texture (formation brine, dilution of surfactant, oil-wet debris, etc.) will make foam less stable, leading to lower frictional pressure loss and less efficient downward displacement of gas kick. Therefore, the calculated values tend to overestimate the maximal injection pressure and underestimate the duration time of operations.

#### 5.4.4 Case Study: Showing the Presence of Two Flow Regimes

This study is developed based on a hypothesis that foams, bullheading the drilling mud or formation gas in the wellbore, should be modeled with two distinct foam flow regimes. This section throws light on the necessity of the two foam flow regimes in modeling by using an evidence from the field-scale testing, that is, a foam-assisted sand-cleanout job in coiled tubing. The job chart, recording injection flow rates, circulation pressure and wellhead pressure, allows the frictional pressure loss during foam circulation to be determined and the pressure contours to be sketched.

Figure 5. 29 shows the well trajectory of the deviated well with survey data. The circulation pressure (i.e., surface injection pressure) is recorded at top of the coiled tubing on the reel, and the wellhead pressure (i.e., back pressure) is recorded at the top of the annulus tubing/pipe. The job intends to clean out fill (that is, a mixture of 20/40 Carbolite proppants and formation fines

(sandy/silty) from the reservoir) by injecting nitrogen foam. The top of fill is 9176 ft (2797 m) MD (measured depth), up inside the tailpipe, down to the TCP (tubing-conveyed perforating) guns at 9245 ft (2818 m) MD. Figure 5. 30 shows the details job chart in real time. At the beginning, the coiled tubing run in hole to 6562 ft (2000 m), and starts foam injection, and then continues running in hole with foam circulation. When the tubing arrives the fill depth around 9185 ft (2800 m), foam starts to circulate and transport sands to surface. During the cleaning period, the tubing is pushed back and forth. Finally, when there is shown no sands returned to surface, the coiled tubing is pulled out from the well and finishes the cleaning job.

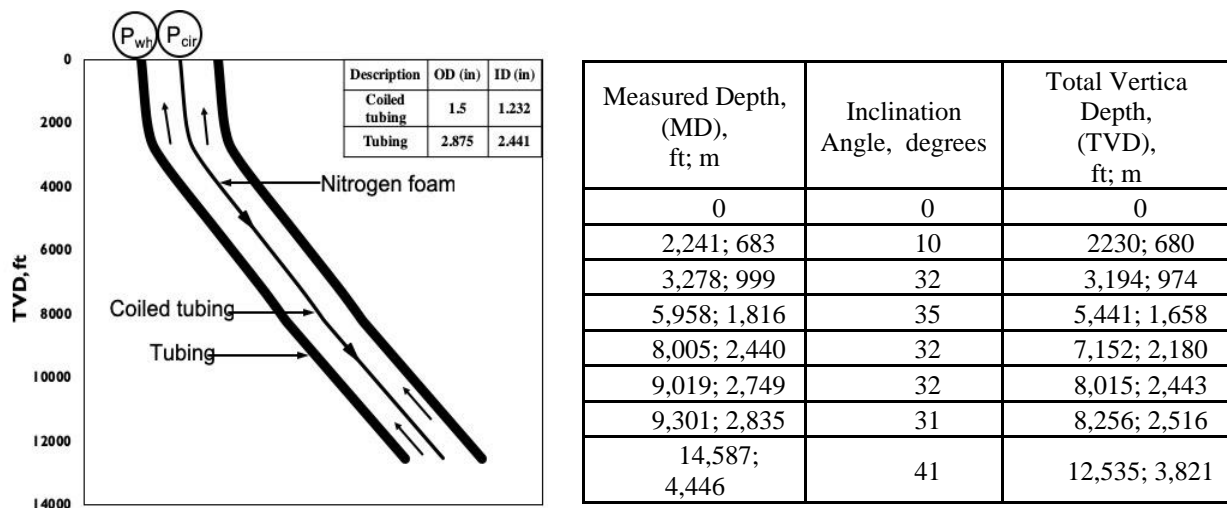


Figure 5. 29 Well trajectory of field-scale testing and survey data

As shown in Figure 5. 30, three sample points, believed to be at or near the steady-state condition at different well depths (6562 ft (2000 m), 9212 ft (2808 m), and 9239 ft (2816 m)), are chosen and denoted as Point A, Point B, and Point C, respectively. Table 5. 3 displays the liquid (i.e., surfactant solution with a similar density with water) and gas (i.e., nitrogen) flow rates together with pressure data. Note that the wellhead pressure and circulating pressure are measured at the same elevation and, thus, the difference between the two is approximately the frictional pressure loss over the entire distance (i.e., down through the coiled tubing and up through the

annulus tubing) assuming the gas and liquid phases are incompressible. The overall frictional pressure gradient,  $\left(\frac{\Delta P}{\Delta z}\right)_f$ , can then be calculated such as 0.2869 psi/ft (6489.8 Pa/m), 0.1832 psi/ft (4144 Pa/m), and 0.1138 psi/ft (2574.2 Pa/m) for Point A, B, and C, respectively.

The results show an interesting aspect. All at the same liquid flow rates, Point A (with  $Q_g = 800$  scfm ( $0.376 \text{ m}^3/\text{s}$ )) has  $\left(\frac{\Delta P}{\Delta z}\right)_f$  higher than Point B (with  $Q_g = 1000$  scfm ( $0.47 \text{ m}^3/\text{s}$ )) that is higher than Point C (with  $Q_g = 700$  scfm ( $0.329 \text{ m}^3/\text{s}$ )). When this response is plotted in a format of two flow regime pressure contours as shown by the three data points in Figure 5.31, it seems obvious that the two-flow regime concept with rheological properties of dry foams and wet foams must be incorporated in the modeling process.

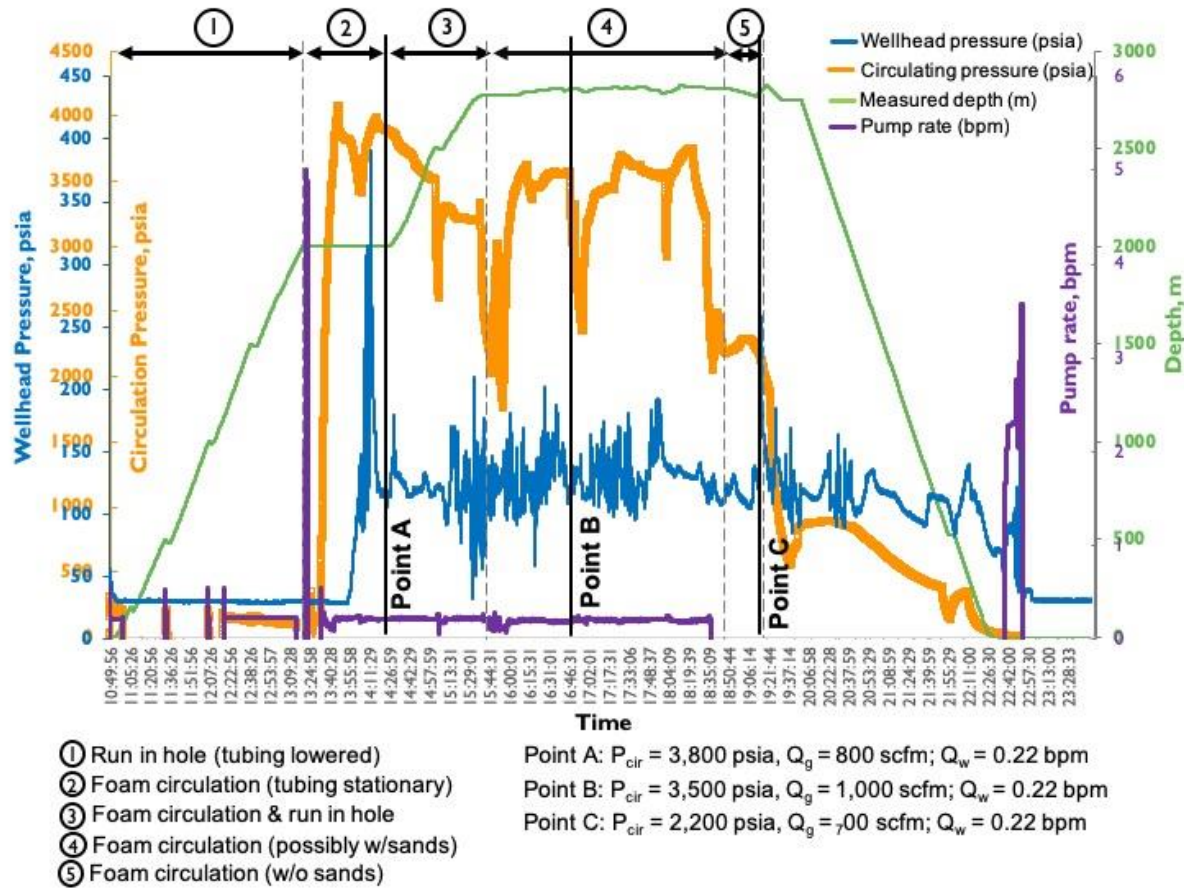


Figure 5.30 Job chart of field-scale testing in real time



Table 5. 3 Flow rate data and measured pressure data for Point A, B, C

Data points	Measured Depth, MD, ft; m	Gas flow rate, $Q_g$ , scfm	Liquid flow rate, $Q_w$ , gpm	Circulating pressure, $P_{cir}$ , psia	Wellhead pressure, $P_{wh}$ , psia	Approximated frictional pressure loss, $P_{cir} - P_{wh}$ , psi	Approximated frictional pressure gradient, $\left(\frac{\Delta P}{\Delta z}\right)_f$ , psi/ft
A	6562; 2000	800	9.24	3880	115	3765	0.2869
B	9212; 2808	1000	9.24	3505	130	3375	0.1832
C	9239; 2816	700	9.24	2238	135	2103	0.1138

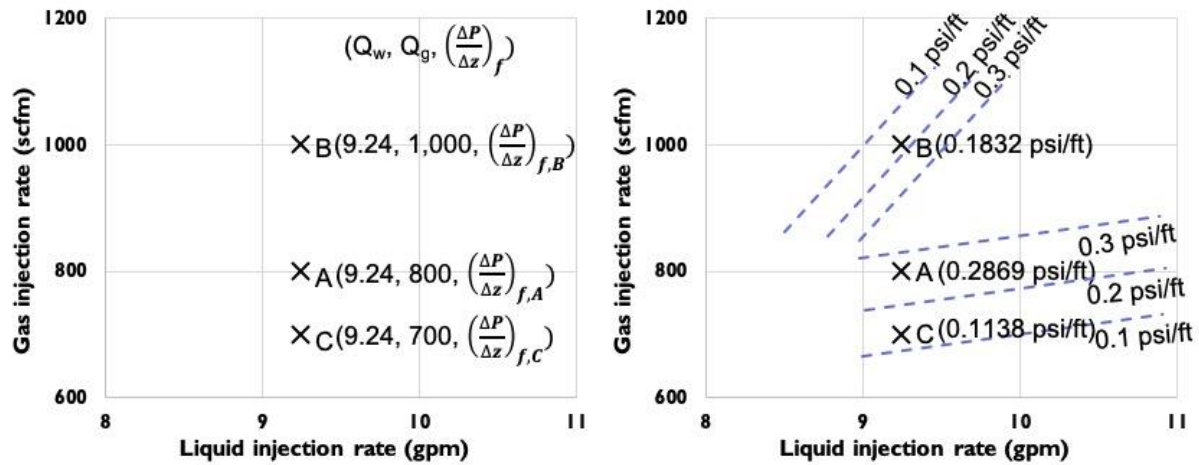


Figure 5. 31 Three near-steady-state data points and the sketch of pressure contours

There are many foam models available in literature. The example calculations for the circulation pressure, by using four different models (i.e., Model A based on Bingham-Plastic, Model B based on Power-Law, and Model C and D based on two empirical models) are shown in Table 5. 4 . Irrespective of the accuracy of different models, this exercise proves how difficult it is to match actual field-scale data that, in turn, highlights the importance of two flow regimes.



Table 5. 4 Comparisons of predicted circulation pressure with different foam models

Data points	Measured Depth, MD, ft; m	Circulating pressure, $P_{cir}$ , psia	Predicted circulating pressure, $P_{cir}$ , psia			
			Model A (Bingham-Plastic)	Model B (Power-Law)	Model C	Model D
A	6562; 2000	3880	3445	2396	3206	1685
B	9212; 2808	3505	4684	2926	4329	1873
C	9239; 2816	2238	3296	2434	3086	1426

## 5.5 Conclusions

This study investigates a process of foam-assisted mud cap drilling with three different scenarios through numerical calculations (Base Scenario, foam bullheading gas kick without making contact; Scenario 1, foam bullheading gas kick by making contact with the formation gas but foam stability not affected; and Scenario 2, foam bullheading gas kick and losing its stability in contact with the formation gas). The complicated foam rheological model, showing the dependence on the total flow rate and foam quality through the high-quality and low-quality regimes, is applied to calculate the frictional pressure loss within the foam zone. The following shows major findings of this study:

1. By investigating a range of possible scenarios, this study shows that the foam model with two flow regimes can be used to predict what happens during foam-assisted mudcap drilling process.
2. The results from simulations show that the two major unknowns in this type of bullheading process, i.e., the maximum injection pressure and overall operation time required for the process, can be determined depending on the scenarios.
3. If the response time is short such that foams do not interact with formation gas, the prediction of the process becomes relatively simple. If the response time is long and if the injected foams are in contact with the formation gas, the results can be more difficult to predict because the

interaction between foam and formation gas at the interface plays a significant role. If the latter happens, it is important to understand and quantify the level of interactions between foam and formation gas from additional investigations.

4. The simulation results clearly show that there is a good chance that foams during this process experience both high-quality regime and low-quality regime over the range of vertical locations and over the range of operation time. This justifies the use of foam model with two flow regimes.
5. The analysis of field-scale data clearly shows the presence of both high-quality regime and low-quality regime. This justifies the use of foam model with two different rheological properties.

## CHAPTER 6. CONCLUSIONS AND FUTURE WORKS

This work focuses on understanding foam fluid flow and its application in drilling, workover, and production stages. We have proposed a new foam rheological model with 9 model parameters based on the concept of Two Foam-Flow Regimes, combining the rheology of both dry and wet foams. This new model has been applied to simulate the well-used foam drilling, controlling gas migration processes to investigate the performance and potential of foam in these areas.

### 6.1 Conclusions

Throughout the whole study, we can make the following conclusions:

- The foam drilling simulation with newly developed foam model demonstrates the necessity of considering both low quality and high quality foams in the foam model. After comparing with the existing models of Chen et al. (2009) and Edrisi and Kam (2013), we conclude that ignoring coarsening foam texture in the high-quality regime can result in significant errors, as much as 40 – 60 %, in the scenarios tested. Even for a model with two flow regimes built in, not incorporating a transition region and two independent foam rheological properties may also lead to a meaningful level of errors in terms of injection pressure and bottom hole conditions.
- Using the complicated foam rheological model, which shows the dependence of total flow rate and foam quality, the transient simulation of foam bullheading gas kick can predict what can happen if foam is assisted. The calculation of maximum injection pressure and overall operation time can be very different in various scenarios, such as different response times and foam interactions at interface zones. The simulation results show that having both high-quality and low-quality regimes foam in the foam model plays a vital role considering such a range of vertical locations and a range of operation times.

- Using the field data from wellbore clean-up process, we can prove the evidence of Two Flow Regimes in terms of foam flow in circulating condition. Models such as the one we proposed in this study can further improve the understanding and interpretation of pressure changes in field operations.

This study covers some new perspectives of foam modeling work and foam-related applications, this can certainly improve the understanding of the fundamentals of foam and handling of foam in field operations, as explained below:

From the study of steady-state foam circulation such as foam drilling and wellbore cleanout, we know foam rheology plays a vital role in the implementation of foam hydraulics simulator. Besides those existing foam models, incorporating this new foam model, which is built on the basis of two flow regimes, into foam hydraulics simulators will improve the accuracy of pressure and foam properties at bottom hole condition.

From the study of foam mud cap drilling application, we learn that although foam interactions at the interface zone is a very complex topic, it still plays a critical role in the foam bullheading/displacement process. Taking into account those three scenarios among many, we find that the two major parameters field engineers most concern about, the maximum injection pressure and overall operation time, greatly depend on foam stabilities. As mentioned in Chapter 5, our modeling results are based on the most ideal case of foam structure. The calculated maximal injection pressure can be treated as the upper bound of the actual maximal injection pressure. Meanwhile, the calculated overall operation time can be treated as the lower bound of the actual required duration time of foam bullheading operation.

## 6.2 Future Works

In the future exploration, we can further improve our work from the following aspects:

- More fundamental knowledge associated with the interface between foam and fluids is demanding. In field operations, foam does not solely exist in borehole, pipe or tube. Mixing with certain amount of oil (from oil-based mud, or from reservoir) or sandy fluid will inevitably affect foam stability and foam properties. Having small-scale experimental works focusing on this field will help us get closer to the actual situations that foam faces in downhole condition.
- To improve the reliability of our developed foam model, despite the field data from a wellbore clean-up case we present in Chapter 5, we need to explore more similar field-scale tests that inject foam especially at high foam quality injection condition, in underbalanced drilling, wellbore clean-up, or other steady state conditions. Pressurized mudcap drilling for bullheading gas kick back to formation is a very novel technology to date. PMCD strictly requires well-trained field engineers upon operation. Using light mud such as foam is still an unmatured attempt. We need more field trials to justify its feasibility.
- We can further explore a broad range of other foam applications such as foam liquid unloading, foam fracturing, foam cementing, foam wellbore clean-up etc.

## REFERENCES

- Ahmed, S., Elraies, K.A., Hanamertani, A.S., Hashmet, M.R., Shafian, S.R.M. and Hsia, I.C.C. 2019. Investigation of Carbon Dioxide Foam Performance Utilizing Different Additives for Fracturing Unconventional Shales. SPE-197964-MS. Presented at the Abu Dhabi International Petroleum Exhibition and Conference, Abu Dhabi, UAE, 11-14 November.
- Al-Awadhi, F. K., Al, A., Fahed, S., Kikuchi, S., and Afifi, A. H. 2014. Making Un-Drillable HPHT Well Drillable using Mud Cap Drilling. SPE-171865-MS. Presented at the Abu Dhabi International Petroleum Exhibition and Conference held in Abu Dhabi, UAE, 10-13 November. (Al-Awadhi, 2014)
- Amit, S., Pathak, A. K., Ojha, K., and Sharma, S. 2017. Experimental and modeling hydraulic studies of foam drilling fluid flowing through vertical smooth pipes. *Egyptian Journal of Petroleum*, 26(2), pp 279-290.
- Benny, B., Andri, M. M. H., Ardia, K., Julius, S. and Julmar, S. T. 2013. Combining Pressurized Mud Cap Drilling (PMCD) and Early Kick Detection (EKD) Techniques for Fractured Formations Overlying a High Pressure Reservoir in Offshore Kalimantan. SPE-165893-MS. Presented at the SPE Asia Pacific Oil and Gas Conference and Exhibition, Jakarta, Indonesia, 22-24 October.
- Bernadiner, M. G. 1991. Foamed Gas Lift. Paper presented at the SPE Production and Operations Symposium held in Oklahoma City, Oklahoma, 7-9 April. SPE-21639-MS. <https://doi.org/10.2118/21639-MS>.
- Bogdanovic, M., Gajbhiye, R. N., and Kam, S. I. 2009. Experimental study of foam flow in horizontal pipes: Two flow regimes and its implications. *Colloids and Surfaces A: Physicochemical and Engineering Aspects*, 344(1), pp 56–71.
- Borre, F. and Sigbjorn, S. 2006. Controlled Mud-Cap Drilling for Subsea Applications; Well-Control Challenges in Deep Waters. SPE-91633-PA. *SPE Drilling and Completion*, 21(02), pp 133-140.
- Bourgoyne, Jr. A. T., Millheim, K., Chenevert, M. E., and Young, Jr. F. S. 1986. Applied Drilling Engineering. (1<sup>st</sup> ed.). TX: Society of Petroleum Engineers.
- Brannon, H.D., Kendrick, D.E., Luckey, E. and Stipetich, A. 2009. Multi-Stage Fracturing of Horizontal Wells Using Ninety-Five Quality Foam Provides Improved Shale Gas Production. SPE-124767-MS. Presented at the 2009 SPE Eastern Regional Meeting, Charleston, West Virginia, USA, 23-25 September.
- Briceno, M. I. and Joseph, D. D. 2003. Self-Lubricated Transport of Aqueous Foams in Horizontal Conduits. *International Journal of Multiphase Flow*, 29(2003), pp1817-1831.

- Bullen, R.S. and Bratrud, T.F. 1976. Fracturing with Foam. *Journal of Canadian Petroleum Technology*, 15(02), pp 27-32.
- Chen, G., Chen, X., Cheng, X., Liu, D., Liu, C., and Wang, D. 2006. The Application of Air and Air/Foam Drilling Technology in Tabnak Gas Field, Southern Iran. SPE-101560-MS. Presented at the IADC/SPE Asia Pacific Drilling Technology Conference and Exhibition, 13-15 November, Bangkok, Thailand.
- Chen, Z., Ahmed, R. M., Miska, S. Z., Takach, N. E., Yu, M., and Pickell, M. B. 2007. Rheology and Hydraulics of Polymer (HEC)-Based Drilling Foams at Ambient Temperature Conditions. SPE-94273-PA. *SPE Drilling and Completion*, 12(01), pp 100–107.
- Chen, Z., Ahmed, R. M., Miska, S. Z., Takach, N. E., Yu, M., Pickell, M. B., and Hallman, J. H. 2007. Experimental Study on Cutting Transport with Foam Under Simulated Horizontal Downhole Conditions. SPE-99201-PA. *SPE Drilling and Completion*, 22(04), pp 304-312.
- Chen, Z., Duan, M., Miska, S. Z., Yu, M., Ahmed, R. M., and Hallman, J. H. 2009. Hydraulic predictions for polymer thickened foam flow in horizontal and directional wells. SPE-105583-PA. *SPE Drilling and Completion*, 24(01), pp 40-49.
- Colbert, John W. and Medley, George 2002. Light Annular Mud Cap Drilling – A Well Control Technique for Naturally Fractured Formations. SPE-77352-MS. Presented at the SPE Annual Technical Conference and Exhibition held in San Antonio, Texas, 29 September – 2 October.
- Davies, R. M. and Taylor, S. G. 1950. The mechanics of large bubbles rising through extended liquids and through liquids in tubes. *Proceedings of The Royal Society-Mathematical, Physical and Engineering Sciences*, 200(1062), pp 375-390.
- Deshpande, N. S. and Barigou, M. 2000. The flow of gas liquid foams in vertical pipes. *Chemical Engineering Science*, 55(19), pp 4297–4309.
- Dipura, Y. S., Ardiyaprana, F. B. and Putra, E. M. F. 2018. Pressurized Mud cap Drilling Drastically Improves Drilling Efficiency in Exploration Well, South Sumatra. SPE/IADC-189398-MS. Presented at the SPE/IADC Middle East Drilling Technology Conference and Exhibition, Abu Dhabi, UAE.
- Doherty D.R. 2007. Implementation of Foamed Cementing for Shallow Water Flow Mitigation in the Caspian Sea. OMC-2007-165. Offshore Mediterranean Conference and Exhibition, 28-30 March, Ravenna, Italy.
- Dusterhoft, D.M. 2003. A Comparison Between Foamed and Lightweight Cements. PETSOC-2003-125. Canadian International Petroleum Conference, June 10-12, Calgary, Alberta.
- Edrisi, A. and Kam, S. I. 2013. A New Foam Model in Pipes for Drilling and Fracturing Applications. SPE-162709-PA. *SPE Journal*, 19(04), pp 576-585.

- Edrisi, A., Gajbhiye, R. N., and Kam, S. I. 2014. Experimental Study of Polymer-Free and Polymer-Added Foams for Underbalanced Drilling: Are Two Foam-Flow Regimes Still There? SPE-162712-PA. *SPE Journal*, 19(01), pp 55-68.
- Edrisi, A. and Kam, S. I. 2015. New Foam Drilling Hydraulics Calculations by Using Two Foam Flow Regimes. SPE-174769-MS. Presented at the SPE Annual Technical Conference and Exhibition, 28-30 September, Houston, Texas, U.S.A.
- Farag, A., Robertson, T., Kerem, M. et al. 2016. Foam Assist in a Gas-Lifted Oil Well. Paper presented at the SPE Middle East Artificial Lift Conference and Exhibition held in Manama, Kingdom of Bahrain, 30 November-1 December. SPE-184217-MS. <https://doi.org/10.2118/184217-MS>.
- Farina, L., Passucci, C., Lullo, A. D. et al. 2012. Artificial Lift Optimization With Foamer Technology in the Alliance Shale Gas Field. Paper presented at the SPE Annual Technical Conference and Exhibition held in San Antonio, Texas, USA, 8-10 October. SPE-160282-MS. <https://doi.org/10.2118/160282-MS>.
- Fomenkov, A., Ilya, P., Viktor, Z. and Artem F. 2018. Foam Cementing in the Volga-Ural Region: Case Study. SPE 191507. SPE Russian Petroleum Technology Conference, Moscow, Russia, 15-17 October 2018.
- Gajbhiye, R. N. and Kam, S. I. 2011. Characterization of foam flow in horizontal pipe by using two-flow-regime concept. *Chemical Engineering Science*, 66(8), pp 1536–1549.
- Gajbhiye, R. N. and Kam, S. I. 2012. The Effect of Inclination Angles on Foam Rheology in Pipes. *Journal of Petroleum Science and Engineering*, 86-87(2012), pp 246-256.
- Hall, D.L. and Roberts, R.D. 1984. Offshore Drilling with Preformed Stable Foam. SPE-12794-MS. Presented at the 1984 California Regional Meeting, Long Beach, California, 11-13 April.
- Hamizan, Azyyati A., Hasbullah, Utvanuddin P., Upadhyay, Abhishek, Buch, M., Eren, S., Zahari, M. Zukhairi, Roslan, M. Rizwan, Hajiyeve, M., Rashid, E. Rashid, Ishak, S. Nadiah, Johari, M. Raimi, Satar, Afzan A., Razali, Ezuan H., Huong, C. S., Payne J., Voshall, A., Mathews, T., and Houng, N. H. 2014. Mud Cap Drilling (MCD) with Continuous Annular Injection – Offshore Malaysia. IADC/SPE-170544-MS. Presented at the IADC/SPE Asia Pacific Drilling Technology Conference held in Bangkok, Thailand, 25-27 August.
- Hasan, A. R. and Kabir, C. S. 1992. Two-phase flow in vertical and inclined annuli. *International Journal of Multiphase Flow*, 18(2), pp 279-293.
- Heller J. 1994. Foams: Fundamentals and Applications in the Petroleum Industry, CO<sub>2</sub> Foams in Enhanced Oil Recovery. In *Advances in Chemistry*, 242 (Chapter 5), pp 201–234.
- Idris, M. F. R., Fabian, O., Hua, L. Y., Arathoon, M., Musa, M. Z., Musa, S., Johari, M. R. 2018. First Pressurized Mud Cap Drilling with Top Kill Application in Malaysia Development Wells.



- OTC-28415-MS. Presented at the Offshore Technology Conference Asia held in Kuala Lumpur, Malaysia, 20-23 March.
- Izadi, M. and Kam, S.I. 2020. Investigating Supercritical CO<sub>2</sub> Foam Propagation Distance: Conversion from Strong Foam to Weak Foam vs. Gravity Segregation. *Transport in Porous Media*, 131(01), pp 223- 250.
- Izadi, M. and Kam, S.I. 2019. Bubble Population Balance Modeling for Supercritical CO<sub>2</sub> Foam EOR Processes: from Pore-scale to Core-scale and Field-scale Events. *SPE Reservoir Evaluation and Engineering*, 22(4), pp 1467–1480.
- Jacobs, T., 2015. Offshore Industry Gets a Fresh Look at Foamed Cement. SPE-0115-0058-JPT. *Journal of Petroleum Technology*, 67 (01), pp 58-63.
- Jean De Rozieres, J. and Ferriere, R. 1991. Foamed-Cement Characterization Under Downhole Conditions and Its Impact on Job Design. *SPE Production Engineering*, 6 (03), pp 297-304.
- Joao A.T., Andrade G. and Alegria, A. 2017. Foam Cement Implementation – Deepwater Angola Case Histories. SPE 188308. Abu Dhabi International Petroleum Exhibition and Conference, Abu Dhabi, UAE, 13-16 November.
- Johnson, A. B. and White, D. B. 1991. Gas-Rise Velocities During Kicks. SPE- 20431-PA. *SPE Drilling Engineering* 6(04), pp 257-263.
- Kam, S. I., Gauglitz, P. A., and Rossen, W. R. 2002. The Yield Stress of Foamy Sands. *Colloids and Surfaces A: Physicochemical and Engineering Aspects*, 202(1), pp 53-62.
- Kam, S. I. and Rossen, W. R. 2002. The Compressibility of Foamy Sands. *Colloids and Surfaces A: Physicochemical and Engineering Aspects*, 202(1), pp 63-70.
- Kuehn, A. L. T. O. 2015. Pressurized Mud Cap Drilling; Feasibility Study for Application in Brazilian Pre-Salt Carbonate Reservoirs and Well Control Issues. SPE-177101-MS. Presented at the SPE Latin American and Caribbean Petroleum Engineering Conference held in Quito, Ecuador, 18-20 November.
- Kuroda, Y., Kudo, H., and Toyoda, K. 2017. Deepwater MPD Operation and Design Method. SPE-188487-MS. Presented at the Abu Dhabi International Petroleum Exhibition and Conference, Abu Dhabi, UAE, 13-16 November.
- Lage, A.C.V.M., Nakagawa, E.Y., Souza, A.A. de and Santos F, M.M. 1996. Recent Case Histories of Foam Drilling in Brazil. SPE-36098-MS. Presented at the Fourth Latin American and Caribbean Petroleum Engineering Conference, Port of Spain, Trinidad and Tobago, 23-26 April.

- Lee, W., Lee, S., Izadi, M. and Kam, S.I. 2016. Dimensionality-Dependent Foam Rheological Properties: How to Go from Linear to Radial Geometry for Foam Modeling and Simulation. *SPE Journal*, 19(1), pp 1669-1687.
- Li, Y. and Kuru, E. 2003a. Numerical Modeling of Cuttings Transport with Foam in Vertical Wells. PETSOC-2003-066. Presented at the Canadian International Petroleum Conference, Calgary, Alberta, 10-22 June.
- Li, Y. and Kuru, E. 2003b. Numerical Modeling of Cuttings Transport with Foam in Horizontal Wells. *Journal of Canadian Petroleum Technology*, 42(10), pp 54-61.
- McAndrew, J., Cisternas, P., Pruvot, A., Kong, X., Tong, S. 2017. Water Consumption and Proppant Transport Aspects of Foam Fracturing Fluids. SPE-2670102-MS. Presented at the Unconventional Resources Technology Conference (URTeC), Austin, Texas, USA, 24-26 July.
- Mooney, M. 1931. Explicit Formulas for Slip and Fluidity. *Journal of Rheology*, 2(02), pp 210-222.
- Moore, R., Daniel, B., Reed, S. and Hernandez, R. 2005. High-Temperature Wells with Lost-Circulation Demands and Reverse-Circulation Techniques Using Foamed-Cement Systems: Two Case Histories. *SPE Drilling and Completion*, 20 (02), pp 133-140.
- Mukherjee, J., Nguyen, Q.P., Scherlin, J., Vanderwal, P. and Rozowski, P. 2016. CO<sub>2</sub> Foam Pilot in Salt Creek Field, Natrona County, WY: Phase III: Analysis of Pilot Performance. SPE-179635-MS. <https://doi.org/10.2118/179635-MS>. Presented at the SPE Improved Oil Recovery Conference, Tulsa, OK. 11-13 April.
- Nakagawa, E. Y., Silva, Jr. V., Boas, M. B. V., Silva, P. R. C., and Shayegi, S. 1999. Comparison of Aerated Fluids/Foam Drilling Hydraulics Simulators Against Field Data. SPE-54319-MS. Presented at the SPE Asia Pacific Oil and Gas Conference and Exhibition, Jakarta, Indonesia, 20-22 April.
- Nugroho, W. A., Sumantri, M., and Wibisono, D. 2017. Design and Application of Aerated and Foam Drilling Fluid, Case Study in Drilling Operation in Indonesia. SPE-186233-MS. Presented at the SPE/IATMI Asia Pacific Oil and Gas Conference and Exhibition, Jakarta, Indonesia, 17-19 October.
- Ocampo, A., Restrepo, A., Cifuentes, H., Hester, J., Orozco, N., Gil, C. and Gonzalez, C. 2013. Successful Foam EOR Pilot in a Mature Volatile Oil Reservoir under Miscible Gas Injection. IPTC-16984-MS. <https://doi.org/10.2523/IPTC-16984-MS>. Presented at the International Petroleum Technology Conference, Beijing, China, 26-28 March.
- Okpobiri, G. A. and Ikoku, C. U. 1986. Volumetric Requirements for Foam and Mist Drilling Operations. SPE-11723-PA. *SPE Drilling Engineering*, 1(1), pp 71-88.

- Ortiz, D.P.M., Izadi, M. and Kam, S.I. 2019. Modeling of Nanoparticle- Stabilized CO<sub>2</sub> Foam Enhanced Oil Recovery. SPE Reservoir Evaluation and Engineering, 22(3), pp 971–989.
- Osunde, O. and Kuru, E. 2006. Numerical Modeling of Cuttings Transport with Foam in Inclined Wells. PETSOC-2006-071. Presented at the Canadian International Petroleum Conference, Calgary, Alberta, 13-15 June.
- Oussoltsev, D., Fomin, I., Butula, K.K., Mullen, K., Gaifullin, A., Ivshin, A., Senchenko, D. and Faizullin, I. 2008. Foam Fracturing: New Stimulation Edge in Western Siberia. SPE-115558-MS. Presented at the 2008 SPE Russian Oil and Gas Technical Conference and Exhibition, Moscow, Russia, 28-30 October.
- Ozbayoglu, M.E., Kuru, E., Miska, S. and Takach, N. 2000. A Comparative Study of Hydraulic Models for Foam Drilling. SPE-65489-MS. Presented at the 2000 SPE/CIM international Conference on Horizontal Well Technology, Calgary, Alberta, Canada, 6-8 November.
- Paknejad, A., Schubert and J., Amani, M. 2007. Foam Drilling Simulator. SPE-105338-MS. Presented at the 15th SPE Middle East Oil and Gas Show and Conference, Kingdom of Bahrain, 11-14 March.
- Paknejad, A., Schubert, J. and Amani, M. 2009. Key Parameters in Foam Drilling Operations. IADC/SPE-122207. Presented at the IADC/SPE Managed Pressure Drilling and Underbalanced Operations Conference and Exhibition, San Antonio, Texas, 12-13 February.
- Rader, D. W., Bourgoyne, A. T., and Ward R. H. 1975. Factors Affecting Bubble-Rise Velocity Of Gas Kicks. SPE-4647-PA. *Journal of Petroleum Technology*, 27(05), pp 571- 584.
- Ridley, K., Jurgens, M., Billa, R. J., and Mota, J. F. 2013. Eagle Ford shale well control: drilling and tripping in unconventional oil and gas plays. SPE-163984-MS. Presented at the SPE Unconventional Gas Conference and Exhibition, Muscat, Oman, 28-30 January.
- Rojas, Y., Vieira, P., Borrell, M., Blanco, J., Ford, M., Nieto, L., Lopez, G., and Atencio, B. 2002. Field application of near-balanced drilling using aqueous foams in western Venezuela. SPE-74449-MS. Presented at the IADC/ SPE drilling conference, Dallas, TX, 26-28 February.
- Rossen, W.R., Ocampo, A., Restrepo, A., Cifuentes, H.D., Marin, J. 2017. Long-time Diversion in Surfactant-Alternating-Gas Foam Enhanced Oil Recovery from a Field Test. SPE 170809-PA. SPE Reservoir Evaluation and Engineering 01(20), pp 1-7. <https://doi.org/10.2118/170809-PA>.
- Safipour, M. J., Mavaddat, Y., Mavaddat, M., A'Rabi, M., Kadkhodaei, N., Abdollahi, A., Behbahani, S. M. Haeri 2017. Applicability of Managed pressure Drilling MPD in a High Sulfur Content Fractured Reservoir. SPE-188694-MS. Presented at the Abu Dhabi International Petroleum Exhibition and Conference, Abu Dhabi, UAE, 13-16 November.

- Sanghani, V. and Ikoku, C. U. 1983. Rheology of Foam and Implications in Drilling and Cleanout Operations. *Journal of Energy Resource Technology*, 105(3), pp 362-371.
- Saxena, Amit, Pathak, A.K., Ojha, Keka, and Sharma, Shivanjali 2016. Experimental and modeling hydraulic studies of foam drilling fluid flowing through vertical smooth pipes. *Egyptian Journal of Petroleum*, 26(2017), pp 279-290.
- Sepulveda, J.J., Falana, O.M., Kakadjian, S., Morales, J.D., Zamora, F., Dibiasio, M.A., Marshall, E., Shirley, G., Benoit, D.J. and Tkach, S.A. 2008. Oil-Based Foam and Proper Underbalanced-Drilling Practices Improve Drilling Efficiency in a Deep Gulf Coast Well. SPE-115536-MS. Presented at the 2008 SPE Annual Technical Conference and Exhibition, Denver, Colorado, USA, 21-24 September.
- Sherif, T., Ahmed, R., Shah, S. and Amani, M. 2015. Rheological behavior of oil-Based drilling Foams. *Journal of Natural Gas Science and Engineering*, 26(2015), pp 873-882.
- Wang, J., Anh, V. Nguyen, and Saeed, Farrokhpay 2016. A critical review of the growth, drainage and collapse of foams. *Advances in Colloid and Interface Science*, 228(2016), pp 55-70.
- Wang, Y., Thiberville, C., and Kam, S. I. 2017. A New Model for Foam Flow in Pipes and Its Application in Drilling Processes. *International Journal of Modern Engineering*, 18(1) (Fall/Winter), pp 21-32.
- Wang, Y., Thiberville, C., and Kam, S. I. 2018. Modeling of Foam-Assisted Wellbore Cleanup and Drilling Processes with Both Dry- and Wet-Foam Rheological Properties. SPE-191263-MS. Presented at the SPE Trinidad and Tobago Section Energy Resources Conference, Port of Spain, Trinidad and Tobago, 25-27 June.
- Xia, G. and Chai, L. 2012. Influence of Surfactant on Two-Phase Flow Regime and Pressure Drop in Upward Inclined Pipes. *Journal of Hydrodynamics*, 24(1), pp 39-49.

## VITA

Yanfang Wang was born in 1991, at Shangqiu City, Henan Province, China. She received her Bachelor of Engineering degree in Petroleum Engineering from China University of Petroleum, Beijing, China in June 2012. She received her Master of Science degree in Petroleum Engineering from University of Louisiana Lafayette, Lafayette, Louisiana in December 2014. In January 2015, she joined the Ph.D. program in Craft & Hawkins Department of Petroleum Engineering in Louisiana State University, Baton Rouge, Louisiana. Over the summer of 2017, 2018, and 2019, she interned with Pegasus Vertex, Inc. at Houston, Texas. She is currently a candidate for the degree of Doctor of Philosophy in Petroleum Engineering.